Stable Isotope Geochemistry of the Okenyenya Igneous Complex, Namibia: Constraints on Contamination and Fluid Interaction.

by

Iúma A. Martinez

Dissertation submitted in fulfilment of the requirements
for the degree of
Master of Science

Department of Geological Sciences
University of Cape Town
March, 1995

Declaration

I hereby declare that all the work presented in this dissertation is my own, except where otherwise stated.

Signed by candidate

I. Martinez

Dedication

This thesis is dedicated to Monique, Erminia, Russell, Tammy

..... & other gentle people.

Contents

Abstract

Oxygen isotope data are presented for silicate minerals separated from the tholeiitic olivine gabbro-quartz monzodiorite suite of rocks, alkaline gabbro, syenite, nepheline syenite, oligoclase essexite and essexite dyke of the Okenyenya igneous complex of northwest Namibia. Carbon and oxygen isotope data from a small number of carbonate-bearing samples are also presented. The calcite within the syenite ($\delta^{18}O$ = + 19.3 ‰), alkaline gabbro ($\delta^{18}O$ = + 16.1 to + 16.6 ‰) and monzodiorite ($\delta^{18}O$ = + 18.0 ‰) is secondary, and the high $\delta^{18}O$ values suggest a low temperature of formation. In contrast, the essexite dyke contains a primary calcite phase, for which the carbonate stable isotope data ($\delta^{18}O$ = + 12.2 ‰; $\delta^{13}C$ = - 4.1 ‰) are consistent with a mantle carbon source. The origin of the calcite may be related to the intrusion of the essexite dyke or ultramafic lamprophyres.

The $\delta^{18}O$ values of coexisting silicate minerals in rocks comprising the tholeiitic olivine gabbro - quartz monzodiorite suite, are consistent with the attainment of isotope equilibrium and largely closed system conditions. The majority of the temperatures calculated by conventional mineral-pair thermometers are spurious, as a result of oxygen isotope diffusion during slow cooling. Closure temperatures for oxygen diffusion of 560 °C and 540 °C have been calculated for the anorthite-clinopyroxene and plagioclase-biotite mineral-pairs in the tholeiitic leucogabbro sample, respectively. The oxygen isotope data for the silicate minerals are consistent with contamination of the magmas by material having the oxygen isotope composition of the southern Etendeka rhyolite ($\delta^{18}O$ = + 11.5 ‰). It is suggested that the assimilant may have been derived from the same source as the southern Etendeka rhyolite, as opposed to the rhyolite itself, which would be expected to occur at a high crustal level. Simple oxygen and strontium isotope mass balance calculations are used to constrain the lower (14 % and 19.5 % respectively) and upper (57 % and 71.6 % respectively) limits of the maximum possible amount of a southern Etendeka rhyolite contaminant assimilated.

Models based on the covariation of $\delta^{18}O$ - $^{87}Sr/^{86}Sr$ indicate that the Outer Zone Units (4 to 6) require lower cumulates / assimilated rock (r) values ($9 > r > 5$) and higher bulk distribution coefficients (β) values (1.3 - 1.6), than the Inner Zone Units (1 to 3)

(r = 9; β = 1.2). Within the tholeiitic suite, for the cases of AFC without and with magma recharge, the ratio (total mass of crust assimilated) / (mass of original magma) (ρ) ranged from 0.2 - 0.12 respectively. For both cases, the rate of assimilation is estimated to have been 5 to 7 times slower than the rate of fractional crystallization. For the case of AFC with magma recharge, the rate of fractional crystallization was 5 to 30 times the recharge rate.

The biotite $\delta^{18}O$ values indicate that the biotite within the tholeiitic suite may have been derived from a deuteric fluid at subsolidus temperatures. The biotite within the nepheline syenite and essexite dyke may have been derived from external fluids, which were respectively characterized by higher and lower initial $\delta^{18}O$ fluid values than the fluid which altered the tholeiitic suite. Both the plagioclase and carbonate oxygen isotope data indicate that the final $\delta^{18}O$ value of the fluid was buffered by the rock. The plagioclase $\delta^{18}O$ values for the tholeiitic suite are in accordance with a greater degree of alteration, by a magmatic fluid, for the inner units with respect to the outer units. Maximum water/rock ratios have been estimated for the most altered tholeiitic and alkaline gabbro samples. Both the tholeiitic and alkaline gabbro experienced localized minor alteration (maximum water/rock ratios in the range of 0.2 to 0.5), by dominantly magmatic fluids ($\delta^{18}O \geq + 5$ ‰) at subsolidus temperatures. The petrographic observations and water/rock ratio calculations indicate that the alteration due to the influx of meteoric water, which is typically associated with caldera collapse, was minimal or absent.

Chapter 1 - Introduction -

1.1 Regional setting

The Okenyenya igneous complex (SACS, 1980) is one of a number of Damaraland anorogenic complexes which lie on a northeast-trending line of intrusions in north-western Namibia (Fig. 1.1). The complexes intrude the Pan-African age Damara metasediments and granites (Miller, 1983) and the Jurassic - early Cretaceous Karoo sedimentary rocks. These high-level sub-volcanic intrusions (Watkins & le Roex, 1991; Watkins *et al.*, 1994) range up to 30 km in diameter and have been interpreted as caldera collapse structures (Korn & Martin, 1939; Simpson, 1954; Martin *et al.*, 1960; Pirajno & Schlögl, 1987; Watkins & le Roex, 1991; le Roex *et al.*, 1995). Martin *et al.* (1960) have grouped the intrusions into: 1) granite plutons, 2) differentiated basic complexes and 3) peralkaline and carbonatitic complexes. The emplacement of these complexes occurred approximately contemporaneously with the Etendeka volcanic rocks 135 - 123 Ma ago and has been related to magmatism associated with to the upwelling Tristan plume and the opening of the South Atlantic Ocean (Milner *et al.*, 1993; 1994). The linear distribution of the complexes has been ascribed to a structurally controlled emplacement mechanism (Milner *et al.*, 1993; 1994) which operated along a Pan-African terrane / Proterozoic cratonic basement discontinuity (Fig. 1.1). A temporally related shift from tholeiitic to alkaline magmatism is observed for the Okenyenya, Paresis, Messum and Cape Cross complexes (Martin *et al.*, 1960; Prins, 1981).

1.2 Previous work on Okenyenya

Preliminary fieldwork by Korn and Martin (1939) led to the initial recognition of gabbroic and syenitic rocks at Okenyenya. The first detailed structural, petrographic and mineral chemistry studies on the complex by Simpson (1950, 1952, 1954) revealed coherent bulk rock and mineral differentiation trends and led to the definition of a tholeiitic and an alkaline series of rock types. The analytical focus of this dissertation is dominated by six units which have been recognized in the olivine gabbro - quartz monzodiorite part of the tholeiitic suite on the basis of mineral and bulk rock geochemistry (le Roex *et al.*, 1995).

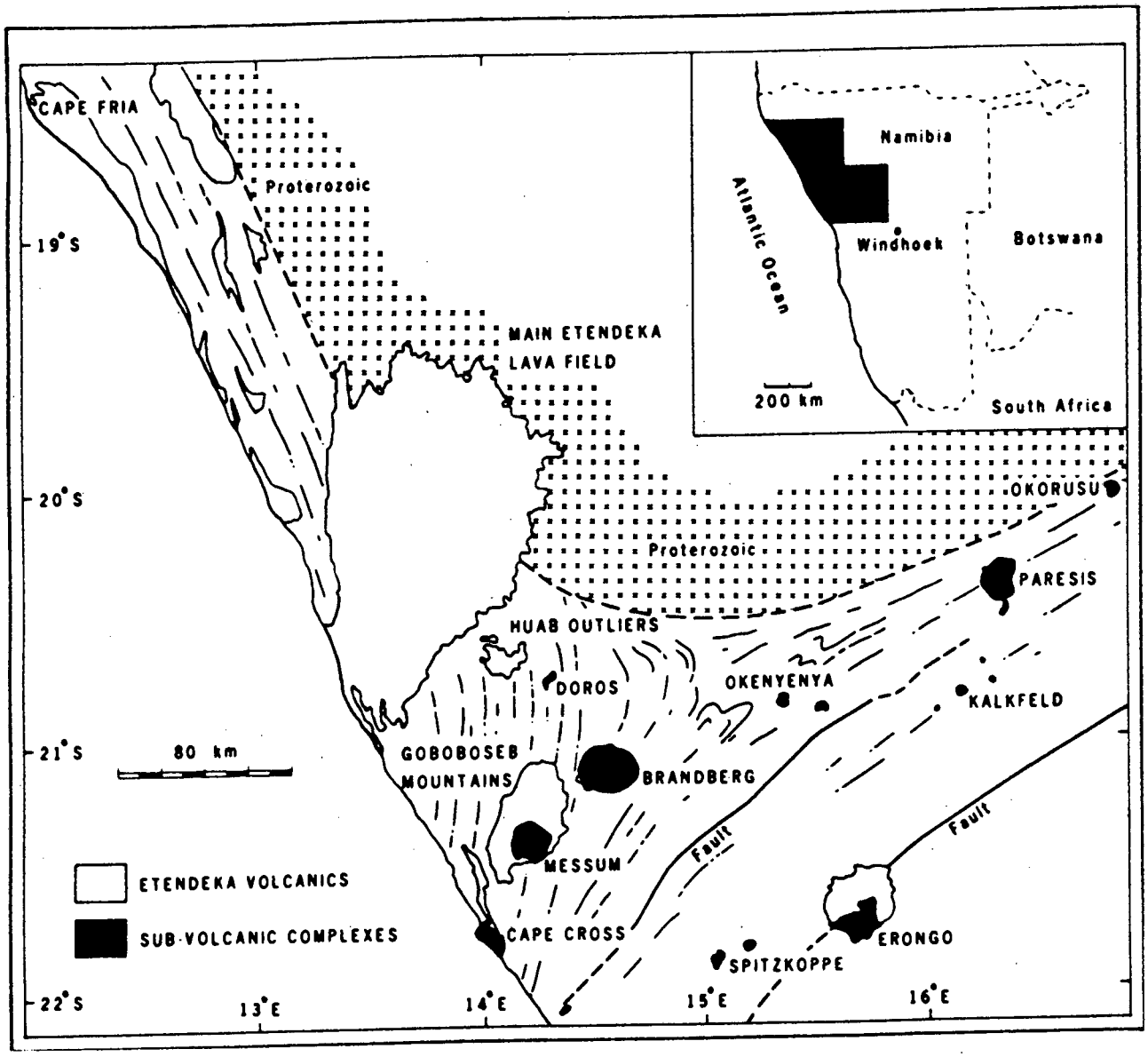

Fig. 1.1

Fig. 1.1 The distribution of the Damaraland sub-volcanic ring complexes in relation to the Etendeka volcanics. The complexes form a Cape Cross - Okorusu lineament which coincides with a structural discontinuity between the Pan-African terrain and the Proterozoic cratonic basement. (Reproduced from: Milner *et al.*, 1994)

Recent Rb-Sr and K-Ar mineral age determinations, which range from 128.6 ± 1.0 Ma to 123.4 ± 1.4 Ma (Milner *et al.*, 1994) and from 133.3 ± 1.4 Ma to 129.2 ± 0.7 Ma (Watkins *et al.*, 1994) respectively, suggest a minimum magmatic lifespan of 5 Ma for the complex.

1.3 Aims

The major aim of this dissertation is to use carbonate and silicate stable isotope data to 1) assess a crustal contamination model for the tholeiitic olivine gabbro - quartz monzodiorite suite, which seems to be required by the existing trace and radiogenic isotope data (le Roex *et al.*, 1995; Milner *et al.*, 1994), 2) examine the cooling history of the pluton in the light of mineral-pair isotope thermometry, and 3) assess the extent of subsolidus fluid-rock interactions.

Mineralogical alteration features are typically absent from gabbroic intrusions which have undergone high-temperature alteration. Oxygen isotope data for coexisting minerals in a suite of rocks might enable high-temperature hydrothermal activity to be recognised (e.g. Taylor, 1987), notwithstanding mineral-magma $^{18}O/^{16}O$ fractionation factor uncertainties. The initial $^{87}Sr/^{86}Sr$ ratio is changed by crustal contamination, but the concentration of Sr in the contaminant is generally not known and may vary by several orders of magnitude. In contrast, most minerals and silicate melts have similar oxygen contents (45 - 50 wt % O) (see Taylor & Sheppard (1986) for a discussion). It should also be noted, that because the oxygen concentration in the magma and assimilant are likely to be similar, the problem of "guessing" the isotope concentration in the assimilant (as in the case of Sr and Nd isotope systems) is no longer applicable. As a result, most recent studies suggest that possible source and crustal contamination models are best constrained by considering the covariation of oxygen and strontium isotope ratios (e.g. Taylor, 1980; James, 1981; Kalamarides, 1984).

The carbon and oxygen isotope composition of the carbonate phase present enable a consideration of: i) the primary or secondary nature of the carbonate present, ii) the source of carbon, iii) the fluid composition and iv) alteration equilibration temperatures. The silicate data may be used to constrain: i) the role of crustal contamination in the

petrogenesis of the complex, ii) the magma source characteristics, iii) the closure temperatures of minerals to isotopic diffusional exchange, and iv) the extent of subsolidus interaction with deuteric and external fluids.

Chapter 2 - Local Geological Setting -

2.1 Introduction

The Okenyenya intrusion is situated 90 km north west of Omaruru (lat.: 20° 50'S long.: 15° 20' E) and occurs as a "ring complex" with an areal extent of 20 km^2. The name "Okenyenya" as recommended by SACS (1980) is synonymous with "Okonjeje" as previously used by Korn & Martin (1939) and Simpson (1950, 1952, 1954). The complex intrudes the Karoo system which lies unconformably on the Damaran system rocks and varies in thickness from 150 - 200 m in the south to a maximum thickness of 600 m (Gevers, 1936). The marginal Karoo system sediments dip from 10° to 15° outwards from the complex and are traversed by a broad east-west zone of near vertical breccia filled fractures. The following summary of the geology of the Okenyenya complex is based largely on revised geological and structural interpretations by Watkins & le Roex (1995).

2.2 Rock types and field relations

Simpson (1952, 1954) recognised a tholeiitic and an alkaline evolutionary series. Watkins & le Roex (1995) subdivide the tholeiitic suite into an olivine gabbro - quartz monzodiorite suite, picritic gabbro, syenite and quartz syenite. The alkaline suite consists of alkaline gabbro, nepheline syenite, essexite, and lamprophyre. The rock type nomenclature used here follows that of Watkins & le Roex (1995). The rock types which have been analysed in this study are listed in Table 2.1 .

On the basis of mineral and bulk rock geochemistry, le Roex *et al.* (1995) identify three inner zone units and three outer zone units, within the tholeiitic olivine gabbro - quartz monzodiorite suite. In the eastern sector of the complex, the inner zone gabbroic units occurr as broken arcuate ridges adjacent to the topographically featureless outer zone of monzodiorite. The inner units are dark, massive, faintly laminated and widely varying in grain size.

The alkaline gabbro consists of a number of discrete intrusions, which are distinguishable by geochemical variations and the development of fine-scale modal layering

Table 2.1 Rock types analysed in this study.

Suite / Rock Type	*Sample number*
Tholeiitic olivine gabbro - quartz monzodiorite suite:	
Monzodiorite, quartz monzodiorite (unit 6)	OKJ-043, OKJ-045, OKJ-047
Monzodiorite, diorite (unit 5)	OKJ-041, OKJ-044, OKJ-046
Olivine gabbro, gabbro (unit 4)	OKJ-004, OKJ-038, OKJ-040
Olivine gabbro, leucogabbro (unit 3)	OKJ-031, OKJ-033
Gabbro, gabbronorite (unit 2)	OKJ-063
Olivine gabbro, leucogabbro (unit 1)	OKJ-062, OKJ-068
Other rock types analysed:	
Alkaline gabbro	OKJ-050, OKJ-069, OKJ-084, OKJ-176
Syenite	OKJ-150, OKJ-164
Nepheline syenite	OKJ-014
Oligoclase essexite	OKJ-088
Essexite dyke	OKJ-018

(le Roex et al., 1995). Discontinuous alkaline gabbro outcrops occur as a coarse-grained massive variety (in which a troctolitic, pyroxenitic and anorthositic facies are recognized), and as a medium grained variety which displays rhythmic banding. The oversaturated syenites occur as a major peripheral ring-dyke and as arcuate intrusive sheets (Watkins & le Roex, 1991). The tholeiitic gabbro forms the most common xenoliths, which occur as partially assimilated, reaction corona-bearing subangular fragments within all the major syenite intrusions (Watkins & le Roex, 1991). In the north, the peripheral ring-dyke is truncated by the Okenyenya Berg ring structure, which consists of three concentrically related and steeply outwardly inclined bodies of nepheline-syenite, andesine- and oligoclase-essexite (Simpson, 1954). Dark rounded xenoliths of andesine-essexite occur within the oligoclase-essexite.

In the south eastern sector of the complex, a series of WNW-ESE trending faults and late-stage lamprophyre dykes transect the tholeiitic and alkaline gabbros (Fig 2.1)

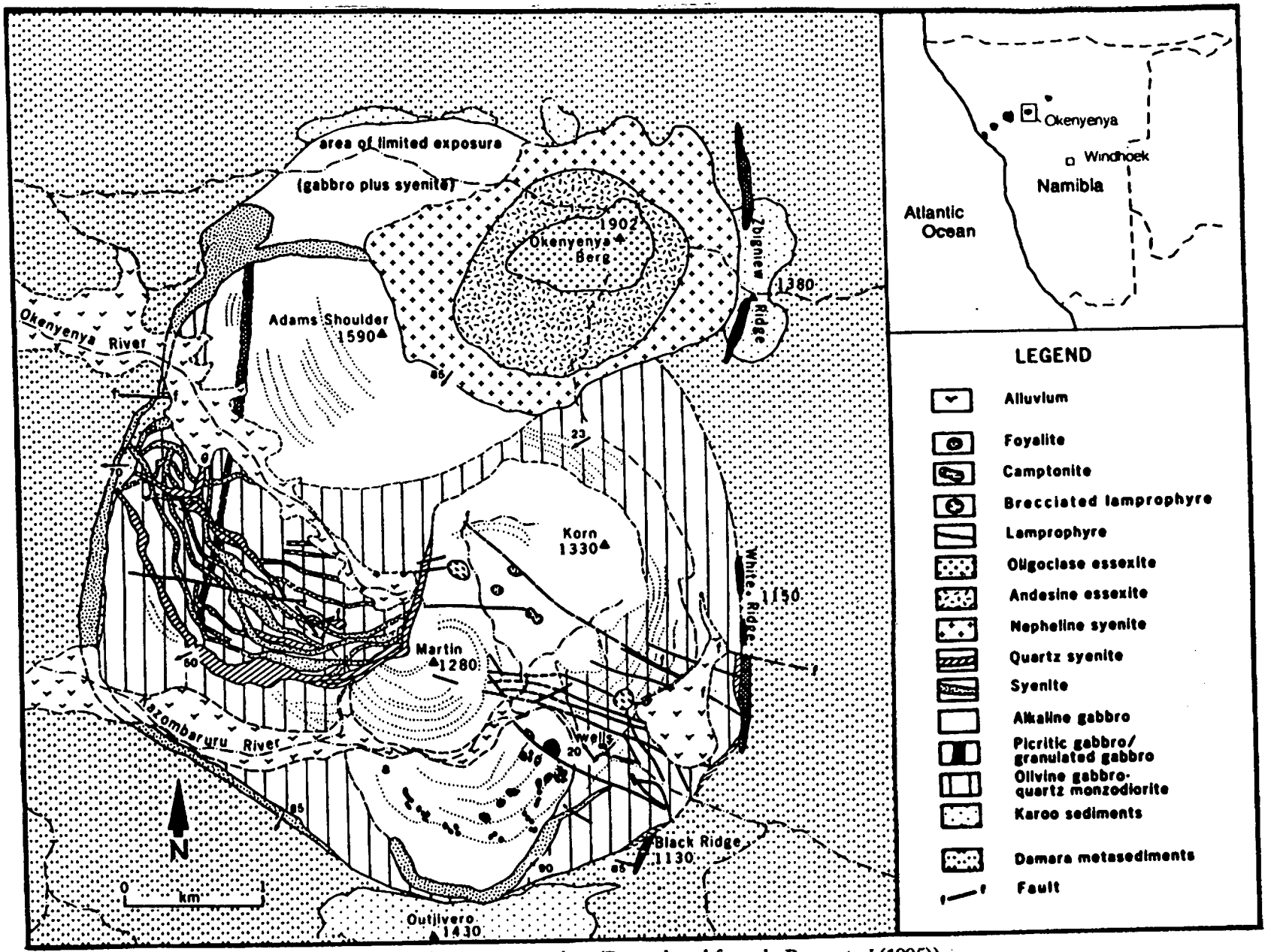

Fig. 2.1 Local intrusive and structural relations in the Okenyenya complex. (Reproduced from le Roex *et al.*(1995))

(Watkins & le Roex, 1995). A volcanic pipe and minor picritic gabbro and quartz syenite outcrops also occur in this area.

Within the picritic gabbro, quartz syenite / nepheline syenite veins are locally associated with serpentinized olivine, granulated pyroxene, sericitized plagioclase and biotite aggregates (Watkins & le Roex, 1991). Alteration of the gabbros, indicated by the presence of secondary hydrated minerals (zeolites), and the growth of biotite plates, have also been attributed to the infiltration of alkaline hydrothermal fluids associated with the intrusion of the lamprophyric magma (Watkins & le Roex, 1995). The field relations of other rock types not analysed in this study are discussed by le Roex *et al.* (1995).

2.3 Tholeiitic olivine gabbro - quartz monzodiorite suite

The tholeiitic olivine gabbro - quartz monzodiorite suite consists of an 800 m thick succession of inward dipping cone sheets and display an "inverted" chemical differentiation trend, in which there is a progression towards more evolved rock types outwards through the complex (Simpson, 1954; le Roex *et. al*; 1995). Within the tholeiitic gabbros, curvilinear features, typical of anorogenic ring complexes, are associated with a major peripheral ring fault (Fig. 2.1) (Watkins & le Roex, 1995).

The intrusion has a multiple sheeted nature and a "pseudostratification" similar to other major tholeiitic gabbroic intrusions which are stratiform and differentiated (Simpson, 1954; Watkins & le Roex, 1995). This is supported by the absence of country rock or alternative intrusive rocks within the gabbro, and the lack of marginal grain size variations (Watkins & le Roex, 1995). The stratification of the gabbro ridges show a consistent inward dip 15° to 30° (Simpson, 1954), and reach 45° where hinge faulting has occurred (Watkins & le Roex, 1995). The regular variation in the composition of the major minerals from the inner towards the outer units defines a cryptic layering similar to that observed for the Skaergaard intrusion (Wager and Deer, 1939), and supports a single intrusive phase for the tholeiitic gabbros (Simpson, 1954). Watkins & le Roex (1995) account for the inverted differentiation trend by an inward tilting of the cone sheets due to subsidence.

2.4 Summary

Watkins & le Roex (1991), Milner *et al.*(1993) and Watkins & le Roex (1995) interpret the Okenyenya intrusion to represent sub-volcanic remains of an early-Cretaceous composite volcano. Watkins & le Roex (1995) recognise six stages in the evolution of the complex, and note that it resembles that of oceanic volcanoes (such as Hawaii; Clague, 1987) in terms of the alternating tholeiitic and alkaline magmatic phases, and the final highly alkaline phase.

Chapter 3 - Petrography, Mineral Chemistry and Bulk Rock Composition -

3.1 Introduction

The discussion which follows focusses on the petrographic, mineral chemistry and bulk rock compositional features of the samples analysed for oxygen isotope ratios in this study, which are indicative of fluid-rock interaction and contamination. In addition, particular attention will be drawn to: (1) variations in the modal abundance along the transect through the tholeiitic olivine gabbro - quartz monzodiorite suite; (2) mineral morphology and textural characteristics; (3) mineral composition ranges, loss on ignition values and variations in the bulk rock chemistry; and (4) the petrogenetic implications of variations in the mineral and bulk rock compositions. The discussion concentrates on the tholeiitic suite, and is largely a summary synthesis of work by Simpson (1954), Watkins & le Roex (1991), Milner *et al.* (1993), and le Roex *et al.* (1995). The locations of samples collected by le Roex *et al.* (1995) along a transect through the tholeiitic olivine gabbro - quartz monzodiorite suite appear in Fig. 3.1 . Sample locations of the remaining rock types analysed may be located on Fig. 2.1 .

3.2 Petrography

Detailed petrographic descriptions, for the samples for which $\delta^{18}O$ values were produced, and the modal abundance and grain size data, appear in Appendix 1.

3.2.1 Tholeiitic suite

3.2.1(a) Tholeiitic olivine gabbro - quartz monzodiorite

The Outer Zone Units 5 - 6 of this suite tend to be characterized by more evolved rock types (monzodiorite, diorite and quartz monzodiorite) than the Inner Zone Units 1 - 3 (olivine gabbro, leucogabbro, gabbro, gabbronorite) (see Table 2.1, Chapter 2).

Modal abundance variations

The modal abundance trends for plagioclase (72 - 37 %) and clinopyroxene (37 - 5 %) are negatively correlated, in the sense that an increase in the one is followed by a corresponding decrease in the other (Fig. 3.2). Olivine follows an irregular variation and ranges from 19 % to trace amounts. The general decline in plagioclase, clinopyroxene

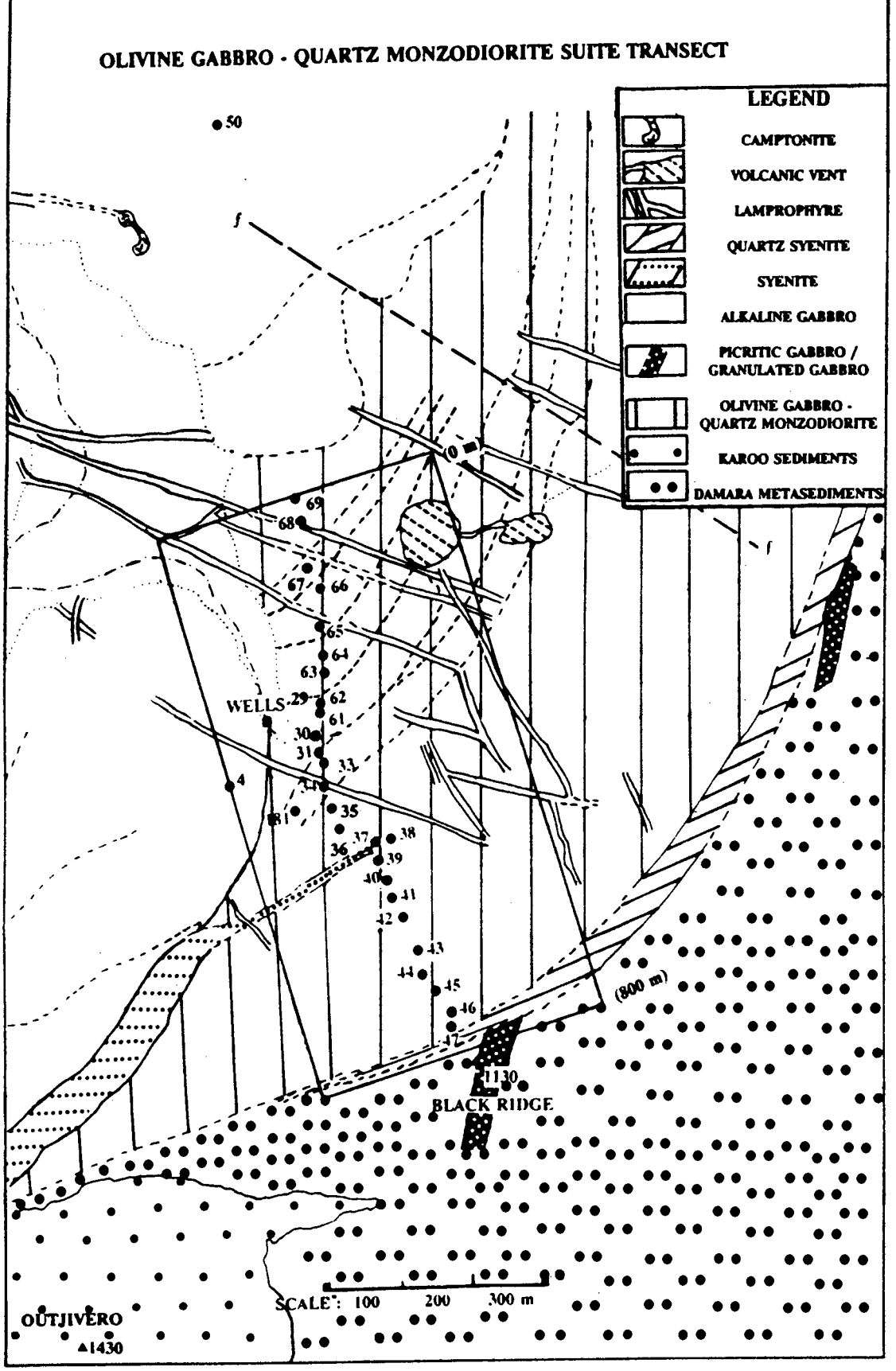

Fig. 3.1

Fig. 3.1 Sampling transect through the tholeiitic olivine gabbro - quartz monzodiorite suite. Samples for which $\delta^{18}O$ values have been determined in this study (and for which $^{87}Sr/^{86}Sr$ data are available) include: 4, 31, 33, 35, 36, 38, 40, 43, 44, 45, 46, 47, 50, 62, 63, 68 and 69. In addition, the locations of samples for which XRF data (29, 30, 34, 35, 36, 42, 65, 66, 67) and modal data (37, 39, 61, 64) are available are shown.

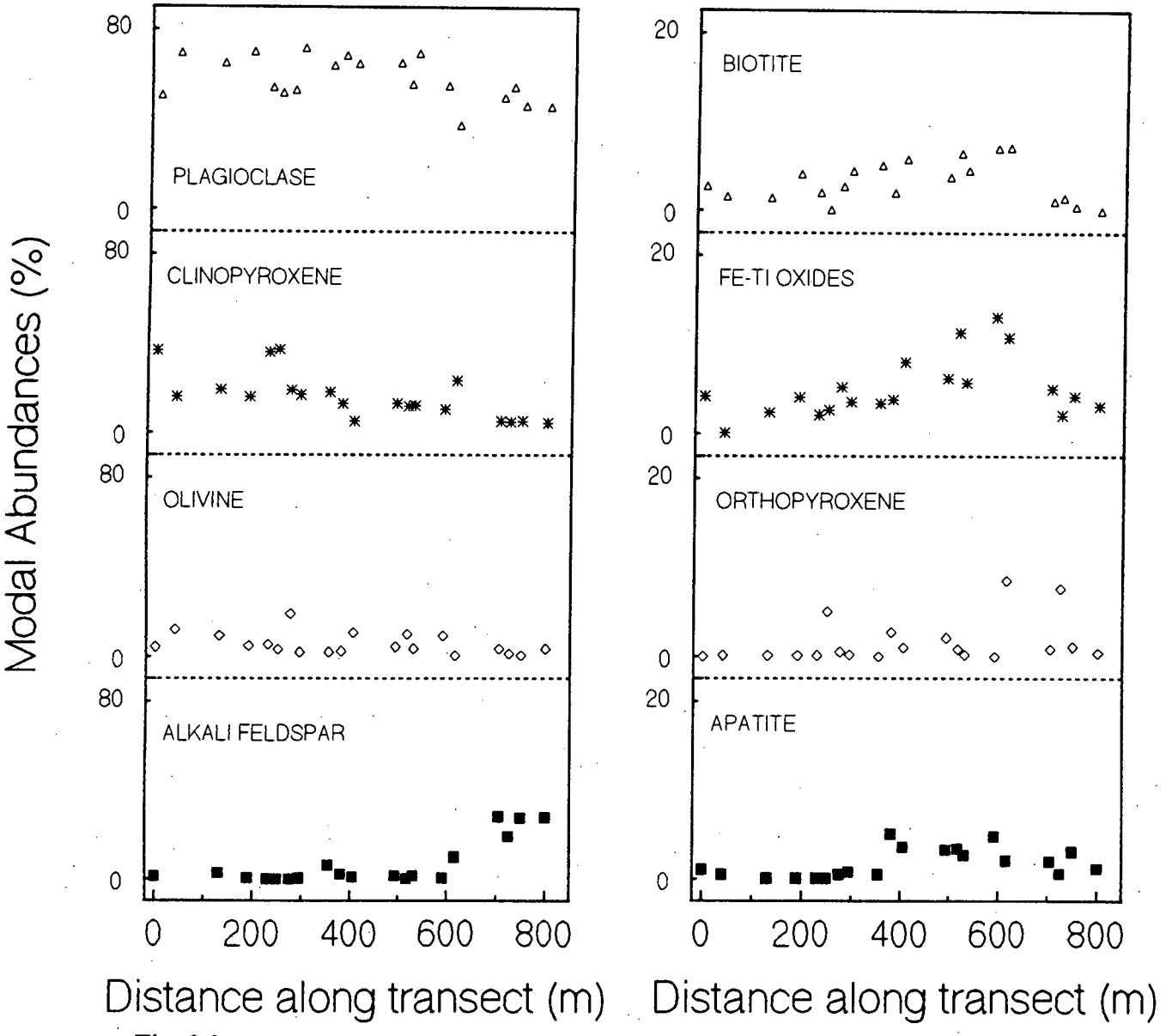

Fig. 3.2

Fig. 3.2 Modal abundance variations of minerals with respect to the sample distance along the transect through the tholeiitic olivine gabbro - quartz monzodiorite suite. Abbreviations used are as follows: plag: plagioclase, cpx: clinopyroxene, oliv: olivine, akfsp: alkali feldspar, biot: biotite, opx: orthopyroxene, apa: apatite, oxid: Fe-Ti oxides. The distances along the transect of samples for which oxygen isotope data were obtained are listed in Table 5.1. Heights for samples not listed therein are as follows: OKJ-034: 405 m, OKJ-037: 493 m, OKJ-039: 516 m, OKJ-061: 295 m, OKJ-064: 230 m, OKJ-065: 190 m and OKJ-066: 130 m.

and olivine towards the outer units is compensated for by an increase in the alkali feldspar from trace amounts to 30 %. The modal abundances of the Fe-Ti oxides (13 % - trace), biotite (7 % - trace) and apatite (5 % - trace), increase outwards towards the contact between Units 4 and 5 (Fig. 3.2). The orthopyroxene is restricted mainly to Unit 5, where it occurs at greater than 7 % within the monzodiorite (OKJ-041, OKJ-044 and OKJ-046). Not shown in Fig. 3.2, are the trends for quartz (2 - 8 %), alteration minerals (chlorite and sericite) (trace) and amphibole (3 %), which are restricted to the outermost Unit 6.

Mineral morphology and textural characteristics

Feldspar

Clouded plagioclase is present in the olivine-leucogabbro (OKJ-068); (Fig. 3.3), gabbro (OKJ-063); (Fig. 3.4), and leucogabbro (OKJ-033), and absent from the subophitic olivine gabbro (OKJ-031, -038, -040, -062); (Fig. 3.5) and monzodiorite (OKJ-041, -044, -046); (Fig. 3.6). Within the monzodiorite (OKJ-043, -044, -045); (Fig. 3.7) and gabbro, plagioclase displays sericitization. Plagioclase in the Inner Zone units (1 - 2) is characterized by biotite inclusions (OKJ-063), and Fe-Ti oxide mantles (OKJ-062). In the Outer Zone units (4 - 6), plagioclase forms corroded laths and is poikilitically enclosed by large sericitized oikocrysts of alkali feldspar (Fig. 3.7 and Fig. 3.8). Myrmekitic intergrowths of quartz and plagioclase occur and the alkali feldspar exhibits plagioclase exsolution lamellae. Alkali feldspar also occurs as a late interstitial phase in the olivine gabbro (OKJ-038, -040), leucogabbro (OKJ-033) and monzodiorites (OKJ-043, -044, -045). Within the quartz monzodiorite (OKJ-047), calcite occurs as patches within the plagioclase. This suggests that the replacement of plagioclase by accessory calcite (Fig. 3.8) occurred.

Clinopyroxene

Clinopyroxene in the Inner Zone units (1 - 3) (OKJ-033, -062, -063, -068), occurrs as large ophitic crystals, which show well developed schiller structures. In the Outer Zone, altered clinopyroxene phenocrysts are mantled by green hornblende (OKJ-043, -044, -045, -047). Clinopyroxene oikocrysts occur within the leucogabbro (OKJ-033), monzodiorite (OKJ-041 - OKJ-045) and olivine leucogabbro (OKJ-068) (Fig. 3.4).

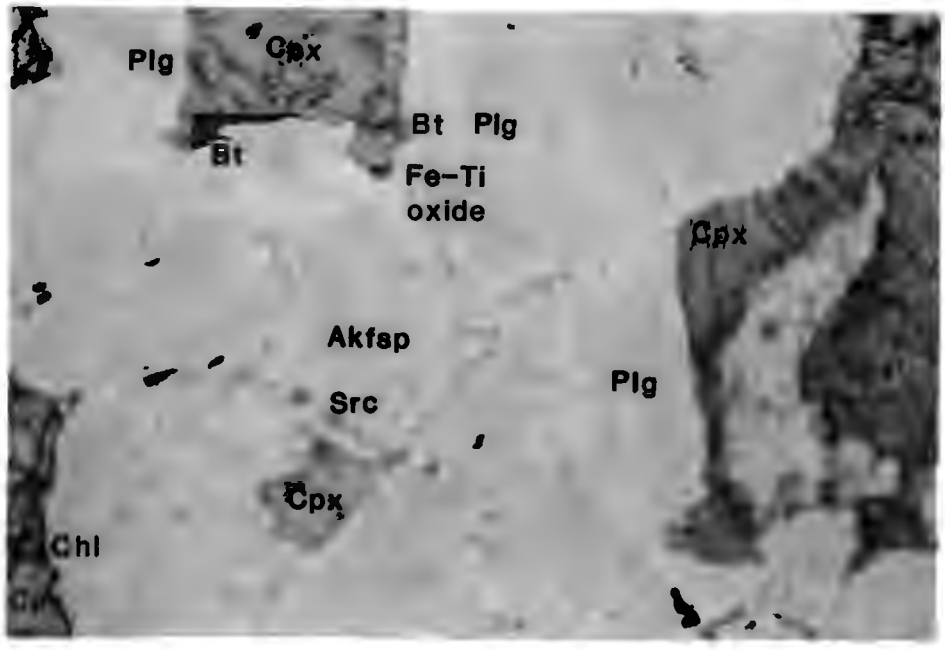

Fig. 3.3 Clouded plagioclase (Plg) (modal abundance: 69.2 %)in olivine-leucogabbro (OKJ-068) from Unit 1. Alkali feldspar (Akfsp) is also present, and trace amounts of Fe-Ti oxides and biotite (Bt) occur as inclusions within the clinopyroxene (Cpx). Anhedral fractured clinopyroxene (16.1 %) grains are also rimmed by chlorite (Chl) and Fe-Ti oxides.

Field of View: 2 mm (Plane polarised light)

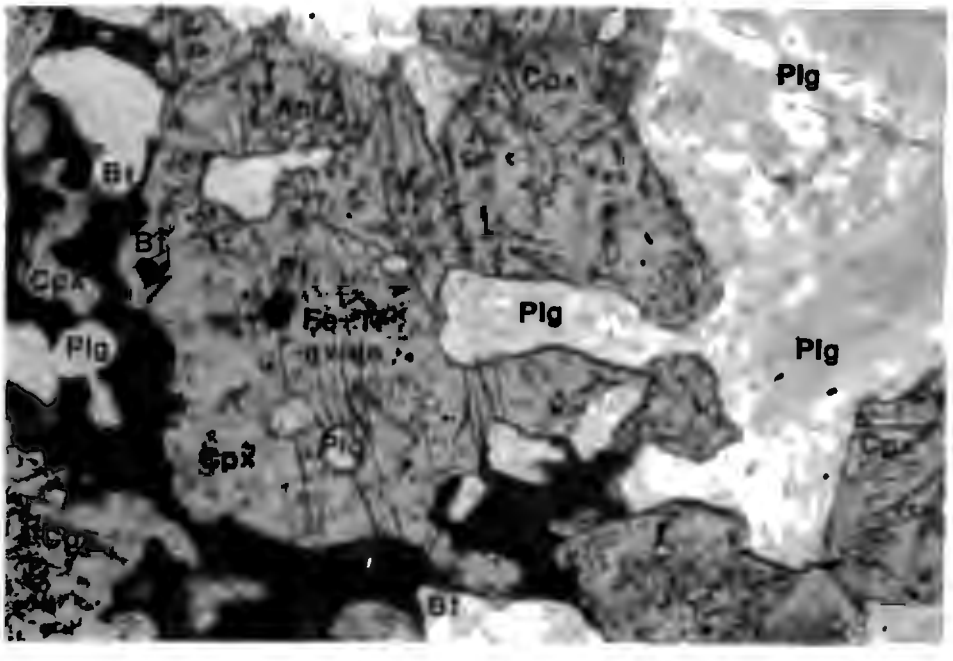

Fig. 3.4 Subophitic clinopyroxene (Cpx) oikocryst within gabbro (OKJ-063) from Unit 2. The oikocryst bears inclusions of plagioclase (Plg), Fe-Ti oxide and apatite (Apt), and is rimmed by biotite (Bt). The clinopyroxene occurs with a coarser grain size, than within the olivine-leucogabbro (OKJ-068).

Field of View: 2 mm (Plane polarised light)

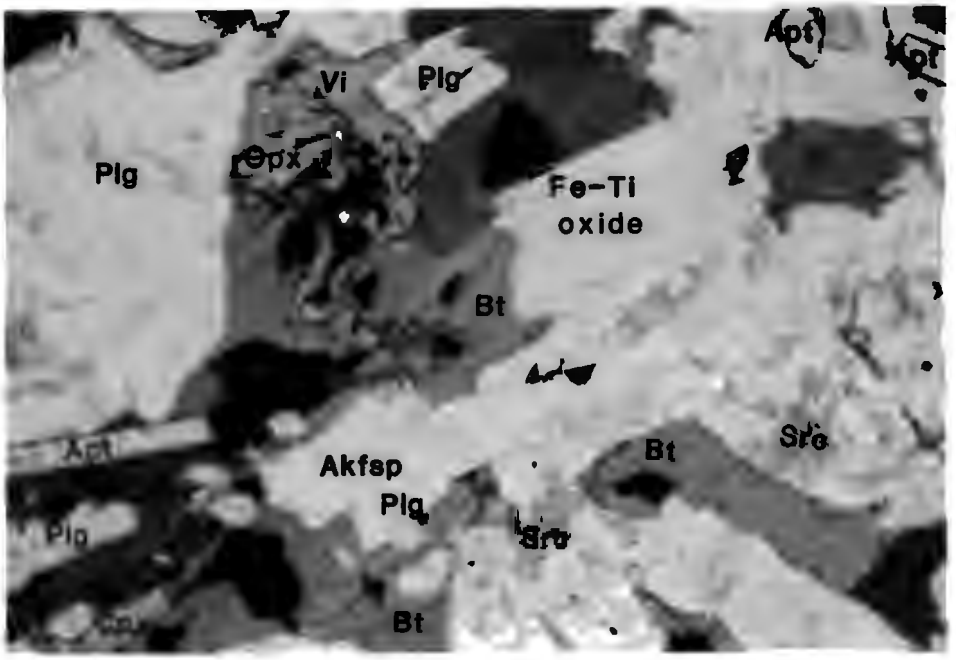

Fig. 3.5 Unclouded plagioclase (Plg) (modal abundance: 54.7 %) within subophitic olivine gabbro (Unit 4) (OKJ-040). Large biotite (Bt) (7 %) flakes are associated with Fe-Ti oxides, which have a higher modal abundance (13.1 %) than observed for rock types from the inner units. The Fe-Ti oxide is also intergrown with orthopyroxene (Opx). Alkali feldspar (Akfsp) (< 1 %) occurs as a late interstitial phase and encloses plagioclase (54.7 %). Apatite (Apt) (4.8 %) is present as an accessory primary phase and forms euhedral prisms.

Field of View: 2 mm (Plane polarised light)

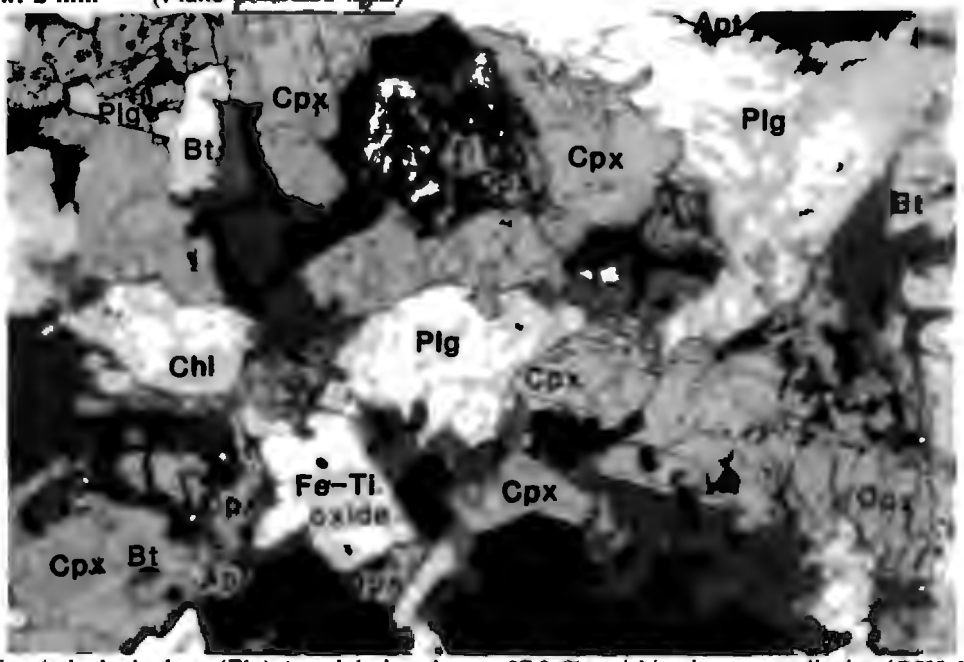

Fig. 3.6 Unclouded plagioclase (Plg) (modal abundance: 37.2 %) within the monzodiorite (OKJ-041) from Unit 5. The orthopyroxene (Opx) (8.5 %) and Fe-Ti oxide minerals (10.8%) have higher modal abundances than in rocks from the inner units, and form vermicular intergrowths (Vi) which replace olivine (< 1% and not visible here). Large biotite (Bt) (7.1 %) flakes are associated with the Fe-Ti oxides, and are less replaced by chlorite (Chl) and opaques than within the monzodiorite (OKJ-045) from Unit 6 (Fig. 3.7). Clinopyroxene (Cpx) (23.2 %) forms subhedral to anhedral oikocrysts and is associated with biotite, Fe-Ti oxides and apatite (Apt) (2.1 %).

Field of view: 2 mm (Plane polarised light)

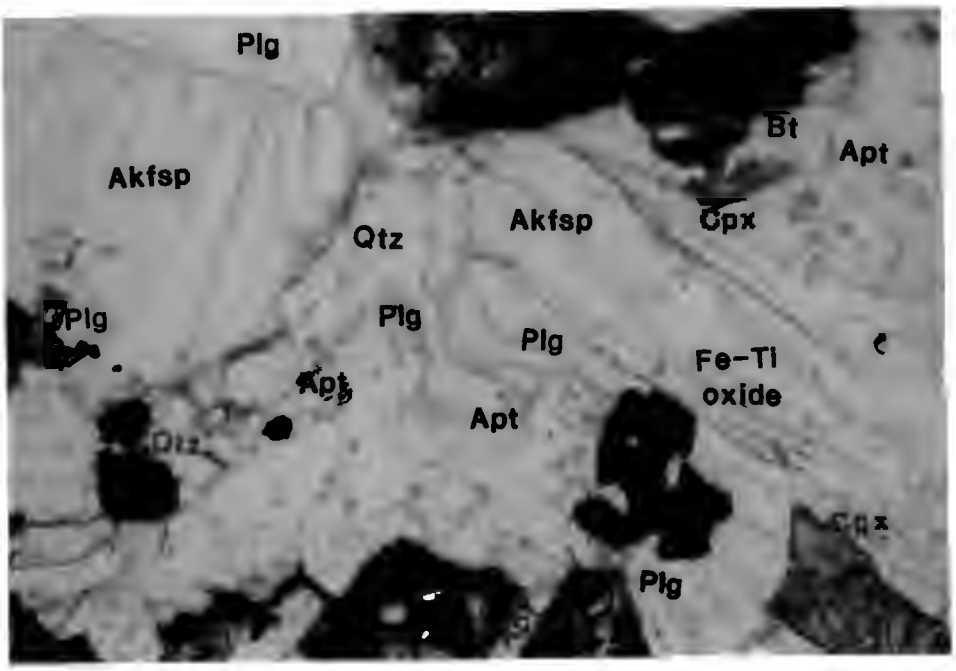

Fig. 3.7 Partially sericitized (Src) alkali feldspar (Akfsp) (modal abundance: 27.6 %) oikocrysts within monzodiorite (OKJ-045) from Unit 6. The alkali feldspar occurs as a late interstitial phase, and is developed as oikocrysts which enclose inclusions of plagioclase (Plg), apatite (Apt), clinopyroxene (Cpx), and olivine (not visible). The plagioclase (46 %) is also sericitized (Src). Anhedral clinopyroxene (5.2 %) grains are altered along fractures and cleavages. Quartz (Qtz) is also present.

Field of View: 2 mm (Plane polarised light)

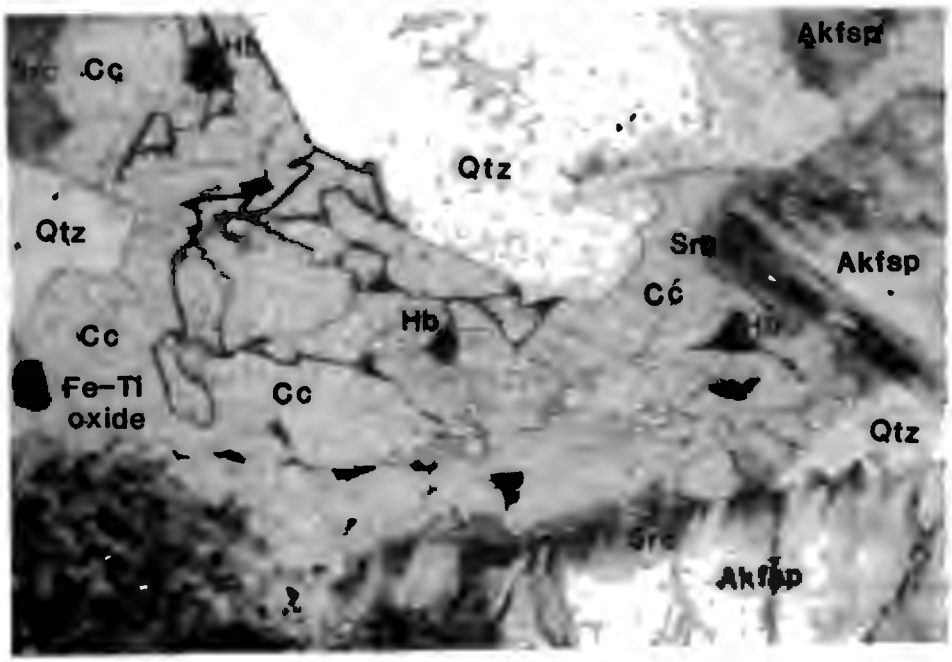

Fig. 3.8 Coarse grained accessory calcite (Cc) within the monzodiorite (OKJ-047) from Unit 6. The occurence of calcite within plagioclase elsewhere in this slide, suggests the replacement of plagioclase by calcite. Hornblende (Hb) (2.4 %) occurs around clinopyroxene (Cpx) (4.4 %) and along calcite grain boundaries. Large sericitized alkali feldspar (Akfsp) (27.8 %) oikocrysts enclose plagioclase, clinopyroxene and apatite (Apt) (1.2 %) inclusions.

Field of View: 2 mm (Plane polarised light)

Biotite

The biotite occurs as late stage laths (1 - 2 mm in length) with euhedral apatite inclusions in leucogabbros (eg. OKJ-033). Biotite in the monzodiorite (OKJ-041) is larger (< 5 mm) and less replaced by chlorite and opaques in OKJ-043, -044, -045 (Fig. 3.7). In the off-transect sample OKJ-004, biotite occurs as 1 mm laths and as mantles to Fe-Ti oxides.

Olivine

Olivine within the gabbro (OKJ-063) is altered. Vermicular intergrowths with orthopyroxene and iron ore occur in the gabbro (OKJ-063) and olivine gabbro (OKJ-062). The olivine gabbros (OKJ-031, 038, -062) also display olivine oikocrysts, which contain inclusions of plagioclase, biotite and Fe-Ti oxides.

Other minerals

Amphibole occurs in Unit 6 (OKJ-047) as mantles of late-stage green-brown hornblende around clinopyroxene, biotite and secondary calcite (see Chapter 4) (Fig. 3.8).

The Fe-Ti oxides are more abundant in Units 4 and 5 (average modal abundance 11.3%) (Fig. 3.5 and Fig. 3.6) than within the remaining units (1 - 3 & 6), and occur as primary ilmenite and as a late stage phase within the olivine gabbros (OKJ-038, -040). Titano-magnetite and pyrrhotite occur within the leucogabbro (OKJ-033) and olivine leucogabbro (OKJ-068), respectively. Quartz occurs as an interstitial phase within Unit 6 (OKJ-043 - OKJ-045, OKJ-047); (Fig. 3.8). Apatite in the leucogabbro (OKJ-033), monzodiorite (OKJ-041 - OKJ-045) and olivine gabbro (OKJ-040, -038) occurs as primary euhedral prisms and as larger anhedral grains which are interstitial to clinopyroxene (Figs. 3.5 - 3.7). Orthopyroxenes within the monzodiorite (OKJ-041 - OKJ-045), contain apatite and plagioclase inclusions, and are partially replaced by chlorite and white mica. The orthopyroxene also occurs as narrow reaction rims around olivine, and forms vermicular intergrowths with titano-magnetite which replaces olivine.

3.2.1(b) Other rock types

Two samples of syenite have been analysed in this study. Sample OKJ-150 is from a syenite sheet in the western area of the complex, whereas sample OKJ-164 is from the

peripheral ring dyke (see Fig. 2.1). In sample OKJ-164 irregular crystal boundaries of the alkali feldspar display symplectic intergrowths and exsolution lamellae occur in the orthoclase microperthite.

The alkaline gabbro samples selected for analysis in this study represent the four groups recognized by le Roex *et al.*(1995) on the basis of modal and geochemical variations: Korn (OKJ-050), Martin summit (OKJ-069), Adams Shoulder (OKJ-084) and Martin flank (OKJ-176) (Fig. 2.1). These gabbros consist predominantly of unaltered plagioclase, clinopyroxene, olivine and Fe-Ti oxides. The plagioclase and clinopyroxene show clouding and schiller structures, respectively.

The oligoclase essexite (OKJ-088) is a medium grained (1 - 2 mm) rock, 70 % of which consists of plagioclase, orthoclase and nepheline. Biotite occurs as an accessory phase and is mantled by kaersutitic amphibole. The essexite dyke (OKJ-018) has a trachytoidal texture, and is characterized by large tabular perthitic orthoclase phenocrysts in a groundmass of alkali feldspar and albite laths (Fig. 3.9). Aegirine-augite forms allotriomorphic crystals and enclose titano-augite cores. Ferrohastingsite forms irregular poikilitic crystals and accessory calcite occurs as isolated primary carbonate grains (Fig. 3.9) (see Chapter 4). Other minerals present in both essexite samples include Fe-Ti oxides, sphene, apatite, and fluorite.

Alkali feldspar within in the nepheline syenite (OKJ-014) is variably altered and forms coarse perthitic intergrowths with plagioclase. Biotite occurs as thin coronas on Fe-Ti oxides and as larger crystals, which together with clinopyroxene, is mantled by amphibole.

3.3 Mineral chemistry and bulk rock compositions

The mineral and bulk rock composition ranges characterizing the six units which comprise the tholeiitic olivine gabbro - quartz monzodiorite suite, and other rock types analysed in this study, are discussed by le Roex *et al.* (1995). The discussion which follows aims to provide a background of the mineral and bulk compositional variations, for the subsequent Chapters 6 and 7, in which the relative importance of contamination and minor alteration processes are evaluated.

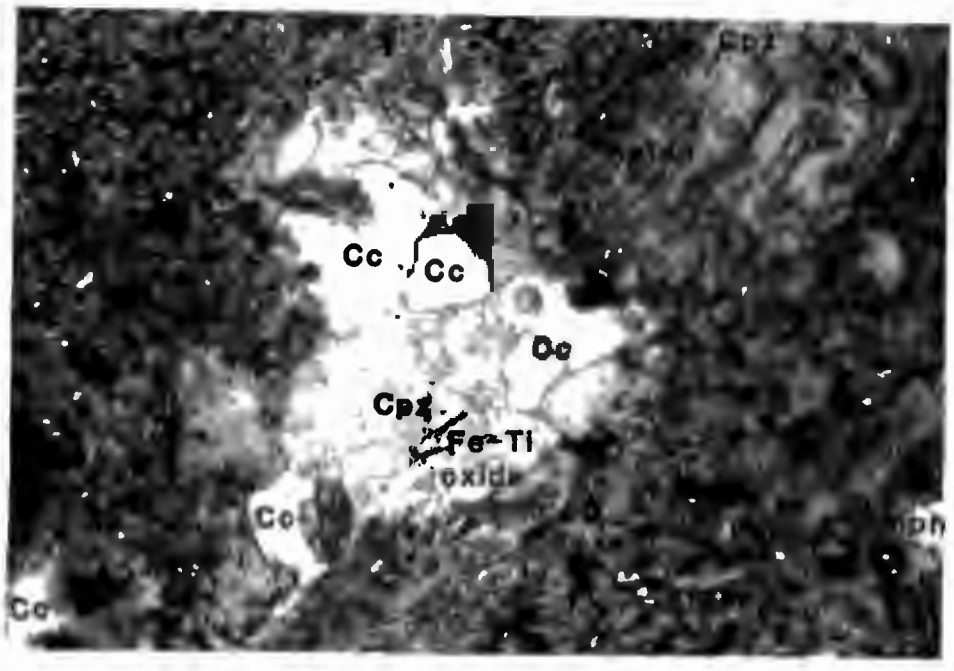

Fig. 3.9 Isolated grains of accessory calcite (Cc) within the essexite dyke (OKJ-018). Altered alkali feldspar (Akfsp) (12.1 %) phenocrysts (5 mm) occur in a groundmass which displays a trachytoidal texture. Clinopyroxene (Cpx), Fe-Ti oxides and amphibole (Amph) are also present.

Field of View: 2 mm (Plane polarised light)

3.3.1 Tholeiitic suite

3.3.1(a) Tholeiitic olivine gabbro - quartz monzodiorite

The range in the plagioclase mineral composition increases progressively from the inner (An_{52} - An_{67}), towards the outer (An_{33} - An_{54}) units (le Roex *et al.*, 1995). Units 1, 2 and 3 have similar most primitive (ie. Mg-rich) olivine (Fo_{63}), clinopyroxene ($Wo_{44}En_{43}Fs_{13}$) and plagioclase (An_{64}) (ie. Ca-rich) mineral compositions. In contrast, the most evolved Unit 3 composition is equivalent to the most primitive Unit 4 composition (Fo_{50}; An_{53}; $Wo_{42}En_{38}Fs_{20}$). The outward increase in the mineral compositional ranges, and the restriction of the most primitive mineral compositions to the inner units, are consistent with an increasing degree of magmatic differentiation and/or contamination by felsic crustal material towards the outer units.

The loss on ignition (L.O.I.) values (le Roex *et al.*, 1995), increase slightly from the inner to the outer units (see Table 3.1). The outer units are characterized by lower MgO, CaO and Al_2O_3 abundances than the inner units, whereas the SiO_2, K_2O, P_2O_5, TiO_2 and FeO abundances increase from the inner to the outer units (Table 3.1). The incompatible elements Rb, Zr, Nb, Zn, Ba and Y increase, whereas the compatible elements Ni, Cr, Co and Cu decrease towards the outer units (Table 3.1).

The low L.O.I. values indicate that the rocks in the tholeiitic olivine gabbro - quartz monzodiorite suite are relatively fresh, and that the outer units are only slightly altered relative to the inner units. The variations in the the MgO, CaO and Al_2O_3 concentrations are consistent with an increasing degree of magmatic differentiation, from the olivine gabbro to quartz monzodiorite, and variable degrees of plagioclase accumulation. The increase in SiO_2 in the outer units suggests that they crystallized from more evolved magmas. The higher P_2O_5, TiO_2, FeO, Zn and Y abundances are attributable to the crystallization of apatite and Fe-Ti-Zn oxides. The higher SiO_2, K_2O, and incompatible element (Rb) abundances, and lower MgO and compatible element (Cr, Ni, Co) abundances in the outer units, are consistent with a greater degree of contamination of the outer units relative to the inner units, but may also be attributed to crystal fractionation.

Table 3.1 Ranges in the abundances of selected major (wt %) and trace (ppm) elements in the inner and outer units of the tholeiitic olivine gabbro - quartz monzodiorite suite. These ranges have been determined only for samples analysed for oxygen in this study. (See Table 1.2 in Appendix 1 for the raw data obtained from le Roex *et al.* (1995).)

Oxides / Trace elements	Inner units	Outer units
SiO_2	46.6 - 48.2 %	44.0 - 55.0 %
TiO_2	0.8 - 2.1 %	2.0 - 3.8 %
Al_2O_3	15.1 - 19.0 %	14.2 - 16.7 %
FeO	6.6 - 10.3 %	9.0 - 13.7 %
MgO	4.2 - 8.5 %	2.2 - 5.2 %
CaO	10.9 - 14.3 %	5.9 - 9.2 %
K_2O	0.3 - 1.1 %	0.9 - 3.1 %
P_2O_5	0.1 - 0.9 %	0.3 - 1.9 %
L.O.I.	0.9 - 1.2 %	1.0 - 2.3 %
Zr	37 - 70 ppm	46 - 206 ppm
Nb	5.4 - 16.4 ppm	18 - 46 ppm
Y	12 - 22 ppm	26 - 53 ppm
Rb	12.1 - 22 ppm	19.7 - 94 ppm
Ba	331 - 619 ppm	650 - 1525 ppm
Co	26 - 56 ppm	10 - 45 ppm
Cr	9.7 - 239 ppm	2 - 19 ppm
Ni	25 - 130 ppm	4 - 12 ppm
Zn	46 - 70 ppm	118 - 154 ppm
Cu	39 - 280 ppm	9 - 20 ppm

Thus the observed bulk compositional variations result from the combined effects of magmatic differentiation, plagioclase accumulation, crystallization and contamination (see Section 6.1). The relative importance of these mechanisms cannot be resolved on the basis of major and trace element data alone. The applicability of a fractional

crystallization - assimilation model will be considered in the light of stable and radiogenic isotope data in Chapter 6.

3.3.1(b) Other rock types

The low L.O.I. value (0.9 %) of the off-transect sample OKJ-004, indicates that it is relatively fresh. The lower Al_2O_3, P_2O_5, incompatible element (Rb, Nb, Ba) and higher MgO and compatible element (Co, Cr, Ni) abundances (Table 1.2, Appendix 1), indicate that it is the least differentiated and/or least contaminated tholeiitic gabbro sample. It should be noted, however, that OKJ-004 more closely resembles the alkaline gabbro OKJ-050 in terms of the oxygen and strontium isotope (see Table 5.1) data, and that the classification of this sample in terms of the alkaline or tholeiitic suites is still in question (le Roex. pers. comm., 1995).

The higher SiO_2 (65.2 %) concentration and lower L.O.I. value (0.9%) of OKJ-164, indicate that it represents a more evolved and less altered sample than the syenite sample OKJ-150 (61 % and 1.8 % respectively). Both samples have significantly high Ba concentrations (1538 - 1363 ppm). The higher SiO_2, K_2O, and incompatible element (Zr, Rb) concentrations, and lower MgO and compatible element (Co, Ni, Cu) concentrations (Table 1.2), are consistent with the more differentiated and/or contaminated nature of these samples relative to the tholeiitic gabbros.

The Martin flank gabbro (eg. OKJ-176) is characterized by mineral compositions which are more evolved than the Martin summit (eg. OKJ-069) and Korn (eg. OKJ-050) gabbros. The Adams Shoulder gabbro (eg. OKJ-084) displays the most evolved mineral compositions. The L.O.I. values allow the analyzed samples to be arranged in an increasing order towards a moderate degree of alteration: OKJ-176 (0.7 %), OKJ-069 (1.0 %), OKJ-084 (1.1 %) and OKJ-050 (2.1 %). The high Sr (773 ppm) concentration in OKJ-050 may also be attributed to a greater degree of alteration as suggested by the L.O.I. value. A comparison of the major (SiO_2, K_2O, TiO_2, FeO) and incompatible (Ba, Nb, Y, Zr, Rb) element abundances is consistent with the following sample arrangement towards the most evolved composition: OKJ-050, OKJ-069, OKJ-176/OKJ-84.

The high L.O.I. value (2.9 %) of the oligoclase essexite sample OKJ-088 indicates that it is highly altered. The essexite dyke sample OKJ-018 has the highest L.O.I. (3.18 %) value and a high Sr (669 ppm) concentration, which indicate that this is the most altered sample analysed for oxygen. The high L.O.I. value is attributable to trace amounts of calcite and pholgopite, which are visible in thin-section. The higher incompatible element (Zr, Nb and Rb) abudances of both essexite samples (Table 1.2), relative to the tholeiitic gabbros, may be attributed to the more differentiated and/or contaminated nature of these samples.

A moderate degree of alteration is indicated for the nepheline syenite (OKJ-014) by an L.O.I. value of 1.7 % (le Roex *et al.*, 1995). This sample is characterized by the highest Ba (2686 ppm), Nb (120 ppm), Na_2O (6.9 %) and K_2O (5.6 %), and the lowest Co (4.6 ppm), Cr (1.7 ppm), Ni (1.9 ppm) and FeO (3.1%) abundances, of all the samples analysed for oxygen. It also has high SiO_2 (59.0 %), Rb (145 ppm) and Zr (255 ppm) concentrations. These abundances indicate that it is the most differentiated and potentially the most contaminated sample analysed for oxygen isotopes.

3.4 Petrogenetic implications

3.4(a) Tholeiitic olivine gabbro-quartz monzodiorite suite

Bulk rock geochemical trends observed for the six units comprising the Inner and Outer Zones of the suite have led to a model involving multiple cone-sheet intrusions, caldera collapse and magma chamber crystallization processes (le Roex *et al.*, 1995). The compositional differences between the Inner and Outer Zone units (Table 2.1) is accountable for by the combined effects of magmatic differentiation, contamination by felsic crust, the tapping of a different primary magma and in-situ crystallisation processes. Elevated P, Ti, Y and REE abundances in Unit 4 are accounted for by the enhanced crystallisation of apatite and Fe-Ti oxides. The derivation from a geochemically enriched mantle source region is indicated by low Zr / Nb, Y / Nb ratios and high La / Sm ratios. Incompatible element ratios are distinctly different from the alkaline gabbro magmas indicating a distinct mantle source region. Ba / Nb ratios are unusually high (56) and attributable to crustal contamination or late stage fluid movement.

3.3.4(b) Other rock types

The petrogenetic implications for other rock types analysed in this study are discussed by le Roex *et. al.* (1995) and are only considered in brief here. le Roex *et al.* (1995) suggest that the syenites, which show evidence for crustal contamination processes, may be genetically related to the outer units (4 to 6) of the tholeiitic gabbros. The alkaline gabbros may have undergone lower degrees of partial melting, or were derived from a less depleted mantle source region than the tholeiitic gabbros, and were subjected to magma chamber crystallization processes. The nepheline syenite and essexite formed by extensive differentiation of the alkaline gabbros and a primitive basanitic magma respectively.

3.5 Summary

Petrographic features indicative of minor hydrothermal alteration (Norton, 1984; Taylor, 1987) within this suite include: 1) clouded plagioclases, 2) clinopyroxene schillerization, 3) the presence of secondary biotite, Fe-Ti oxides and amphibole, and 4) quartz - plagioclase myrmekitic intergrowths. The myrmekitic intergrowths may also be attributed to a magmatic process such as magma mixing. Plagioclase clouding and pyroxene schillerization decrease, whereas sericitization, chloritization and the abundances of orthoclase, quartz and Fe-Ti oxides increase from the inner to the outer margins of the group. The clouding of the plagioclase and schillerization of the clinopyroxene from the inner units, may be ascribed to the intrusion of the alkaline gabbro.

The increased concentration of NW - SE trending lamprophyre dykes and ring fracture-related faulting, indicates that the transect lies in a region which could, potentially, have interacted with a late stage fluid related to the lamprophyre intrusion. The local geology (Fig. 3.1) suggests that the tholeiitic gabbros may also have been subjected to metasomatic effects related to the intrusion of the alkaline gabbro, quartz syenite, syenite, picritic / granulated gabbro, and a recent volcanic pipe.

Chapter 4 - The $\delta^{18}O$ and $\delta^{13}C$ values of Carbonates in the Okenyenya Complex -

4.1 Introduction

The replacement of plagioclase by calcite and its occurrence as a fine-grained disseminated trace mineral suggests a secondary origin for the carbonate within the syenite (OKJ-050), alkaline gabbro (OKJ-084 & OKJ-150) and quartz monzodiorite (OKJ-047) (Fig. 3.8). The isolated occurrence of carbonate grains within the essexite dyke (OKJ-018) is consistent with either a secondary or primary origin (Fig. 3.9). The $\delta^{13}C$ and $\delta^{18}O$ values of the carbonate material have been determined with the following aims in mind: (1) to distinguish the primary or secondary nature of the carbonate, 2) to determine a possible temperature range for calcite in equilibrium with fluids of various $\delta^{18}O$ values, and (3) to characterize the composition and source of the fluid.

4.2 Results

The calcite CO_2-extraction technique used is discussed in Appendix 2. The oxygen and carbon isotopes were obtained for samples of alkaline gabbro, syenite, monzodiorite and the essexite dyke. The $\delta^{18}O$ and $\delta^{13}C$ values of the data reported in Table 4.1, are precise to ± 0.2 ‰ and ± 0.1 ‰ respectively. The $\delta^{18}O$ values range from + 12.2 ‰ to + 19.3 ‰, and the $\delta^{13}C$ values from - 4.4 ‰ to - 3.7 ‰. The systematic variation of the carbon and/or oxygen isotope composition of a rock with the L.O.I. value, would imply that the isotope composition was dominantly determined by the composition of the of the altering fluid. This is clearly not the case for the $\delta^{13}C$ data (Fig. 4.1a). However, the negative trend in Fig. 4.1b indicates that it may be true for the $\delta^{18}O$ bulk carbonate data. It should also be noted, that a plot of the plagioclase $\delta^{18}O$ value with respect to the L.O.I. value suggests a strong negative correlation (R = - 0.99) (Fig. 4.1c).

The essexite dyke sample exhibits the highest L.O.I. (3.2 %) and lowest $\delta^{18}O$ (12.2 ‰) values (Table 4.1). The former suggests that the essexite dyke is the most altered sample, whereas the latter implies the highest temperature of formation of all the calcites analysed. The essexite dyke is therefore the rock type sampled, which most probably records the maxiumum temperature of a fluid that equilibrated with the bulk

Table 4.1 Carbonate stable isotope data. The corresponding L.O.I. values (wt %), the Ba (ppm), Sr (ppm) and Ca (wt %) concentrations (le Roex *et al.*, 1995) are also shown for comparison. The $\delta^{18}O$ and $\delta^{13}C$ data are precise to ± 0.2 ‰ and ± 0.1 ‰ respectively.

Rock type	*Sample*	$\delta^{18}O$ (‰)	$\delta^{13}C$ (‰)	*L.O.I.* (%)	*Ba* (ppm)	*Sr* (ppm)	*Ca* (wt %)
Essexite dyke	OKJ-018	+ 12.2	- 4.1	3.2	976	669	7.5
Monzodiorite	OKJ-047	+ 18.0	- 4.4	1.0	1525	317	6.1
Alkaline gabbro	OKJ-050	+ 16.1	- 3.7	2.1	213	773	12.8
Alkaline gabbro	OKJ-084	+ 16.6	- 3.9	1.1	792	613	12.7
Syenite	OKJ-150	+ 19.3	- 4.3	1.8	1538	131	2

Note: The initial $^{87}Sr/^{86}Sr$ ratios (Milner *et al.*, 1993) for these samples are listed in Table 5.1. Not listed therein is the initial $^{87}Sr/^{86}Sr$ ratio for the syenite (OKJ-150), which is 0.70923 .

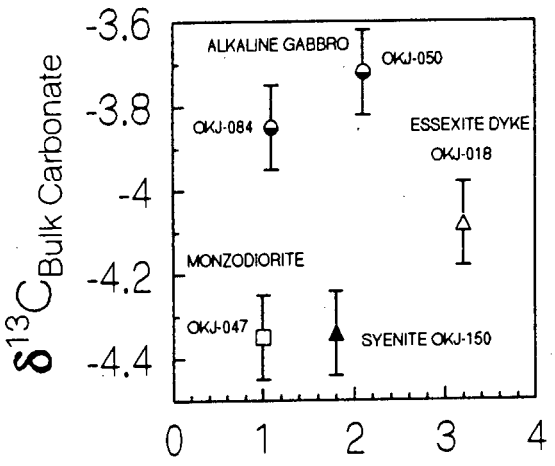

Fig. 4.1a

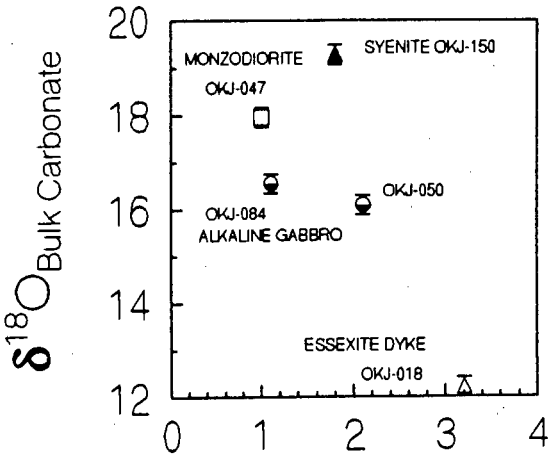

Fig. 4.1b

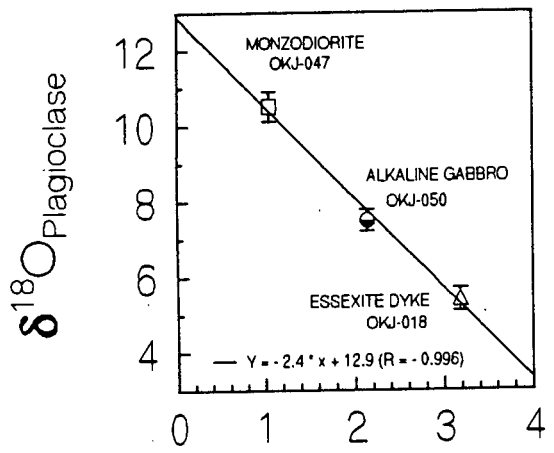

Fig. 4.1c

Fig. 4.1a - b Plots of $\delta^{13}C$ (a) and $\delta^{18}O$ (b) (both ‰) of the total bulk carbonate versus loss on ignition (L.O.I.) (wt %) values.
Fig. 4.1c Plot of $\delta^{18}O$ of the plagioclase (‰) versus loss on ignition (L.O.I.) (wt %) values. The plot suggests a strong negative correlation, albeit based on three points only.
Symbols used represent the following rock types: (1) monzodiorite (□), (2) alkaline gabbro (⊖), (3) syenite (▲), and (4) essexite dyke (▲).

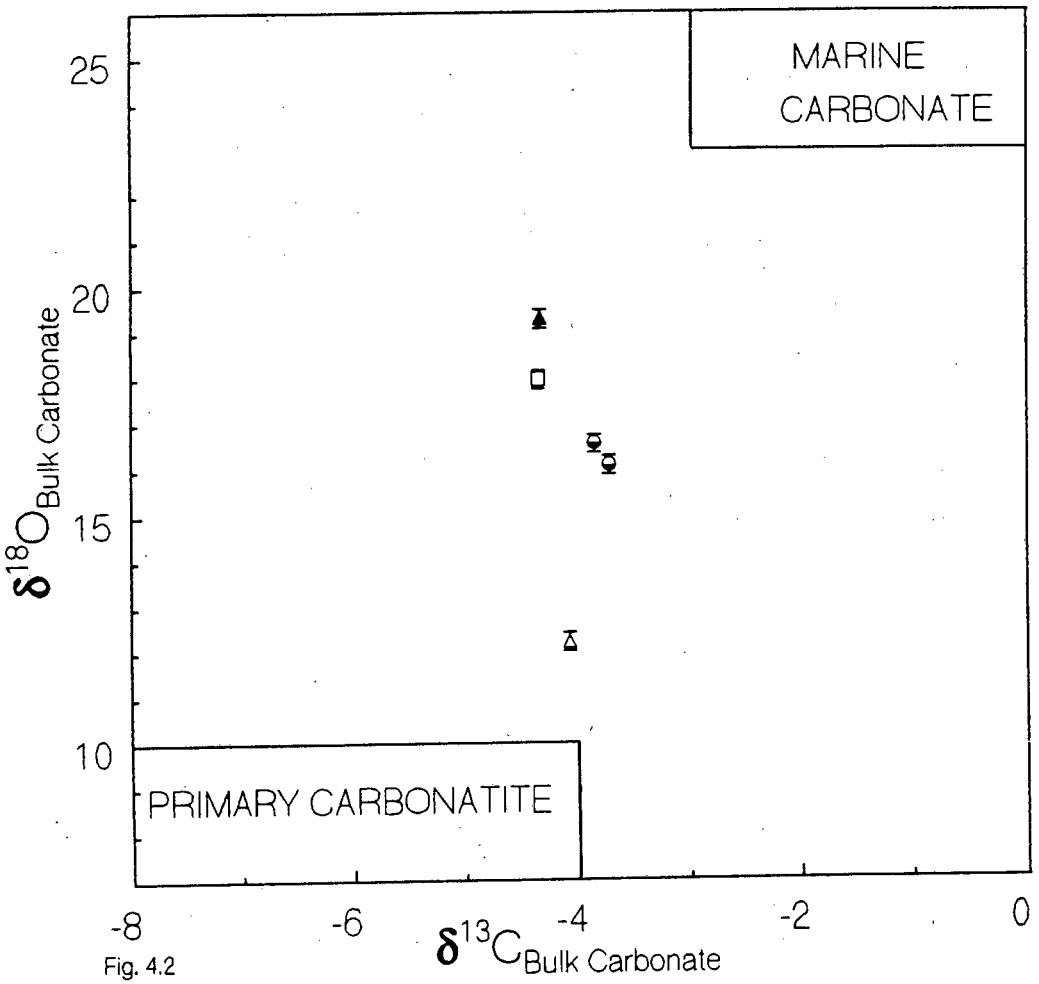

Fig. 4.2 Plot of $\delta^{18}O$ versus $\delta^{13}C$ of the total bulk carbonate (both ‰), shown relative to the $\delta^{18}O$ fields recognized for primary carbonatite and marine carbonate $\delta^{18}O$ values (Taylor *et al.*, 1967).
Symbols used represent the following rock types: (1) monzodiorite (□), (2) alkaline gabbro (⊖), (3) syenite (▲), and (4) essexite dyke (△).

carbonate. The sample OKJ-018 has thus been selected to characterize the possible carbon and oxygen components, and equilibration temperature of the altering fluid.

4.3 Bulk carbonate $\delta^{18}O$ - $\delta^{13}C$ variation

The syenite and monzodiorite are characterized by the most ^{13}C-depleted (- 4.3 ‰ and - 4.4 ‰ respectively) and the most ^{18}O-enriched (+ 19.3 ‰ and + 18.0 ‰ respectively) compositions. The essexite dyke $\delta^{18}O$ and $\delta^{13}C$ values are + 12.2 ‰ and - 4.1 ‰ respectively. The $\delta^{13}C$ values are close to typical mantle values of - 7 ‰ (Kyser, 1986). The remaining carbonates lie within the field of secondary low temperature hydrothermal carbonates on Fig. 4.2 . The alkaline gabbro $\delta^{13}C$ values (- 3.9 to - 3.7 ‰), are slightly higher (by 0.1 ‰ to 0.7 ‰) than the other samples. This suggests that the carbonate in the alkaline gabbro equilibrated with a slightly less "primary" fluid than in the other rock types. The large $\delta^{18}O$ value variation (extrema differ by 7.07 ‰) may be accounted for by a variation in the equilibration temperature. In contrast, the $\delta^{13}C$ values, which are affected to a much lesser extent by temperature changes, span a very narrow range (0.7 ‰).

4.4 Variation of bulk carbonate $\delta^{18}O$ and $\delta^{13}C$ values with other chemical parameters

A plot of the plagioclase $\delta^{18}O$ values versus the bulk carbonate $\delta^{18}O$ values for the essexite dyke, alkaline gabbro and quartz monzodiorite, shows a statistically significant positive correlation (R = + 0.95) (Fig. 4.3). The bulk carbonate $\delta^{13}C$ values correlate negatively with the bulk rock initial $^{87}Sr/^{86}Sr$ (R = - 0.97) and Ba (R = - 0.98), and positively with Sr (R = + 0.96) concentrations (Figs. 4.4, 4.5, 4.6). Similarly, the CaO concentration shows a negative correlation with respect to the Ba (R = - 0.97), and a positive correlation with respect to the Sr (R = + 0.84) concentrations. The bulk carbonate $\delta^{18}O$ values correlate positively with the bulk rock $^{87}Sr/^{86}Sr_i$ values (R = + 0.98) (Fig. 4.7) and negatively with the Sr (R = - 0.99) (Fig. 4.8) and CaO (R = - 0.99) (Fig. 4.9) concentrations. It should also be noted, that the $\delta^{18}O$ values of plagioclase in these samples also correlate positively with the initial $^{87}Sr/^{86}Sr$ (R = + 0.97) value, and negatively with the Sr (R = - 0.85) concentration.

The $\delta^{18}O$ value of the calcite correlates with the $\delta^{18}O$ value of the plagioclase because

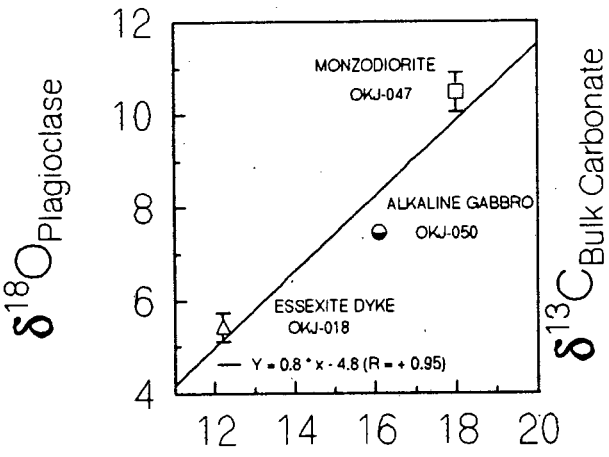

Fig. 4.3

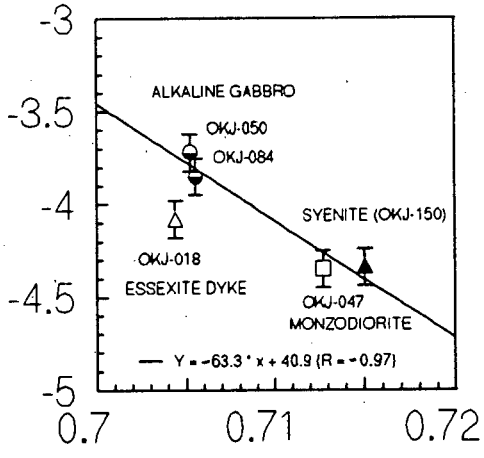

Fig. 4.4

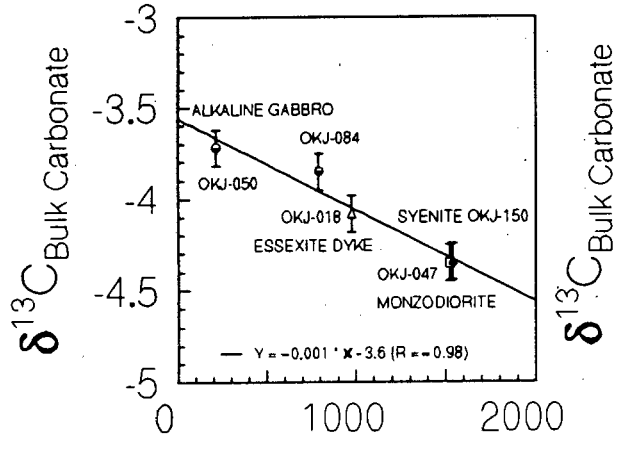

Fig. 4.5

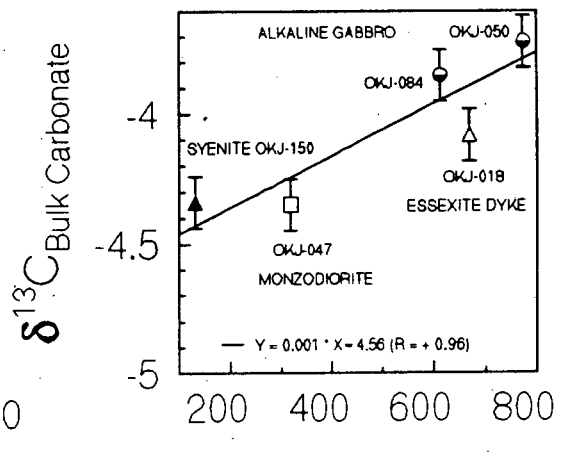

Fig. 4.6

Fig. 4.3 Plot of the $\delta^{18}O$ value of the plagioclase versus the total bulk carbonate $\delta^{18}O$ value (both ‰).
Fig. 4.4 Plot of the $\delta^{13}C$ value (‰) of the total bulk carbonate versus the initial ^{87}Sr / ^{86}Sr values of the bulk rock (silicate and carbonate).
Fig. 4.5 Plot of the $\delta^{13}C$ value (‰) of the total bulk carbonate versus the Ba concentration (ppm).
Fig. 4.6 Plot of the $\delta^{13}C$ value (‰) of the total bulk carbonate versus the Sr concentration (ppm).
Symbols used represent the following rock types: (1) monzodiorite (□), (2) alkaline gabbro (◒), (3) syenite (▲), and (4) essexite dyke (△).

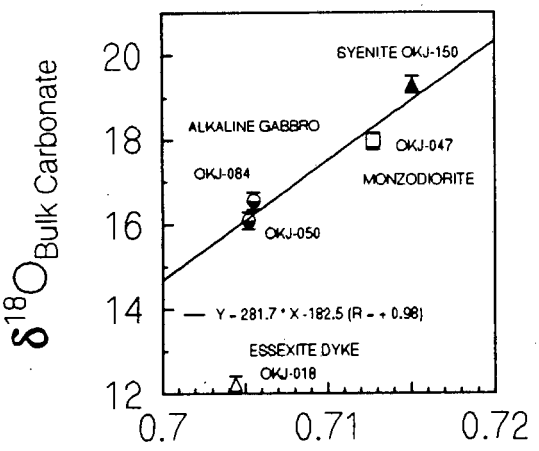

Fig. 4.7 $^{87}Sr/^{86}Sr_{initial}$

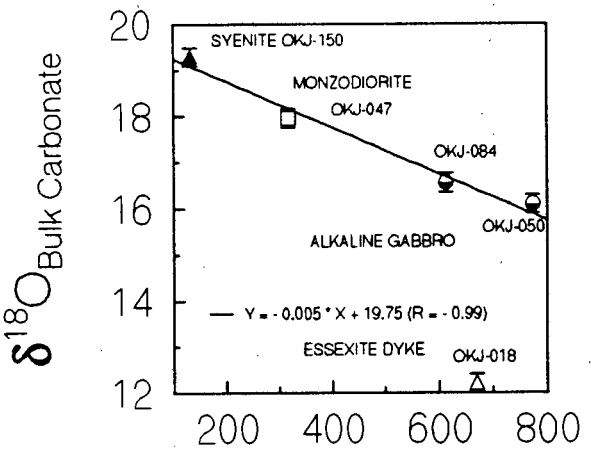

Fig. 4.8 Sr (ppm)

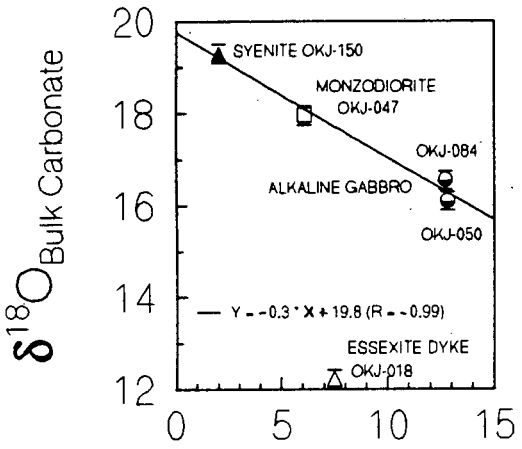

Fig. 4.9 Ca (wt %)

Fig. 4.7 Plot of the $\delta^{18}O$ value (‰) of the total bulk carbonate versus the initial ^{87}Sr / ^{86}Sr values of the bulk rock (silicate and carbonate).
Fig. 4.8 Plot of the $\delta^{18}O$ value (‰) of the total bulk carbonate versus the Sr concentration (ppm).
Fig. 4.9 Plot of the $\delta^{18}O$ value (‰) of the total bulk carbonate versus the Ca concentration (wt %).
Symbols used represent the following rock types: (1) monzodiorite (□), (2) alkaline gabbro (●), (3) syenite (▲), and (4) essexite dyke (△).(Note: The data for which the correlation coefficients, in Figs. 4.7 - 4.9 have been calculated, exclude the essexite dyke sample (OKJ-018).)

the fluid $\delta^{18}O$ value (and hence the calcite $\delta^{18}O$ value) is rock buffered, and plagioclase is the major constituent of the rock. The $\delta^{18}O$ value of the plagioclase correlates with the initial $^{87}Sr/^{86}Sr$ ratio because of crustal contamination (see Chapter 6). These two correlations result in the positive correlation between the calcite $\delta^{18}O$ value and the initial $^{87}Sr/^{86}Sr$ ratio (ie. this correlation results from two separate events). The correlation of the calcite $\delta^{18}O$ value with Sr, is a consequence of the Sr correlation with the plagioclase $\delta^{18}O$ value, which also results from contamination.

The low $\delta^{18}O$ values observed for the essexite dyke bulk carbonate are characteristic of lamprophyre carbonates (Rock, 1991), and may be attributed to the magmatic nature of the carbonate grains. The negative bulk carbonate $\delta^{18}O$ - CaO correlation (R = - 0.99) and the replacement of plagioclase by calcite suggests that the carbonate was probably produced by the interaction of a carbon bearing fluid with the rock. The similar $\delta^{13}C$ and CaO correlations with respect to Ba and Sr suggest that the $\delta^{13}C$ variation may be directly related to the extent to which this replacement reaction occurred within the individual samples.

4.5 Equilibration temperature

The equilibration temperature for the calcite - water system may be expressed as a function of the final $\delta^{18}O$ fluid composition by using the O'Neil *et al.* (1969) fractionation equation:

$$10^3 \ln \alpha_{\text{calcite-water}} \approx \delta^{18}O_{\text{calcite}} - \delta^{18}O_{\text{water}} \qquad (1)$$
$$= 2.78\ (10^6\ T^{-2}) - 2.89$$
$$(\ 0\ ^{\circ}C - 500\ ^{\circ}C)$$

A series of equilibration temperature curves (Fig. 4.10) and values (Table 4.2) have been calculated. The locus of the calculated temperatures may be used to determine equilibration temperature ranges for selected $\delta^{18}O$ values of fluids in equilibrium with the observed carbonate $\delta^{18}O$ values. The "normal" mantle oxygen isotope compositional range based on mantle xenoliths is 5 to 6.5 ‰ (Deines *et al.*, 1991). The equilibration temperatures in Table 4.2 have been calculated for "normal" mantle (+ 5 ‰, + 6 ‰),

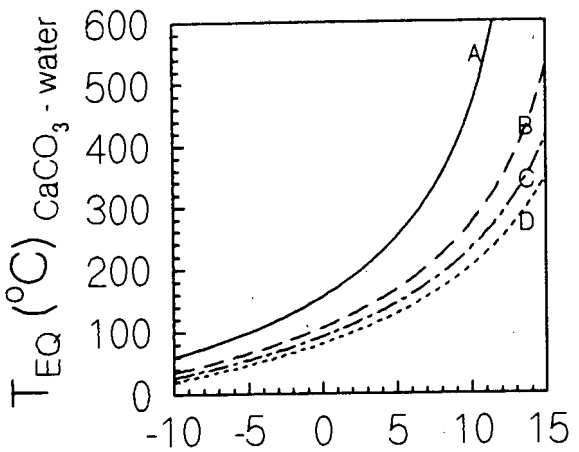

Fig. 4.10

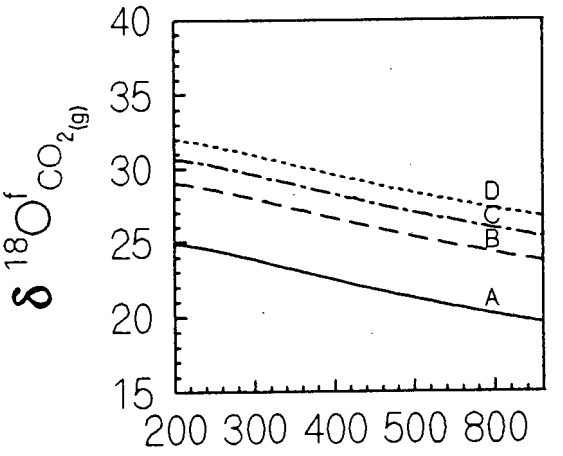

Fig. 4.11

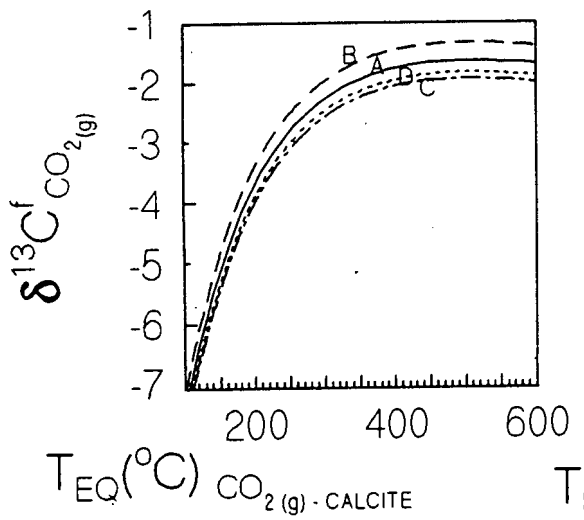

Fig. 4.12

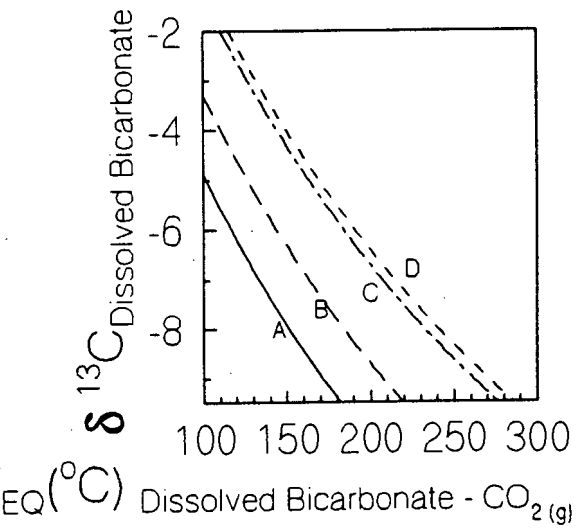

Fig. 4.13

Fig. 4.10 Locus of the calculated temperatures (°C) versus the $\delta^{18}O$ values of fluids in equilibrium with the observed carbonate $\delta^{18}O$ values (‰). The equation for $\alpha_{calcite\text{ - }H2O}$ of O'Neil *et al.* (1969) (ie. $10^3\ln a$ = $2.78(10^6T^{-2})$-2.89) was used in the calculations. (Note: in Figs. 4.10 - 4.12, the curves calculated for the various rock types are denoted by: A = essexite dyke, B = alkaline gabbro, C = monzodiorite, and D = syenite.)

Fig. 4.11 Locus of the calculated temperatures (°C) versus the $\delta^{18}O$ values of a CO_2 gas (‰) in equilibrium with the observed carbonate $\delta^{18}O$ values. The equation for $\alpha_{CO2(g)\text{ - calcite}}$ of Bottinga (1968) (ie. $10^3\ln a$ = $-1.8034(10^6T^{-2})+10.611(10^3/T)-2.7798$) was used in the calculations.

Fig. 4.12 Locus of the calculated temperatures (°C) versus the $\delta^{13}C$ values of a CO_2 gas (‰) in equilibrium with the observed carbonate $\delta^{13}C$ values. The equation for $\alpha_{CO2(g)\text{ - calcite}}$ of Bottinga (1968b) (ie. $10^3\ln a$ = $-2.9880(10^6T^{-2})+7.6663(10^3/T)-2.4612$) was used in the calculations.

Fig. 4.13 Locus of the calculated temperatures (°C) versus the $\delta^{13}C$ values of a dissolved bicarbonate (‰) in equilibrium with the observed carbonate $\delta^{13}C$ values. The equation for $\alpha_{Dissolved\ Bicarbonate\text{ - }CO2(g)}$ of Mook *et al.*(1974) (ie. $10^3\ln a$ = $9.552(10^3/T)-24.10$) was used in the calculations. The curves have been calculated for various $\delta^{13}C$ compositions of possible CO_2 gases (ie. A = - 6.4 ‰,B = - 4.8 ‰, C = - 2.8 ‰, and D = - 2.5 ‰), which may have equilibrated with the bulk carbonate (see Table 4.3).

Table 4.2 Possible equilibration temperatures (°C) for a variety of initial fluid $\delta^{18}O$ compositions. The equilibration temperatures, which were calculated by the O'Neil *et al.* (1969) fractionation equation, for the $\delta^{18}O$ carbonate value of each rock type, assuming possible initial fluid $\delta^{18}O$ values in the range of meteoric to magmatic compositions (- 3 to + 11 ‰) (see text for further details).

Rock type	*Possible equilibration temperatures (°C) for a variety of fluid $\delta^{18}O$ values:*				
	Moderately Depleted Meteoric: (- 3 ‰)	*Sea Water:* (0 ‰)	*"Normal" Mantle:* (+ 5 ‰)	*"Normal" Mantle:* (+ 6 ‰)	*Magmatic:* (+ 11 ‰)
Essexite dyke	120 °C	160 °C	250 °C	280 °C	550 °C
Monzodiorite	70 °C	90 °C	150 °C	160 °C	260 °C
Alkaline gabbro	80 °C	110 °C	170 °C	180 °C	310 °C
Syenite	60 °C	80 °C	130 °C	140 °C	230 °C

Table 4.3 Final fluid, CO_2 gas and dissolved carbon isotope compositions for selected equilibration temperatures, which were calculated by the O'Neil *et al.* (1969), Bottinga (1968 b), Malinin *et al.* (1967), and Mook *et al.* (1969) fractionation equations. These values were calculated by substituting the $\delta^{18}O$ and $\delta^{13}C$ values of the essexite dyke (OKJ-018) sample, into equations (1) to (3) (see text). In other words, the compositions have been calculated for the sample which records the maximum equilibration temperature.

$Temperature_1$	$\delta^{18}O^{f}_{fluid}$	$\delta^{13}C^{f}_{CO2(g)\ 2}$	$\delta^{13}C_{bicarbonate\ 3}$	$\delta^{13}C_{carbonate\ 4}$
120 ° C	- 3 ‰	- 6.4 ‰	- 4.1 ‰	- 6.2 ‰
160 ° C	0 ‰	- 4.8 ‰	- 4.8 ‰	- 6.9 ‰
250 ° C	+ 5 ‰	- 2.8 ‰	- 7.8 ‰	- 8.6 ‰
280 ° C	+ 6 ‰	- 2.5 ‰	- 9.1 ‰	- 9.3 ‰
550 ° C	+ 11 ‰	- 1.7 ‰	-	-

Notes:
1. Temperature estimates based on the O'Neil, Clayton and Mayeda (1969) equilibration curve for the selected $\delta^{18}O$ values of possible fluids. (Calibrated for: 0 °C - 500 °C)
2. The $\delta^{13}C$ compositions of possible CO_2 gases, which may have equilibrated with the bulk carbonate, based on Bottinga (1968 b). (Calibrated for: 0 °C - 700 °C)
3. The $\delta^{13}C$ compositions of possible dissolved bicarbonates which may have equilibrated with the bulk carbonate, based on Malinin, Kropotova & Grinenko (1967). (Calibrated for: 23 °C - 286 °C)
4. The $\delta^{13}C$ compositions of possible dissolved bicarbonates which may have equilibrated with the bulk carbonate, based on Mook, Bommerson, Staverman (1974). (Calibrated for: 5 °C - 125 °C)

meteoric (- 3 ‰), sea water (0 ‰), and magmatic (+ 11 ‰) (Faure, 1986) initial fluid $\delta^{18}O$ values. The near mantle $\delta^{13}C$ value (- 4.1 ‰) of the essexite dyke suggests that a "normal" mantle initial fluid $\delta^{18}O$ composition range (+ 5 ‰ to + 6 ‰) may be assumed for an estimate of the maximum equilibration temperature. The highest corresponding equilibration temperature range may be extrapolated from the essexite dyke curve as 250 °C to 280 °C.

4.6 Fluid composition and source

The origin of the secondary and possibly primary carbonates may be ascribed to the interaction of a carbon bearing fluid with Ca bearing silicates within the rock. Most mantle carbon isotope values range from - 5 to - 8 ‰ (Kyser, 1986). A series of curves have been calculated which illustrate possible final $\delta^{18}O$ and $\delta^{13}C$ carbon dioxide compositions as a function of the equilibration temperature for the Bottinga (1968) and Bottinga (1968b) thermometers respectively:

$$10^3 \ln \alpha_{CO2(g)\text{-}calcite} \approx \delta^{18}O_{CO2(g)} - \delta^{18}O_{calcite} \qquad (2)$$
$$= -1.8034\,(10^6\,T^{-2}) + 10.611\,(10^3/T) - 2.7798$$
$$(0\ ^\circ C - 750\ ^\circ C)$$

$$10^3 \ln \alpha_{CO2(g)\text{-}calcite} \approx \delta^{13}C_{CO2(g)} - \delta^{13}C_{calcite} \qquad (3)$$
$$= -2.9880\,(10^6 T^{-2}) + 7.6663\,(10^3/T) - 2.4612$$
$$(0\ ^\circ C - 700\ ^\circ C)$$

For an equilibration temperature in the range of 250 °C - 280 °C, the bulk rock carbonate may have equilibrated with a final carbon dioxide gas component characterized by the average $\delta^{18}O$ and $\delta^{13}C$ values of + 22.9 ‰ (Bottinga; 1968) and - 2.7 ‰ (Bottinga; 1968 b) respectively (Figs. 4.11 & 4.12). Alternatively, if equilibration occurred with a dissolved bicarbonate or carbonate fluid species, the possible average $\delta^{13}C$ values of - 8.5 ‰ and - 9.0 ‰ are suggested by the Malinin *et al.* (1967) and Mook *et al.* (1974) equilibration curves respectively (see Table 4.3). A series of equilibration curves have been produced for the Mook *et al.* (1974) geothermometer (Fig. 4.13):

$$10^3 \ln \alpha_{\text{Dissolved bicarbonate-CO2(g)}} \approx \delta^{13}O_{\text{Dissolved bicarbonate}} - \delta^{13}O_{CO2(g)} \quad (4)$$

$$= 9.552\ (10^3 / T) - 24.10$$

$$(5\ ^\circ C - 125\ ^\circ C)$$

The reliability of the above temperature and fluid composition estimates is restricted by 1) the calibrated ranges of the equilibration curves (Table 4.3) and 2) the assumption that all the disseminated carbonate present is calcite of the same generation.

4.7 Summary

Carbonate with carbon and oxygen isotope compositions that are most like those for magmatic sources occur in the essexite dyke. The essexite data suggest that the calcite equilibrated at about 270 °C with a CO_2 and H_2O bearing fluid, with a $\delta^{18}O$ of + 22.9 ‰ and $\delta^{13}C$ of - 2.7 ‰, or a dissolved bicarbonate with a $\delta^{13}C$ of about - 8.7 ‰. The bulk carbonate $\delta^{13}C$ and $\delta^{18}O$ values are uncorrelated with L.O.I. values. This indicates that carbon-bearing species was not the dominant component in the fluid which produced the carbonates. In contrast, the $\delta^{18}O$ values for plagioclase within the same samples show a strong negative correlation with the L.O.I. value (R = - 0.99), albeit based on three samples only. This suggests that the infiltrating fluid, which led to the minor alteration recorded in the plagioclase $\delta^{18}O$ values (see Chapter 7), may have been dominated by the H_2O component. The equilibration temperatures calculated for the essexite data lie within the suggested lamprophyre melt crystallization range of 250 °C - 450 °C (Nemec, 1977a; Montel & Weisbrod, 1986). Rock (1991) suggests that such temperatures may imply a crystal laden status.

It should be noted that the essexite dyke sample was obtained from an area far north of the transect region (Fig. 2.1). The $\delta^{13}C$ values of the essexite dyke, quartz monzodiorite, alkaline gabbro and syenite (Table 4.1), all lie slightly above the range of $\delta^{13}C$ values of carbonates within ultramafic lamprophyres occurring in the transect region (- 4.9 to - 5.7 ‰) (Lanyon & le Roex, unpublished data). This suggests that the carbonate within these rocks, and in particular the quartz monzodiorite transect sample, may have equilibrated with a fluid related to the intrusion of the ultramafic lamprophyres, or the essexite dyke.

- Chapter 5 Oxygen isotope data on silicates and oxygen isotope thermometry -

5.1 Introduction

Oxygen isotope data may be used to determine whether the minerals coexisting in an igneous rock are in isotopic equilibrium or disequilibrium. This in turn may reveal whether crystallization occurred under open or closed system conditions (Gregory & Criss, 1986; Gregory *et al.*, 1989). The effects of open system exchange with fluids may be quantified in terms of possible water/rock ratios and alteration temperatures. Equilibration temperatures may also be calculated for conventional mineral-pair thermometers. Bearing in mind the limiting effects of oxygen isotope diffusion (Giletti, 1986), hydrothermal alteration, and crustal contamination, one may be able to determine possible closure and crystallization temperatures. Systematic variations in the oxygen isotope data with various geochemical parameters, such as the initial $^{87}Sr/^{86}Sr$ ratio, may be used to assess the importance of crustal contamination in the petrogenetic process.

The mineral and bulk rock compositional variations within the tholeiitic olivine gabbro - quartz monzodiorite suite, are consistent with an increasing degree of magmatic differentiation and/or contamination by felsic crustal material, towards the outer units. Petrographic observations and loss on ignition (L.O.I.) values indicate that these rocks are relatively fresh, and that the outer units are only slightly altered relative to the inner units. The major aims of obtaining oxygen isotope data on the silicates were (i) to assess the importance of crustal contamination indicated by existing radiogenic isotope and trace element data, and (ii) to quantify the minor hydrothermal (?) alteration suggested by the petrography. The analysis of pyroxene is especially important, as it is more resistant than plagioclase to the exchange of oxygen during alteration, and provides a measure of the original $\delta^{18}O$ value of the magma (Taylor & Forester, 1979; Gregory & Taylor, 1981). Together these two phases comprise more than 70 % of the mode of rocks from the tholeiitic suite. The $\delta^{18}O$ values for biotite and olivine were also determined.

5.2 Results

The $\delta^{18}O$ values for the silicates analysed in this study are reported in Table 5.1.

Table 5.1 Oxygen isotope composition of silicates. The corresponding initial $^{87}Sr/^{86}Sr$ whole-rock data, loss on ignition (L.O.I.) values (wt %), and distances along the tholeiitic suite transect (m) (Milner et al., 1993; le Roex et al., 1995), are also shown for comparison. The oxygen analyses for feldspar in the nepheline syenite (OKJ-014) and syenite (OKJ-150, -164) represent the $\delta^{18}O$ values of alkali feldspar within these samples. The tholeiitic suite rock type is followed by the corresponding unit number in brackets.

Rock type / (unit)	Sample	Plagioclase $\delta^{18}O$ (‰)	Pyroxene $\delta^{18}O$ (‰)	Biotite $\delta^{18}O$ (‰)	Olivine $\delta^{18}O$ (‰)	L.O.I. (wt %)	Distance (m)	Whole-rock $^{87}Sr/^{87}Sr_i$
Gabbro (4)	OKJ-004	+ 7.1 (0.47)	+ 6.5 (0.09)	+ 6.2 (0.09)	-	0.88	-	0.70523
Nepheline syenite	OKJ-014	+ 10.9 (0.21)	+ 6.7 (0.08)	+ 10.1 (0.08)	-	1.73	-	0.70433
Essexite dyke	OKJ-018	+ 5.4 (0.31)	+ 5.9 (0.11)	-	-	3.18	-	0.70378
Leucogabbro (3)	OKJ-031	+ 8.8 (0.24)	+ 8.1 (0.09)	+ 7.6 (0.16)	+ 8.1 (0.09)	1.17	355	0.70881
Leucogabbro (3)	OKJ-033	+ 9.0 (0.19)	-	+ 7.1 (0.35)	-	1.24	380	0.70900
Leucogabbro (3)	OKJ-033	+ 8.6 (0.20)	+ 8.1 (0.13)	-	-	-	-	-
Olivine gabbro (4)	OKJ-038	+ 9.5 (0.10)	+ 8.8 (0.06)	+ 8.4 (0.29)	+ 7.8 (0.35)	0.96	530	0.71228
Olivine gabbro (4)	OKJ-040	+ 9.7 (0.20)	+ 8.6 (0.22)	+ 8.0 (-)	-	1.06	590	0.71184
Monzodiorite (5)	OKJ-041	+ 9.2 (-)	-	+ 7.9 (0.14)	-	1.36	615	0.70891
Monzodiorite (6)	OKJ-043	+ 9.7 (0.30)	+ 9.0 (0.08)	+ 8.0 (0.18)	-	2.32	705	0.71161
Monzodiorite (5)	OKJ-044	+ 10.1 (0.41)	+ 8.5 (0.14)	-	-	2.32	725	0.71167
Monzodiorite (6)	OKJ-045	+ 9.9 (0.35)	+ 8.2 (0.22)	-	-	1.72	750	0.71196
Monzodiorite (5)	OKJ-046	+ 10.0 (0.31)	-	-	-	1.27	770	0.71223
Quartz monzodiorite (6)	OKJ-047	+ 10.5 (0.42)	+ 9.0 (0.03)	-	-	1.05	800	0.71116
Quartz monzodiorite (6)	OKJ-047	+ 10.0 (0.21)	-	-	-	-	-	-
Alkaline gabbro	OKJ-050	+ 7.5 (0.27)	-	-	-	2.14	-	0.70519
Olivine gabbro (1)	OKJ-062	+ 8.6 (0.32)	+ 8.2 (0.16)	+ 7.3 (0.24)	+ 7.9 (0.16)	0.92	275	0.70875
Gabbro (2)	OKJ-063	+ 8.8 (0.33)	-	+ 7.1 (0.26)	+ 6.2 (0.02)	1.22	250	0.70733
Olivine leucogabbro (1)	OKJ-068	+ 7.7 (0.07)	+ 6.9 (0.02)	-	-	-	40	0.70595
Alkaline gabbro	OKJ-069	+ 8.8 (0.01)	+ 7.1 (0.15)	-	+ 6.3 (-)	1.02	-	0.70635
Oligoclase essexite	OKJ-088	-	-	+ 5.5 (0.21)	-	2.93	-	0.70490
Syenite	OKJ-164	+ 10.2 (0.02)	+ 7.0 (0.35)	-	-	0.90	-	0.71497
Alkaline gabbro	OKJ-176	+ 8.5 (0.32)	+ 7.1 (0.34)	-	-	0.71	-	0.70491

Note: 1. The errors quoted in brackets represent the mean deviation of repeat analyses.
(The analytical technique which was followed is outlined in Appendix 3.)

5.2.1 Plagioclase

The plagioclase and alkali feldspar, when they occur together, could not be separated from each other for analysis. The oxygen analyses for feldspar in the nepheline syenite (OKJ-014) and syenite (OKJ-150, -164) samples represent the $\delta^{18}O$ values of alkali feldspar within these samples. Significant quantities of alkali feldspar are also present in samples from Units 5 and 6 of the tholeiitic suite (OKJ-043, -045, -046, -047). Nevertheless, the average modal abundance of plagioclase (46 %) within the these tholeiitic suite samples, by far exceeds that of alkali feldspar (26 %). In the remainder of the samples analysed for oxygen isotopes, alkali feldspar is either absent or present only as a minor constituent. Thus the majority of the $\delta^{18}O$ values of feldspar in Table 5.1 represent the plagioclase compositions. Infact, it should also be noted that the fractionation factor between alkali feldspar and plagioclase ($\Delta_{\text{alkali feldspar - plagioclase}}$) is very small or non existent (O'Neil & Taylor, 1967).

The tholeiitic suite $\delta^{18}O$ data set has a mean value of + 9.4 ‰ (± 0.8) (Fig. 5.1a). The samples from Units 1 - 3, which have clouded plagioclase grains, are characterized by lower $\delta^{18}O$ values (+ 7.7 ‰ to + 8.8 ‰). The outer unit samples, which show sericitization, resorbed grain boundaries and alkali feldspar rims, are characterized by higher values (+ 9.7 ‰ to + 10.1 ‰). The highest value (+ 10.9 ‰) is displayed by the feldspar in the nepheline syenite (OKJ-014). The lowest value (+ 5.4 ‰) is displayed by the feldspar of the essexite dyke. Alkaline gabbro plagioclase $\delta^{18}O$ values range from + 7.5 ‰ to + 8.5 ‰. The syenite alkali feldspar has a value of + 10.2 ‰.

5.2.2 Pyroxene

The coexisting orthopyroxene and clinopyroxene were not separated for analysis, however, it should be noted that the per mil fractionation between these two phases is near zero (Kyser *et al.*, 1981). Nevertheless, the restricted occurrence and low modal abundance of the orthopyroxene means that the pyroxene data largely represent the clinopyroxene compositions. The tholeiitic suite pyroxene $\delta^{18}O$ values have a mean value of + 7.7 ‰ (± 0.6) (Fig. 5.1b). Schillerized clinopyroxenes from the inner units of the

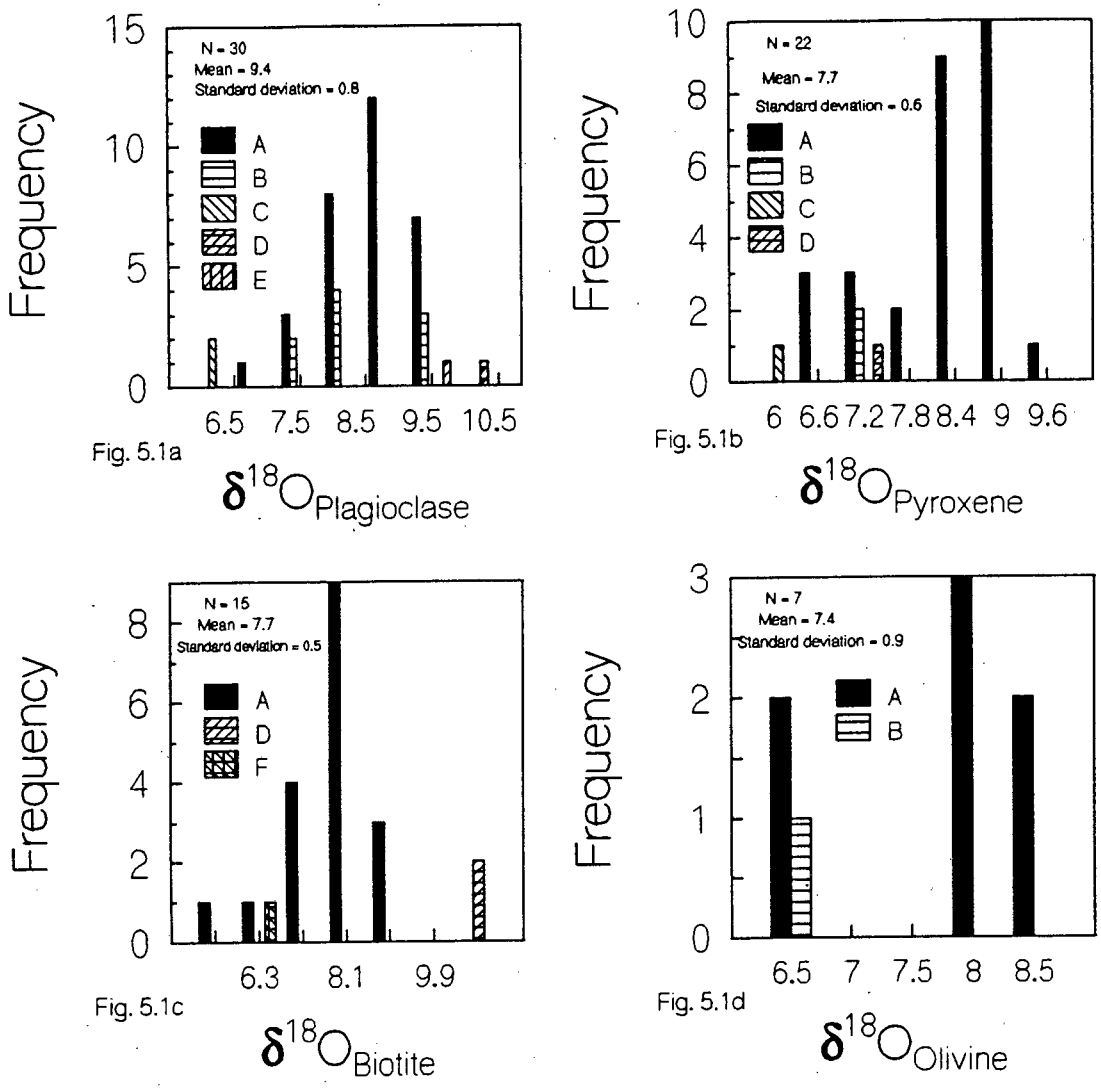

Fig. 5.1a - d Histograms of the $\delta^{18}O$ (‰) values obtained for plagioclase (a), pyroxene (b), biotite (c) and olivine (d). The mean and standard deviation values calculated for the tholeiitic olivine gabbro - quartz monzodiorite suite (A) are shown for each data set (n = number of samples). Other rock types shown include the alkaline gabbro (B), essexite dyke (C), nepheline syenite (D), syenite (E), and oligolcase essexite (F).

tholeiitic suite are characterized by lower $\delta^{18}O$ values (+ 6.9 ‰ to + 8.2 ‰). Higher values (+ 8.2 ‰ to + 9 ‰) are shown by samples bearing clinopyroxene mantled by hornblende. (It should be noted that the clinopyroxene was analysed after removal of the hornblende.) The nepheline syenite, alkaline gabbro and essexite dyke have values of + 6.7 ‰, + 7.1 ‰ and + 5.9 ‰ respectively.

5.2.3 Biotite

The mean $\delta^{18}O$ value for biotite in the tholeiitic suite lies at + 7.7 ‰ (± 0.5) (Fig. 5.1c). Biotite from Units 1 to 3 of the tholeiitic suite have $\delta^{18}O$ values in the range of + 7.1 ‰ to + 7.6 ‰. Samples from Units 4 to 6 have values in the range of + 7.9 to + 8.4 ‰. Biotite from the Unit 4 gabbro sample (OKJ-004), which lies off the transect through the tholeiitic suite, occurs as large flakes, and has a $\delta^{18}O$ value (+ 6.2 ‰) which closely resembles the pyroxene $\delta^{18}O$ compositon (+ 6.5 ‰). Biotite from the oligoclase essexite (OKJ-088) has a value of + 5.5 ‰.

5.2.4 Olivine

The mean value for the very limited $\delta^{18}O$ data for the tholeiitic suite olivine lies at + 7.4 ‰ (± 0.9) (Fig. 5.1d). The inner Units 1 and 2 of the tholeiitic suite have values which range from + 6.2 ‰ to + 7.9 ‰. Units 3 and 4 have values ranging from + 7.8 ‰ to + 8.1 ‰. Olivine in the alkaline gabbro has a value of + 6.3 ‰.

5.3 Discussion

The highest $\delta^{18}O$ values for all four data sets are restricted to the outer units, which are characterized by: 1) higher modal abundances of alkali feldspar, amphibole, quartz, secondary minerals (chlorite and sericite) and orthopyroxene, 2) myrmekitic intergrowths of quartz and plagioclase, and 3) plagioclase exsolution lamellae within the alkali feldspar.

The silicate $\delta^{18}O$ and loss on ignition (L.O.I.) values do not show any statistically significant positive correlations (Fig. 5.2). The $\delta^{18}O$ value of the plagioclase shows a positive covariation with the initial $^{87}Sr/^{86}Sr$ ratio (Fig. 5.3a). The tholeiitic suite data show correlations of the plagioclase $\delta^{18}O$ value with distance along the transect

Table 5.2 Correlation matrix of selected geochemical parameters monitored along the transect through the tholeiitic olivine gabbro - quartz monzodiorite suite.

	Distance																	
Distance	+ 1.00	SiO_2																
SiO_2	+ 0.70	+ 1.00	TiO_2															
TiO_2	+ 0.30	- 0.43	+ 1.00	Al_2O_3														
Al_2O_3	- 0.63	- 0.46	- 0.01	+ 1.00	Fe_2O_3													
Fe_2O_3	+ 0.27	- 0.42	+ 0.82	- 0.37	+ 1.00	MnO												
MnO	+ 0.71	- 0.14	+ 0.68	- 0.67	+ 0.80	+ 1.00	MgO											
MgO	- 0.89	- 0.70	- 0.27	+ 0.27	- 0.04	- 0.49	+ 1.00	CaO										
CaO	- 0.97	- 0.70	- 0.26	+ 0.53	- 0.27	- 0.68	+ 0.88	+ 1.00	Na_2O									
Na_2O	+ 0.90	+ 0.65	+ 0.28	- 0.32	+ 0.20	+ 0.58	- 0.92	- 0.94	+ 1.00	K_2O								
K_2O	+ 0.93	+ 0.90	- 0.03	- 0.57	- 0.06	+ 0.46	- 0.89	- 0.91	+ 0.84	+ 1.00	P_2O_5							
P_2O_5	- 0.43	- 0.16	+ 0.85	+ 0.02	+ 0.51	+ 0.58	- 0.49	- 0.39	+ 0.44	+ 0.17	+ 1.00	Rb						
Rb	+ 0.91	+ 0.93	- 0.07	- 0.57	- 0.12	+ 0.44	- 0.87	- 0.89	+ 0.83	+ 0.99	+ 0.16	+ 1.00	Sr					
Sr	- 0.64	- 0.88	+ 0.40	+ 0.76	+ 0.26	- 0.25	+ 0.49	+ 0.57	- 0.42	- 0.81	+ 0.28	- 0.83	+ 1.00	Ba				
Ba	+ 0.95	+ 0.85	+ 0.07	- 0.55	+ 0.02	+ 0.52	- 0.90	- 0.93	+ 0.91	+ 0.98	+ 0.25	+ 0.97	- 0.73	+ 1.00	Zr			
Zr	+ 0.88	+ 0.87	- 0.06	- 0.57	- 0.10	+ 0.39	- 0.84	- 0.85	+ 0.78	+ 0.98	+ 0.12	+ 0.96	- 0.81	+ 0.94	+ 1.00	Cr		
Cr	- 0.64	- 0.25	- 0.52	- 0.06	- 0.35	- 0.48	+ 0.78	+ 0.74	- 0.82	- 0.52	- 0.57	- 0.48	- 0.04	- 0.59	- 0.45	+ 1.00	Ni	
Ni	- 0.79	- 0.31	- 0.61	+ 0.15	- 0.45	- 0.64	+ 0.85	+ 0.84	- 0.88	- 0.63	- 0.66	- 0.59	+ 0.10	- 0.69	- 0.57	+ 0.96	+ 1.00	Nd
Nd	+ 0.90	+ 0.58	+ 0.42	- 0.55	+ 0.27	+ 0.73	- 0.84	- 0.86	+ 0.81	+ 0.79	+ 0.63	+ 0.81	- 0.51	+ 0.81	+ 0.72	- 0.59	- 0.74	+ 1.00
Nb	+ 0.94	+ 0.80	+ 0.17	- 0.61	+ 0.08	+ 0.62	- 0.89	- 0.90	+ 0.86	+ 0.93	+ 0.37	+ 0.95	- 0.72	+ 0.93	+ 0.87	- 0.57	- 0.69	+ 0.93
Zn	+ 0.97	+ 0.57	+ 0.43	- 0.70	+ 0.46	+ 0.84	- 0.81	- 0.95	+ 0.85	+ 0.85	+ 0.48	+ 0.82	- 0.56	+ 0.87	+ 0.81	- 0.63	- 0.79	+ 0.89
Co	- 0.81	- 0.64	- 0.30	+ 0.27	+ 0.01	- 0.50	+ 0.93	+ 0.76	- 0.79	- 0.80	- 0.60	- 0.81	+ 0.46	- 0.81	- 0.76	+ 0.60	+ 0.71	- 0.86
Cu	- 0.72	- 0.28	- 0.56	+ 0.06	- 0.43	- 0.57	+ 0.81	+ 0.79	- 0.86	- 0.57	- 0.60	- 0.53	+ 0.03	- 0.64	- 0.51	+ 0.99	+ 0.98	- 0.65
R_{OSr}	+ 0.82	+ 0.37	+ 0.56	- 0.36	+ 0.44	+ 0.76	+ 0.77	- 0.84	+ 0.79	+ 0.65	+ 0.77	+ 0.64	- 0.23	+ 0.69	+ 0.59	- 0.70	- 0.81	+ 0.89
R_{ONd}	- 0.79	- 0.48	- 0.40	+ 0.30	- 0.20	- 0.51	+ 0.88	+ 0.74	- 0.71	- 0.74	- 0.50	- 0.70	+ 0.39	- 0.72	- 0.74	+ 0.71	+ 0.80	- 0.74
$\delta^{18}O_{Plag}$	+ 0.94	+ 0.64	+ 0.32	- 0.63	+ 0.26	+ 0.71	- 0.81	- 0.89	+ 0.84	+ 0.86	+ 0.51	+ 0.85	- 0.60	+ 0.90	+ 0.82	- 0.51	- 0.68	+ 0.91
$\delta^{18}O_{Pyr}$	+ 0.78	+ 0.36	+ 0.35	- 0.64	+ 0.38	+ 0.64	- 0.56	- 0.73	+ 0.70	+ 0.61	+ 0.47	+ 0.59	- 0.47	+ 0.70	+ 0.54	- 0.52	- 0.68	+ 0.62
$\delta^{18}O_{Bt}$	+ 0.79	- 0.43	+ 0.74	- 0.49	+ 0.88	+ 0.93	- 0.39	- 0.79	+ 0.65	+ 0.39	+ 0.62	+ 0.32	+ 0.17	+ 0.58	+ 0.27	- 0.45	- 0.62	+ 0.74

	Nb							
Nb	+ 1.00	Zn						
Zn	+ 0.88	+ 1.00	Co					
Co	- 0.85	- 0.74	+ 1.00	Cu				
Cu	- 0.62	- 0.71	+ 0.64	+ 1.00	R_{OSr}			
R_{OSr}	+ 0.74	+ 0.86	- 0.80	- 0.75	+ 1.00	R_{ONd}		
R_{ONd}	- 0.75	- 0.75	+ 0.80	+ 0.77	- 0.70	+ 1.00	$\delta^{18}O_{Plag}$	
$\delta^{18}O_{Plag}$	+ 0.90	+ 0.92	- 0.81	- 0.60	+ 0.83	+ 0.91	+ 1.00	$\delta^{18}O_{Pyr}$
$\delta^{18}O_{Pyr}$	+ 0.61	+ 0.77	- 0.59	- 0.66	+ 0.71	+ 0.61	+ 0.77	+ 1.00
$\delta^{18}O_{Bt}$	+ 0.57	+ 0.91	- 0.35	- 0.56	+ 0.83	+ 0.74	+ 0.83	+ 0.77

Notes:

1. OKJ-068 has been excluded from the correlation matrix. The correlation coefficient between the plagioclase $\delta^{18}O$ value and the sample distance along the transect, for a data set which includes OKJ-068 is 0.96.

2. The $\delta^{18}O$ - initial $^{87}Sr/^{86}Sr$ ratio correlation coefficient is higher for the full pyroxene data set (R = + 0.95).

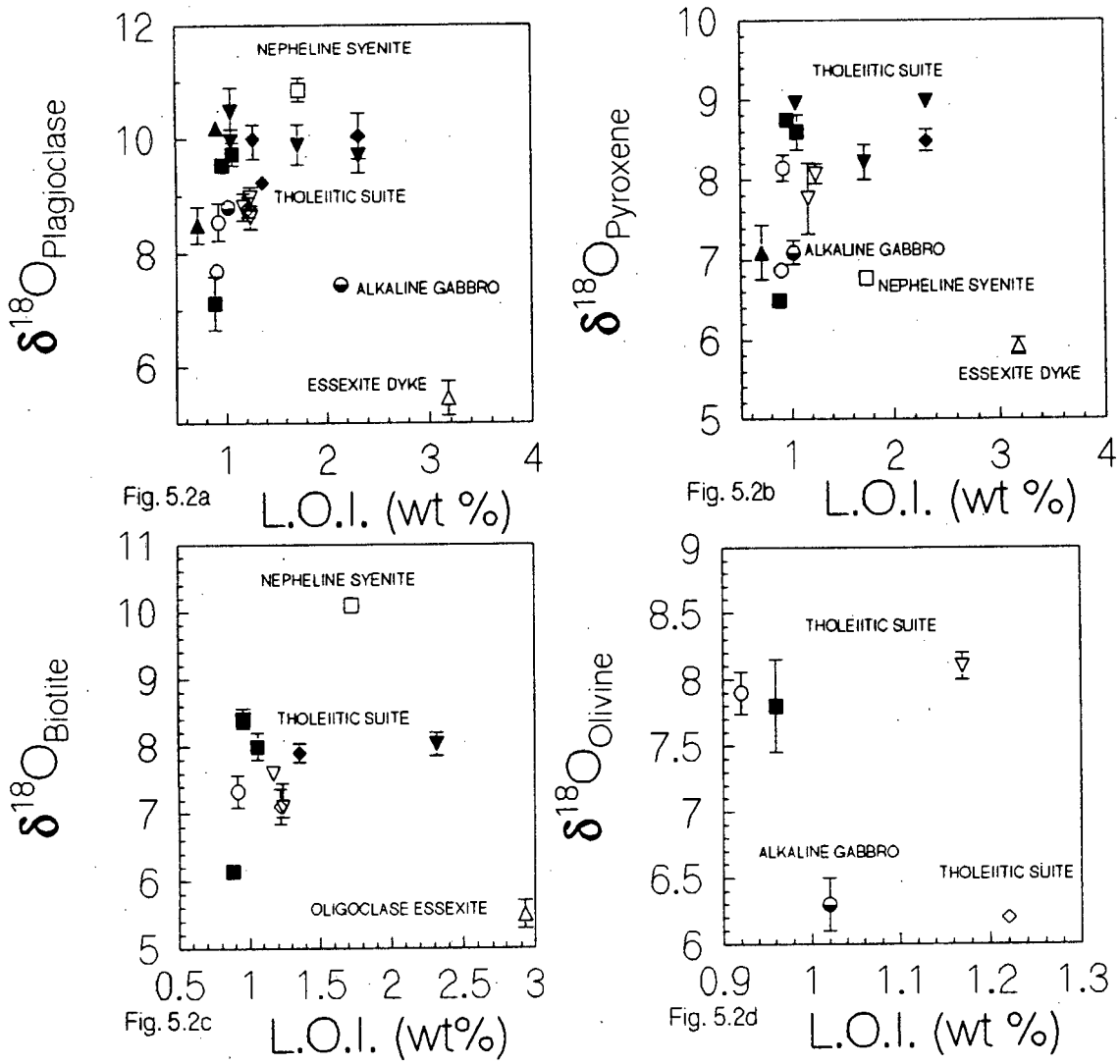

Fig. 5.2a - d The variation in the $\delta^{18}O$ (‰) values obtained for plagioclase (a), pyroxene (b), biotite (c) and olivine (d) with respect to the loss on ignition (L.O.I.) values (wt %). The correlation coefficients of the tholeiitic olivine gabbro - quartz monzodiorite suite data, for all four minerals, lie below the value of 0.4. Symbols used are: (1) tholeiitic suite units: 1 (○), 2 (◇), 3 (▽), 4 (■), 5 (♦) and 6 (▾), (2) alkaline gabbro (◒), (3) syenite (▲), (4) nepheline syenite (□) and (5) essexite dyke / oligoclase essexite (△).

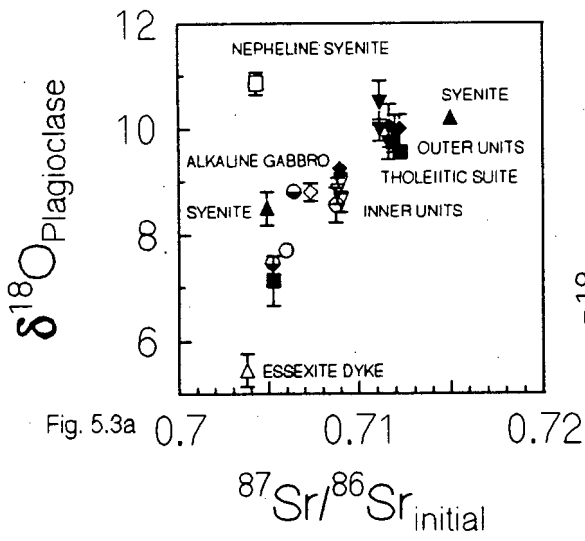

Fig. 5.3a

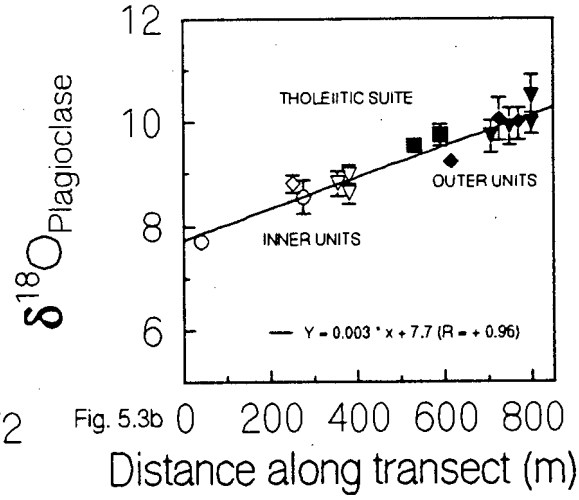

Fig. 5.3b

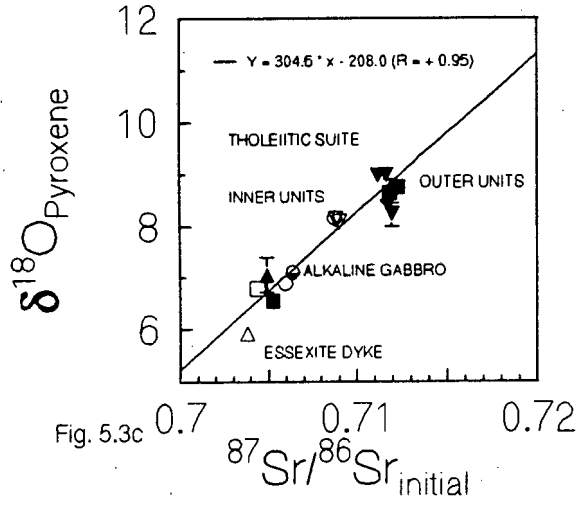

Fig. 5.3c

Fig. 5.3a - b Variations in the plagioclase $\delta^{18}O$ value (‰) with respect to the initial $^{87}Sr/^{86}Sr$ ratio (a), and the distance along the transect (m) (b). Symbols used are: (1) tholeiitic suite units: 1 (○), 2 (◇), 3 (▽), 4 (■), 5(♦) and 6 (▾), (2) alkaline gabbro (◒), (3) syenite (▲), (4) nepheline syenite (□) and (5) essexite dyke / oligoclase essexite (△).
Fig. 5.3c Variation in the pyroxene $\delta^{18}O$ value (‰) with respect to the initial $^{87}Sr/^{86}Sr$ ratio. Symbols used are the same as for Figs. 5.3a - b. (Note that where errors are absent, the magnitude of the error is smaller than the symbol size.)

(R = + 0.96) (Fig. 5.3b), Ba (+ 0.90), Nd (+ 0.91), Nb (+0.90), Zn (+0.92), Ce (+0.95) and $^{144}Nd/^{143}Nd$ (+ 0.91) (Table 5.2). Less significant correlations exist between the $\delta^{18}O$ value and MgO, CaO, Na_2O, K_2O, Rb, Zr, Co, and the initial $^{87}Sr/^{86}Sr$ value. The full pyroxene data set correlates positively with the initial $^{87}Sr/^{86}Sr$ ratio (R = + 0.95) (Fig. 5.3c). The pyroxene transect data show poor correlations with the distance, CaO, Na_2O, Ba, Zn, initial $^{87}Sr/^{86}Sr$ ratio and the plagioclase $\delta^{18}O$ value (Table 5.2). The biotite $\delta^{18}O$ data correlates with the Fe_2O_3 (+ 0.88), MnO (+ 0.93) and Zn (+ 0.91) concentrations. Poorer correlations are observed with respect to the initial $^{87}Sr/^{86}Sr$ ratio, plagioclase and pyroxene $\delta^{18}O$ values, distance, TiO_2 and CaO concentration. The numerous correlations observed between the silicate $\delta^{18}O$ data for the tholeiitic suite and other geochemical parameters strongly suggest that the variation in the $\delta^{18}O$ values may be accounted for by crustal contamination as opposed to alteration. This will be dealt with in detail in Chapter 6.

5.4 Mineral - pair thermometry

5.4.1 Introduction

The condition of isotopic equilibrium or disequilibrium for coexisting minerals may be evaluated by δ - δ plots (Gregory & Criss, 1986; Gregory *et al.*, 1989). The δ - δ diagrams for minerals with different isotopic exchange rates may be used to determine open or closed system conditions (eg. Gregory & Criss, 1986). Closed system equilibria are characterized by arrays which lie on a 45° line of constant Δ on δ-δ plots (Gregory & Taylor, 1986). The constant value fractionation line, $\Delta_{a\text{-}b} = \delta_a - \delta_b$, is an isotherm by definition. Data arrays which do not conform to a 45° line indicate open system behaviour. Data arrays steeper than 45° will result if the faster exchanging mineral (in this case plagioclase, rather than the other phases analysed) is plotted on the y-axis (Gregory & Criss, 1986).

5.4.2 Results

On a plot of the plagioclase versus clinopyroxene $\delta^{18}O$ values, the data lie on an array subparallel to, and are bracketed by, the Δ = 0.3 and Δ = 1.8 fractionation lines (Fig. 5.4a). Similarly, the $\delta^{18}O$ values of the plagioclase-biotite mineral-pair are bracketed by the Δ = 0.2 and Δ = 2.0 fractionation lines (Fig. 5.4b). Large differences in the

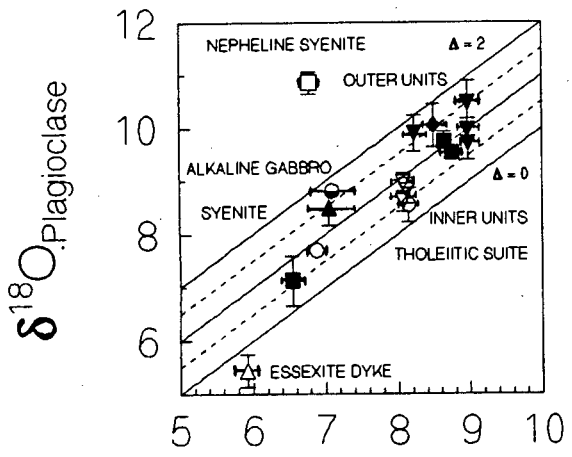

Fig. 5.4a

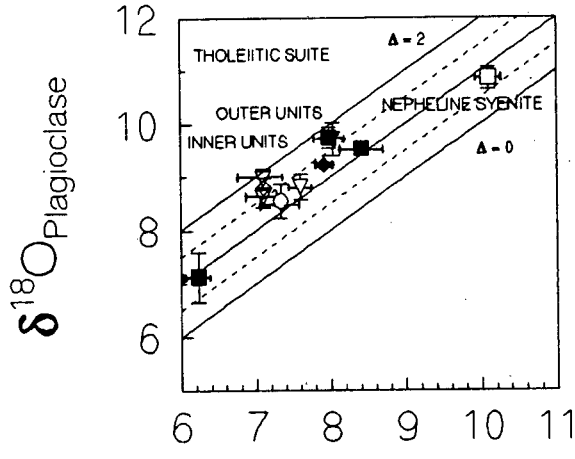

Fig. 5.4b

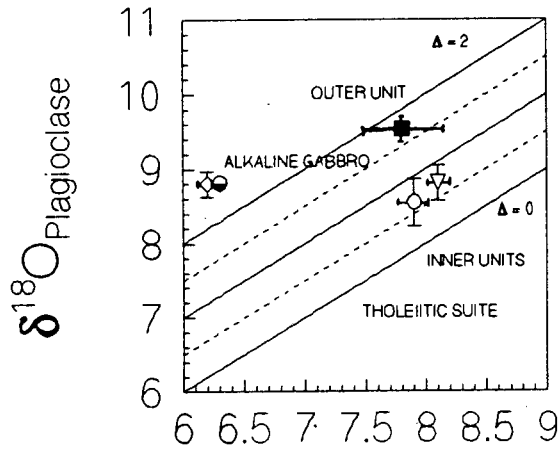

Fig. 5.4c

Fig. 5.4a - c The $\delta^{18}O$ - $\delta^{18}O$ plots for the plagioclase-pyroxene (a), plagioclase-biotite (b) and plagioclase-olivine (c) mineral-pair data (‰). Also shown are the fractionation lines for Δ = 0, 1 and 2. Symbols used are: (1) tholeiitic suite units: 1 (○), 2 (◇), 3 (▽), 4 (■), 5 (♦) and 6 (▾), (2) alkaline gabbro (◒), (3) syenite (▲), (4) nepheline syenite (□) and (5) essexite dyke / oligoclase essexite (△).

plagioclase and olivine $\delta^{18}O$ values are observed for the alkaline gabbro and tholeiitic gabbro (bracketed by the Δ = 0.2 and Δ = 1.8 fractionation lines), on the plagioclase-olivine mineral-pair data plot (Fig. 5.4c).

Equilibration temperatures calculated for the $\delta^{18}O$ silicate data, together with fractionation factors applied, are listed in tables 5.3.1 and 5.3.2. The average anorthite mole fraction in the tholeiitic suite (0.494) may be used to determine the temperature ranges bracketed by the above mentioned isotherms. The majority of the temperatures (Table 5.3.1) calculated for the various plagioclase-pyroxene, plagioclase-olivine, plagioclase-biotite and pyroxene-olivine mineral-pair thermometers (Mathews *et al.*, 1983; Bottinga & Javoy, 1974; 1975), lie beyond the maximum range of solidus to liquidus crystallization temperatures (1000 °C to 1200 °C) suggested for a gabbro pluton (Taylor, 1987). It should be noted that in general, calculated equilibration temperatures yield neither crystallization nor closure temperatures, as a result of oxygen isotope diffusion during slow cooling (Giletti, 1986; Deines, 1977; Javoy, 1977; Cole & Ohmoto, 1986; Valley, 1986). Minerals which are mantled by Fe-Ti oxides and/or amphibole, display vermicular intergrowths, or bear inclusions (see Chapter 3), are particularly susceptible to isotopic diffusion. The variability in the calculated temperatures may also be attributed to alteration and crustal contamination. In addition, the application of plagioclase-based thermometers to samples OKJ-043, -045 and -047, is less appropriate, due to the greater modal abundance of alkali feldspar within these samples.

The low temperatures (< 350 °C) calculated for the tholeiitic suite and alkaline gabbro by the plagioclase and biotite based thermometers (Table 5.3.1), are clearly inappropriate, and may be ascribed to the re-equilibration of these minerals with a derived fluid at subsolidus temperatures (see Chapter 7). Plagioclase from the essexite dyke appears to have remained in isotopic equilibrium with the coexisting pyroxene.

The error due to oxygen diffusion may be minimized by selecting temperatures calculated for samples which are essentially bimineralic. A comparison of the modal abundances (Table 1.1, Appendix 1) of the samples for which the anorthite mole fractions are listed (Table 5.3.1), reveals that OKJ-033 has the highest plagioclase (68.3 %) and pyroxene

Table 5.3.1 Equilibration temperatures (°C) calculated for the Okenyenya oxygen isotope silicate data. Note that the coefficients given by Bottinga and Javoy (1975, Table 2) have been recalculated for plagioclase of variable anorthite content.

Sample	*Rock type / (unit)*	*Anorthite mole fraction*	*Matthews et al. (1983) Albite-Cpx*	*Matthews et al. (1983) Anorthite-Cpx*	*Bottinga & Javoy (1975) Plag-Pyroxene*	*Bottinga & Javoy (1975) Plag-Olivine*	*Bottinga & Javoy (1975) Pyroxene-Olivine*	*Bottinga & Javoy (1975) Plag-Biotite*	*Bottinga & Javoy (1975) Plag-Olivine*	*Bottinga & Javoy (1975) Plag-Pyroxene*
OKJ-004	Gabbro (4)	-	1350	630	> 900	-	-	-	-	-
OKJ-018	Essexite dyke	-	1500	720	> 1000	-	-	-	-	-
OKJ-031	Leucogabbro (3)	-	1230	560	> 900	-	-	-	-	-
OKJ-033	Leucogabbro (3)	0.595	1230	560	> 900	> 1000	-	540	-	970
OKJ-038	Olivine gabbro (4)	-	1230	560	> 900	-	-	-	-	-
OKJ-040	Olivine gabbro (4)	0.440	930	390	700	850	840	620	-	790
OKJ-041	Monzodiorite (5)	0.423	-	-	-	-	-	710	-	-
OKJ-043	Monzodiorite (6)	0.514	1230	560	> 900	-	-	570	-	960
OKJ-044	Monzodiorite (5)	-	720	280	550	-	-	-	-	-
OKJ-045	Monzodiorite (6)	-	690	260	540	-	-	-	-	-
OKJ-047	Monzodiorite (6)	0.390	750	300	560	-	-	-	-	660
OKJ-062	Olivine gabbro (1)	-	1710	830	> 1000	> 1000	1760	-	-	-
OKJ-063	Gabbro (2)	0.599	-	-	-	670	-	570	660	-
OKJ-068	Olivine leucogabbro (1)	-	1130	510	850	-	-	-	-	-
OKJ-069	Alkaline gabbro	-	690	260	540	680	970	-	-	-
OKJ-176	Alkaline gabbro	-	790	320	600	-	-	-	-	-

Table 5.3.2 Fractionation factors, used to calculate equilibration temperatures, which are not listed in the text. A and B are coefficients of the equation: $1000 \ln \alpha = A (10^6 T^{-2}) + B$ where T is the absolute temperature. The mole fraction of anorthite in the feldspar is β. Note that the coefficients given by Bottinga and Javoy (1975, Table 2) have been recalculated for plagioclase of variable anorthite content.

Mineral-pair	A	B	Temperature range (°C)	Reference
Albite-diopside	1.58	0	400 - 800	Matthews *et al.* (1983)
Anorthite-diopside	0.49	0	400 - 800	Matthews *et al.* (1983)
Plagioclase-biotite	(2.27 - 1.04 β)	-0.60	> 500	Bottinga & Javoy (1975)
Plagioclase-olivine	(2.90 - 1.04 β)	0	> 500	Bottinga & Javoy (1975)
Plagioclase-pyroxene	(1.70 - 1.04 β)	0	> 500	Bottinga & Javoy (1975)
Pyroxene-olivine	1.24	0	> 500	Bottinga & Javoy (1975)

(13 %) modal abundances. Other minerals such as biotite, olivine, Fe-Ti oxides and alkali feldspar have minor abundances within this sample. The anorthite mole fraction (0.595) value of OKJ-033 indicates that the anorthite-clinopyroxene (Matthews *et al.*, 1983) thermometer may be applied to calculate the closure temperature (560 °C) for this mineral-pair. Of the samples for which plagioclase-biotite temperatures (Bottinga & Javoy, 1975) (Table 5.3.1) were calculated, OKJ-033 has the highest plagioclase modal abundance, and generally lower pyroxene, olivine, Fe-Ti oxide, alkali feldspar and biotite abundances. This suggests that the best plagioclase-biotite closure temperature estimate is 540 °C. These temperatures compare favourably with the plagioclase-biotite closure temperatures (± 550 °C) calculated for a closed system (Vennemann, 1989).

The average modal abundance of olivine (3.8 %) in the samples for which plagioclase-olivine and pyroxene-olivine (Bottinga & Javoy, 1975) equilibration temperatures have been calculated (Table 5.3.1), is by far exceeded by the plagioclase, pyroxene and Fe-Ti oxide abundances. Subsequent to the closure of olivine, plagioclase would have continued exchanging oxygen with pyroxene and Fe-Ti oxides. These temperatures are therefore unlikely to represent the true closure temperatures.

5.5 Closed- and open-system equilibria

The plagioclase-clinopyroxene δ-δ plot indicates, with the exception of the nepheline syenite, attainment of isotope equilibrium and closed system conditions for this mineral-pair (Fig. 5.4a). The attainment of isotope equilibrium is also suggested by the plagioclase-biotite δ-δ plot. The low average equilibration temperature (600 °C) calculated for this mineral-pair (Table 5.1) is typical of closed system closure temperatures (about 570 °C) (eg. Vennemann, 1989). The δ-δ plots therefore suggest minimal open system exchange. Evidence for minor fluid infiltration into the tholeiitic suite and alkaline gabbro will be discussed in Chapter 7.

The apparent isotopic equilibrium observed for the pyroxene-biotite mineral-pair in the unit 4 gabbro sample (OKJ-004), which lies off the transect through the tholeiitic suite, suggests that the biotite may be primary. The large differences in the $\delta^{18}O$ value observed for the alkaline gabbro and tholeiitic gabbro (Unit 2), on the plagioclase-olivine

plot (Fig. 5.4c), suggest isotopic disequilibrium and open system conditions for these rocks.

5.6 Possible causes for the observed silicate $\delta^{18}O$ covariations

The wide ranges in the $\delta^{18}O$ value observed for plagioclase, pyroxene, biotite and olivine are strongly consistent with crustal contamination as suggested by the radiogenic isotope data. Crystal fractionation alone can only shift the $\delta^{18}O$ value by ± 1 ‰ (Sheppard & Harris, 1985). The increase in the $\delta^{18}O$ values towards the outer units may be attributed to a greater degree of assimilation, as suggested by systematic variations in the bulk rock compositions and initial $^{87}Sr/^{86}Sr$ ratio with distance along the transect. Davidson and Harmon (1989) have attributed positive correlations between the $\delta^{18}O$ and L.O.I. to low-temperature alteration. The absence of such correlations for the Okenyenya data indicates that the observed $\delta^{18}O$ covariations cannot be simply ascribed to low-temperature alteration. Instead, the correlations are more likely the result of crustal contamination.

The broad correlations observed for the pyroxene data with distance along the transect (+ 0.78) and $^{87}Sr/^{86}Sr$ ratio, may be explained by the limited data set and by the greater resistance of this mineral to hydrothermal alteration. The correlations observed for the biotite $\delta^{18}O$ value with respect to the Fe_2O_3, MnO and TiO_2 concentrations suggests that the biotite replaced, or was generated from the same fluid as the Fe - Ti oxide minerals. The TiO_2 - P_2O_5 (R = + 0.85) correlation suggests that the apatite may also have been generated from the same fluid.

5.7 Summary

Closure temperatures calculated for the anorthite-plagioclase and biotite-plagioclase mineral-pairs, from the leucogabbro Unit 3 (OKJ-033) sample, are 560 °C and 540 °C, respectively. The absence of disequilibrium arrays in the silicate oxygen isotope δ - δ diagrams is consistent with isotopically equilibrated closed system behaviour (eg. Gregory & Taylor, 1986). The plagioclase-biotite mineral-pair data are also consistent with closed system crystallization. These observations are in accordance with petrographic features which are indicative of only minor hydrothermal alteration.

The numerous correlations observed between the silicate $\delta^{18}O$ data for the tholeiitic suite and other geochemical parameters strongly suggest that the variation in the $\delta^{18}O$ values may be accounted for by crustal contamination. The increase in the plagioclase $\delta^{18}O$ value with distance along the transect indicates an increase in the amount of high $\delta^{18}O$ value crustal material assimilated by the parent magma.

Chapter 6 - Contamination models -

6.1 Introduction

The high $\delta^{18}O$ values and the correlation between $\delta^{18}O$ and the initial $^{87}Sr/^{86}Sr$ ratio, strongly suggest that contamination occurred within the tholeiitic suite. The correlations observed for the tholeiitic suite may be used to characterize the nature of the contaminant. The simple mixing of a parental magma with felsic crustal material is usually associated with 1) negative correlations between initial $^{87}Sr/^{86}Sr$ ratios and elements with low abundances in felsic rocks (e.g. Mg, Cr, Ni and Co) and 2) positive correlations between initial $^{87}Sr/^{86}Sr$ ratios and elements with high abundances in felsic rocks (e.g. SiO_2, K_2O, Rb etc.) (eg. Bristow *et al.*, 1984). These correlations may be modified by fractional crystallization, which causes a magma to differentiate towards more felsic components, and are considered as strong indicators of crustal contamination (Faure *et al.*, 1979; Bristow *et al.*, 1984).

Indicators of a crustal contaminant for the tholeiitic suite are 1) the wide range in the initial $^{87}Sr/^{86}Sr$ ratio, 2) the positive correlations between the $^{87}Sr/^{86}Sr$ ratio and the K_2O ($r = + 0.65$) and Rb ($r = + 0.64$) contents, 3) the negative correlations between the $^{87}Sr/^{86}Sr$ ratio and the Cr ($r = - 0.70$), Ni ($r = - 0.81$) and Co ($r = - 0.80$). The positive correlations between the distance along the transect and SiO_2 ($r = + 0.70$), K_2O ($r = + 0.93$) and Rb ($r = + 0.91$), and the negative correlations between the distance and MgO ($r = - 0.89$), Cr ($r = - 0.64$), Ni ($r = - 0.79$) and Co ($r = - 0.81$) concentrations (Table 5.2), are consistent with an increase in the degree of contamination and differentiation towards the outer units.

The aim of modelling the crustal contamination process are 1) to evaluate the $\delta^{18}O$ value of the most likely contaminant, 2) to quantify the crustal contribution in terms of the percentage of material assimilated and crust / magma ratio, and 3) to quantify the average relative rates of assimilation, fractional crystallization and possible magma recharge during an assimilation fractional crystallization (AFC) process.

The pyroxene $\delta^{18}O$ data have been used to constrain the contamination models as this

mineral exhibits a greater resistance to hydrothermal alteration than plagioclase, and is therefore more likely to reflect changes in the magma $\delta^{18}O$ value. In addition, the value of $\Delta_{CPX\ -\ magma}$ lies close to zero (about 0.5 ‰) for the maximum solidus-liquidus crystallization temperature range (1000 °C to 1200 °C), and its effect cancels out, if only the clinopyroxene $\delta^{18}O$ data is modelled throughout (ie. the difference between the maximum and minimum $\delta^{18}O$ values of the magma is equal to the difference between the maximum and minimum $\delta^{18}O$ values of the clinopyroxene). This allows the $\delta^{18}O$ values of the pyroxene to serve as an estimate of the change in the $\delta^{18}O$ value of the magma.

6.2 The $\delta^{18}O$ value and initial $^{87}Sr/^{86}Sr$ ratio of the uncontaminated magma

The wide range observed for the tholeiitic suite pyroxene $\delta^{18}O$ value and its correlation with the distance along the transect, suggest a gradual shift in the $\delta^{18}O$ composition of the magma from about + 6.9 ‰ to + 9.0 ‰. The shift observed for the $\delta^{18}O$ value may be explained by a gradual increase in the amount of crustal material assimilated by the parent magma in a shallow (within plagioclase stability field) magma chamber. The alkaline gabbro $\delta^{18}O$ values fall within the range of $\delta^{18}O$ values observed for the tholeiitic gabbros. The $\delta^{18}O$ data are thus not consistent with distinctly different magma sources for the tholeiitic suite and alkaline gabbro, as suggested by the incompatible element ratios (le Roex *et al.*, 1995). In contrast, the lower pyroxene $\delta^{18}O$ values for the nepheline syenite (+ 6.7 ‰) and essexite dyke (+ 5.9 ‰), and their distinctly younger ages are consistent with a derivation from less contaminated magma sources.

Since the assimilation of crustal material results in an increase in the $\delta^{18}O$ and $^{87}Sr/^{86}Sr$ values of the magma, estimates of these values for the uncontaminated magma should lie below the $\delta^{18}O$ (+ 6.9 ‰ ± 0.02) and $^{87}Sr/^{86}Sr$ (0.70595) values of the most primitive tholeiitic gabbro transect sample (OKJ-068) (ie. the sample with the lowest values for these parameters). In the contamination models which follow, the $\delta^{18}O$ value of 5.7 ‰ of MORB (Ito *et al.*, 1987; Harmon & Kempton, 1990), and the most primitive mantle-like $^{87}Sr/^{86}Sr$ ratio of 0.70378 (ie. lowest ratio measured throughout the complex), have been selected for the uncontaminated magma to determine the maximum amounts of

assimilation may be obtained by recalculating the contamination models for a less primitive parental magma.

6.3 Possible contaminants

The Okenyenya igneous complex is contemporaneous and spatially associated with the Etendeka quartz latites ("rhyolites" sensu lato; Harris, 1995) (130 - 135 Ma) (Milner & Duncan, 1987), which have high $^{87}Sr/^{86}Sr$ ratios and $\delta^{18}O$ values ranging from 7.3 ‰ to 11.6 ‰. The Etendeka rhyolites have a bimodal distribution of $\delta^{18}O$ values with means at + 10 ‰ and + 7 ‰. The high $\delta^{18}O$ variety is found in the southern part of Etendeka, and is interpreted to be a crustal melt (Harris, 1995). This variety of rhyolite is dominant (Harris, 1995).

Possible contaminants considered in this work include 1) the high $\delta^{18}O$ value southern Etendeka rhyolite ($\delta^{18}O$ pyroxene: + 11.5 ‰) and 2) the low $\delta^{18}O$ value northern Etendeka rhyolite ($\delta^{18}O$ pyroxene: + 6.5 ‰) (Harris *et al.*, 1990; Harris, 1994). Note that the Etendeka rhyolites are not likely to be present at the crustal depth required to contaminate the Okenyenya magmas. However, the source material from which the high $\delta^{18}O$ southern Etendeka rhyolites were derived is a more likely potential contaminant. Assimilants chosen to represent the lower continental crust include igneous ($\delta^{18}O$ + 7.5 ‰) and metasedimentary ($\delta^{18}O$ + 9.7 ‰) granulite xenoliths (Fowler & Harmon, 1990; Downes *et al.*, 1990). Damaran granitoids and metasediments which are spatially closely associated with the Okenyenya complex and which may have also provided material for crustal contamination include: the Sorris-Sorris Granite ($\delta^{18}O$: + 11.4 ‰) (Haack *et al.*, 1982), and the Kuiseb mica schists ($\delta^{18}O$: + 17.0 ‰) (C. Harris, pers. comm. 1995), which have been dated at 495 ± 15 Ma and 548 ± 56 Ma respectively (Hawkesworth & Marlow, 1983; Hawkesworth *et al.*, 1981; 1984). The value of + 17 ‰ represents the maximum $\delta^{18}O$ value of the metasedimentary schists in the Damara belt (average = + 13.2 ‰), and has been selected to calculate the minimum amount of metasedimentary contamination required to produce the measured pyroxene $\delta^{18}O$ compositions. The geochemical data for the selected possible contaminants appear in Table 6.1.

Table 6.1 Geochemical data for the selected possible assimilants considered in the simple mixing models and in the calculation of the $\delta^{18}O$ versus $^{87}Sr/^{86}Sr$ curves.

Description	*Sr (ppm)*	$\delta^{18}O$ (‰)	$^{87}Sr/^{86}Sr_i$	*Reference*
Southern Etendeka Rhyolite	167	+ 11.5	0.72136	(1)
Northern Etendeka Rhyolite	346	+ 6.6	0.70586	(1)
Metasedimentary granulite	287	+ 9.7	0.71364	(2)
Igneous granulite	304	+ 7.5	0.70538	(2)
Sorris-sorris granite	118	+ 11.4	0.74972	(3)
Kuiseb mica schists	130	+ 17.0	0.74100	(3)

Notes:
1. The $^{87}Sr/^{86}Sr$ initial ratios have been recalculated to t = 130 Ma by:
$^{87}Sr/^{86}Sr_t = {}^{87}Sr/^{86}Sr_{present} - {}^{87}Rb/^{86}Sr\ (e^{\lambda t} - 1)$ where $\lambda = 1.42 \times 10^{-11}$.
2. The Etendeka rhyolite and granulite $\delta^{18}O$ data are for pyroxene and whole-rock analyses respectively.
3. The granulite $^{87}Sr/^{86}Sr$ ratios are based on the whole-rock sample data for granite facies xenoliths from the French Massif Central (Downes *et al.*, 1990). The average values for metasediment granulites without Al_2SiO_5 (n=2, average age = 1159 Ma) and granulites derived from basic liquids (n=8, average age = 576 Ma) are listed above. Sources of data: (1) Harris *et al.* (1990); Harris (1994), (2) Fowler & Harmon (1990); Downes *et al.* (1990); (3) Haack *et al.*, 1982; Hawkesworth & Marlow, 1983; Hawkesworth *et al.*, 1981; 1984).

6.4 Simple oxygen and strontium isotope mixing models

Mass balance calculations based on the oxygen isotope data may be used to constrain the amount of crustal contamination (James, 1981; Graham & Harmon, 1983; Schiffries & Rye, 1989). The $\delta^{18}O$ value of the contaminated magma ($\delta^{18}O_m$) may be approximated by:

$$\delta^{18}O_m = (1 - x)\ \delta^{18}O^{\circ}_m + x\ \delta^{18}O_a \qquad (1)$$

where x is the mole fraction of oxygen contributed by the crustal contaminants, and $\delta^{18}O^{\circ}_m$ and $\delta^{18}O_a$ are the mean $\delta^{18}O$ values of the uncontaminated magma and assimilant respectively. A series of solutions have been calculated for the maximum amounts of crustal material assimilated, by assuming a mantle-like $\delta^{18}O$ value, equal to the value of 5.7 ‰ of MORB (Ito *et al.*, 1987; Harmon & Kempton, 1990), for the uncontaminated magma (Fig. 6.1). For the observed range of pyroxene $\delta^{18}O$ values (+ 6.5 ‰ to + 9.0 ‰), the amounts of crustal contaminant assimilated (%) required are: 14 - 57 % (southern Etendeka rhyolite), 20 - 83 % (metasedimentary granulite) and > 44 % (igneous granulite).

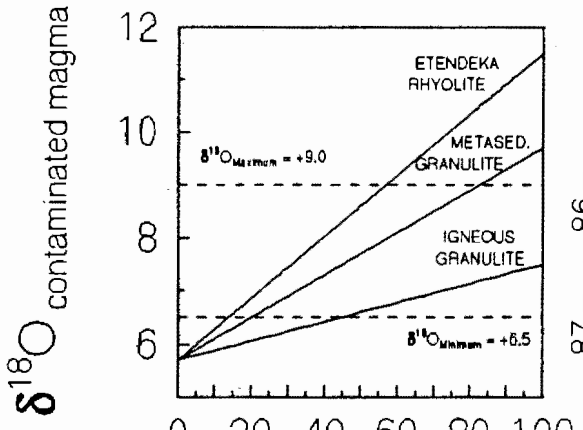

Fig. 6.1

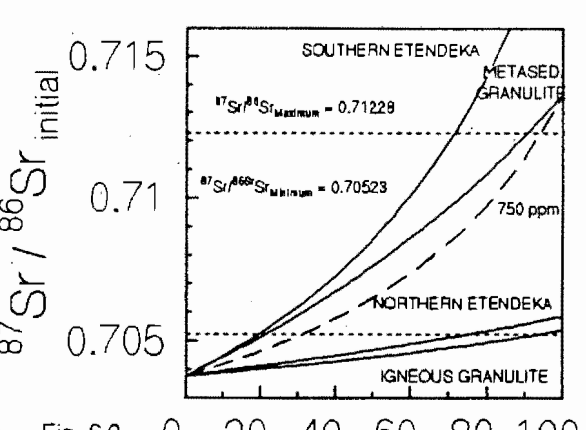

Fig. 6.2

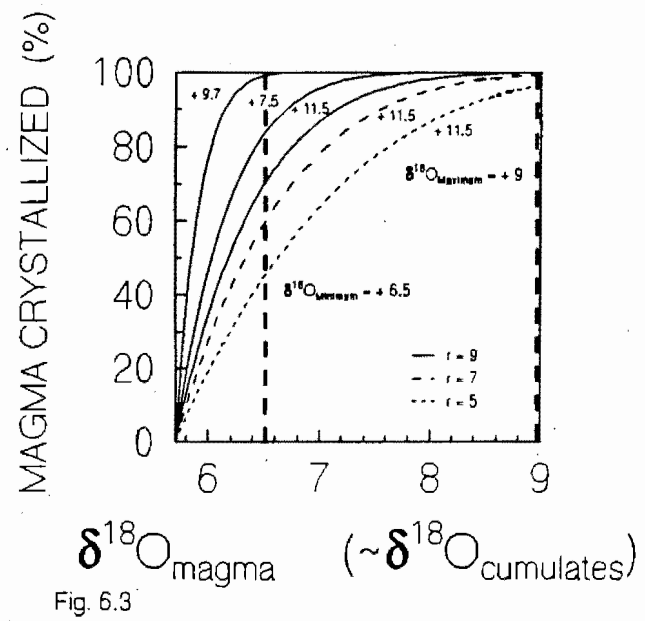

Fig. 6.3

Fig. 6.1 Solutions to the mass balance equation (1) for oxygen isotopes at different values of $\delta^{18}O_a$. The $\delta^{18}O$ value of the uncontaminated magma is assumed to be + 5.7 ‰. The geochemical data for the possible contaminants are listed in Table 6.1 . The range of the pyroxene $\delta^{18}O$ values (+ 6.5 ‰ to + 9.0 ‰) observed for the tholeiitic olivine gabbro - quartz monzodiorite suite is also shown.

Fig. 6.2 Solutions to the mass balance equation (2) for strontium isotopes at different values of $^{87}Sr/^{86}Sr_a$. The solid line curves have been calculated for initial magma $^{87}Sr/^{86}Sr$ ratio and concentration values of 0.70378 and 450 ppm. A curve for an initial magma Sr concentration of 750 ppm is also shown for the metasedimentary (metased.) granulite contaminant. The tick marks indicate the minimum (0.70523) and maximum (0.71228) $^{87}Sr/^{86}Sr$ values observed for the tholeiitic suite. The geochemical data for the contaminants are listed in Table 6.1. The C^o_m = 750 ppm curve illustrates that higher degrees of contamination are required for higher C^o_m values. A C^o_m = 750 ppm curve for the southern Etendeka rhyolite, would illustrate that an unrealistic amount of contamination (80 %) would be required to produce the maximum $^{87}Sr/^{86}Sr$ ratio measured.

Fig. 6.3 The plot of $\delta^{18}O$ versus per cent of magma crystallized (100[1-f]), showing calculated changes in $\delta^{18}O$ of a magma that is undergoing combined fractional crystallization and wall rock assimilation (AFC) (equation (3)). The curves have been calculated for various assimilant $\delta^{18}O$ values (+ 7.5, + 9.7 and + 11.5 ‰). Different values of r (9, 7, and 5) are also considered for each assimilant. A $^{18}O/^{16}O$ fractionation of zero is assumed between the melt and the bulk cumulates crystallizing at any instant. The initial $\delta^{18}O$ of the melt is assumed to be + 5.7 ‰. The tick marks indicate the minimum (+ 6.5 ‰) and maximum (+ 9.0 ‰) $\delta^{18}O$ pyroxene values observed for the tholeiitic suite.

A similar plot may be produced for the $^{87}Sr/^{86}Sr$ ratio of the contaminated magma by applying (Faure,1986):

$$(^{87}Sr/^{86}Sr)_m = (^{87}Sr/^{86}Sr)_a\, Sr_a\, f + (^{87}Sr/^{86}Sr)^\circ_m\, Sr^\circ_m\, (1-f) \,/\, (Sr_a\, f + Sr^\circ_m\, (1-f)) \qquad (2)$$

where f is the weight fraction of the assimilant, and the Sr concentration and the $^{87}Sr/^{86}Sr$ ratio of the assimilant and initial magma are denoted by $_a$ and $^\circ_m$ respectively (Fig. 6.2). Curves have been calculated for the maximum amounts of assimilation, by assuming that the uncontaminated magma had an initial $^{87}Sr/^{86}Sr$ ratio equal to the most primitive whole-rock ratio (ie. the lowest $^{87}Sr/^{86}Sr$ ratio, which most closely resembles the ratio of a mantle-derived magma ($^{87}Sr/^{86}Sr \approx 0.704$; Taylor & Sheppard, 1986)) measured throughout the complex (0.70378), and a Sr concentration of 450 ppm. If the magma $^{87}Sr/^{86}Sr$ value is approximated by the whole-rock value, then the observed range (0.70523 - 0.71228) indicates that the most likely material assimilated (19.5 to 71.6 %) was the southern Etendeka rhyolite. If a higher initial magma Sr concentration (750 ppm) is assumed, an unrealistic degree of contamination of up to 80 % is required to produce the higher $^{87}Sr/^{86}Sr$ ratios measured.

6.5 Effects of the AFC process on oxygen isotopes

Taylor & Sheppard (1986) have shown that by assuming 1) the oxygen content of assimilated country rocks, the cumulates and silicate melt are identical and 2) an $^{18}O/^{16}O$ fractionation of zero between the melt and the bulk cumulates crystallizing at any instant, the AFC process may be approximated by:

$$\delta_{magma} \approx \delta_a\, (1-f^{(1/(r-1))}) \quad [\text{ normalized to } \delta^\circ_{magma} = 0 \text{ }] \qquad (3)$$

where δ_{magma} and δ_a are respectively the $\delta^{18}O$ values of the magma and the assimilated country rocks normalized to an initial $\delta^{18}O$ magma value of zero (ie. $\delta^\circ_{magma} = 0$), r is the ratio of cumulates to assimilated rock, and f is the fraction of melt remaining at any stage. Fig. 6.3 shows the percentage of magma crystallized versus the $\delta^{18}O$ value of the magma (‰), which may be approximated from the $\delta^{18}O$ value of the cumulates (‰). By assuming an initial primary mantle $\delta^{18}O$ value close to the value of + 5.7 ‰ of MORB

(Ito *et al.*, 1987; Harmon & Kempton, 1990), curves have been calculated for a series of possible $\delta^{18}O$ values of the assimilant (+ 7.5, + 9.7, + 11.5‰) and r (9, 7, 5). The maximum $\delta^{18}O$ value of pyroxene (9.00 ‰) provides an estimate of the $\delta^{18}O_{magma}$ value at the maximum amount of contamination. Considering that the highest ratio of cumulates to assimilated rock (r) requires the least amount of contamination, the best solution has a $\delta^{18}O$ value of + 11.5 ‰, and an r value of 9. For an assimilant with a $\delta^{18}O$ value of 11.5 ‰, 11.1 % contamination and 58 % crystallization would be required to shift the $\delta^{18}O$ value of a mantle-derived magma (ie. + 5.2 ‰, from a mantle-derived pyroxene) to that of the lowest pyroxene value measured (+ 6.5 ‰). Lower degrees of contamination and crystallization would be required for a parental magma with a higher $\delta^{18}O$ value.

Taylor & Sheppard (1986) argue that the value of r may be reduced to less than 1:1 if the country rocks were very hot or partially molten prior to assimilation. The higher $\delta^{18}O$ values of the outer units may be explained by a lower cumulate / assimilant ratio and intrusion into heated country rocks.

6.6 Effects of the AFC process on the coupled $\delta^{18}O$ - $^{87}Sr/^{86}Sr$ variation

6.6.1 Introduction

Taylor & Sheppard (1986) illustrate how the effects of AFC processes on the $^{87}Sr/^{86}Sr$ - $\delta^{18}O$ system may be modelled by:

$$\gamma_{ox} = [(1 / \gamma_{Sr} - 1) \lambda C^{o}_{m} / C_a + 1]^{-1/\lambda} \qquad (4)$$

where $\gamma = (\varepsilon_m - \varepsilon_a) / (\varepsilon^{o}_{m} - \varepsilon_a)$, $\lambda = 1 - r (1 - \beta)$ and C^{o}_{m} and ε^{o}_{m}, C_m and ε_m, and C_a and ε_a, are respectively, the concentrations and isotope ratios of the particular element in the initial magma, in the magma at any stage f, or in the assimilated country rocks. Here β is defined as the bulk distribution coefficient for the element (bulk crystals/bulk liquid) and is regarded as a constant. The definitions of r and f are the same as for equation (3) above.

6.6.2 Estimation of parameters

The initial magma Sr composition may be estimated from the Sr bulk rock distribution

coefficient and concentration by applying:

$$C^{o}_{m} \approx C_{rock} / (\Sigma^{n}_{i=1} W_i k_{Di}) \quad (5)$$

where W_i and k_{Di} are respectively the weight proportion and distribution coefficient of each mineral (see Table 6.2) (Cox *et al.*, 1979; Aitcheson & Forrest, 1994). The low plagioclase (+ 7.7 ‰) and pyroxene (+ 6.9 ‰) $\delta^{18}O$ values for the olivine leucogabbro (OKJ-068) (Unit 1), suggest that it represents the least contaminated tholeiitic gabbro

Table 6.2 Calculated Sr and Nd bulk distribution coefficients (β) and initial magma concentration estimates for the samples, on which the AFC Aitcheson & Forrest (1994) contamination models for the tholeiitic suite are based.

Sample	β_{Sr}	β_{Nd}	*Sr* C^{o}_{m}	*Nd* C^{o}_{m}
OKJ-018	1.50	0.33	446	58.5
OKJ-031	2.02	0.23	234	57.4
OKJ-033	2.12	1.17	231	17.6
OKJ-038	1.99	0.67	270	54.2
OKJ-040	1.67	1.11	298	39.5
OKJ-041	1.67	0.57	232	38.9
OKJ-043	3.05	0.50	128	79.8
OKJ-044	1.95	0.20	199	205
OKJ-045	2.98	0.73	107	80.8
OKJ-046	2.44	0.61	123	70.2
OKJ-047	2.88	0.33	110	140.6
OKJ-062	1.35	0.14	361	62.1
OKJ-063	1.33	0.15	266	86
OKJ-068	1.78	0.22	274	487

Notes:

1) The bulk rock distribution coefficients have been calculated for the partition coefficients listed in Table 4.1 of Appendix 4.

2) The initial magma Sr and Nd compositions have been estimated from the Sr and Nd bulk rock distribution coefficients and concentrations by applying: $C^{o}_{m} \approx C_{rock} / (\Sigma^{n}_{i=1} W_i k_{Di})$, where W_i and k_{Di} are respectively the weight proportion and distribution coefficient of each mineral (Cox *et al.*, 1979; Aitcheson & Forrest, 1994).

sample. The minimum initial magma Sr concentration may be estimated to lie close to 274 ppm, by substituting the Sr concentration (487 ppm) and calculated Sr bulk distribution coefficient (1.78) (see Appendix 4) of OKJ-068 into equation (5). In addition, the simple oxygen and strontium mixing models indicate that 1) the initial magma Sr concentration was probably closer to 450 than 750 ppm (Fig. 6.2), and 2) the northern Etendeka rhyolite and igneous granulite assimilants require unrealistically large degrees of contamination. The average for the minimum C^{o}_{m}/C_{a} values calculated for the Sr concentrations in the southern Etendeka rhyolite (167 ppm), metasedimentary granulite (287 ppm), Sorris-sorris granite (118 ppm) and Kuiseb micaschists (130 ppm), and the minimum initial magma Sr concentration (274 ppm), lies at 1.73 ± 0.6 .

Considering that the average modal abundance of plagioclase in the tholeiitic gabbros is 57.6 % ± 10.3, and assuming that the partition coefficient of plagioclase equals 2.5 (Korringa, 1977; see Appendix 4), it may be seen that the average Sr bulk distribution coefficient (ß) will lie above 1.44 ± 0.3 . These arguments are in accordance with Taylor & Sheppard (1986), who argue that 1) the value of C^{o}_{m}/C_{a} may be assumed ≥ 1 and 2) the value of β for plagioclase crystallizing as a cumulate phase in a crustal magma chamber is greater than 1. For the $\delta^{18}O$ - $^{87}Sr/^{86}Sr$ model curves calculated here, the values of C^{o}_{m}/C_{a} and β are varied from 1 to 10 and from 1.0 to 2.0 respectively. The β = 1.0 curves coincide with simple mixing hyperbolae.

The lower limit of the $\delta^{18}O$ - $^{87}Sr/^{86}Sr$ model curves is constrained by an initial primary mantle $\delta^{18}O$ value of 5.7 ‰ (Ito *et al.*, 1987; Harmon & Kempton, 1990), and the most primitive mantle-like (0.704; Taylor & Sheppard, 1986) initial $^{87}Sr/^{86}Sr$ ratio (ie. the lowest ratio) measured throughout the complex, which is 0.70378. The upper limit of the curves trend towards the oxygen and strontium isotope composition of the selected assimilant.

The $^{87}Sr/^{86}Sr$ initial ratios of the possible assimilants (Table 6.1) have been recalculated to t = 130 Ma by:

$$^{87}Sr/^{86}Sr_{t} = {}^{87}Sr/^{86}Sr_{present} - {}^{87}Rb/^{86}Sr\ (e^{\lambda t} - 1) \qquad (6)$$

where $\lambda = 1.42 \times 10^{-11}$.

6.6.3 Results

The results of the simple mixing models and the characteristics, discussed in section 6.3, strongly suggest that the assimilant may have been derived from the same source as the the southern Etendeka rhyolite. A number of model curves have been calculated for the southern Etendeka rhyolite to illustrate the effects of varying the different model parameters (Figs. 6.4a - d). The curves are arbitrarily terminated where the original magma is 99 % crystallized (f = 0.01). From Fig. 6.4a, it may be seen that reducing the ratio of the cumulates to assimilated rock (r), has the same effect as reducing the bulk distribution coefficient (β) value. For a constant C^{o}_{m}/C_{a} value of 10, the outer units (4 to 6) require lower r ($9 > r > 5$) and higher β (1.3 - 1.6) values than the inner units (1 & 3) ($r = 9$; $\beta = 1.2$). It may be seen from Fig. 6.4b that steeper curves may be generated by increasing the C^{o}_{m}/C_{a} value. Most of the data values may be constrained by the $\beta = 1.0$ and 1.1 curves for $C^{o}_{m}/C_{a} = 2$.

Curves have also been produced for initial magma Sr concentrations of 450 ppm ($C^{o}_{m}/C_{a} = 2.7$) and 360 ppm ($C^{o}_{m}/C_{a} = 2.2$) (Fig. 6.4c). If one assumes that the minimum ß value exceeds 1.4 (see section 6.6.2), then both figures 6.4b and 6.4c suggest that the C^{o}_{m}/C_{a} ratio exceeded 3. The low $\delta^{18}O$ and $^{87}Sr/^{86}Sr$ values for the olivine leucogabbro (Unit 1) (OKJ-068), gabbro (Unit 4) (OKJ-004) and monzodiorite (OKJ-045) samples may be explained by higher r values (ie. lower amounts of assimilation). The progressive increase in the $\delta^{18}O$ values of the outer Units 4 to 6 may be explained by an increase in the percentage of magma crystallized and a decrease in the r value (ie. an increase in the amount of assimilated material).

Curves for the Sr concentration versus initial $^{87}Sr/^{86}Sr$ ratio for various C^{o}_{m}/C_{a}, β, r and C^{o}_{m} parameter value combinations are shown in Fig. 6.4d . The model curves generated for a β value equal to 1.4, and a southern Etendeka rhyolite assimilant may be reconciled with the measured Sr concentrations of the tholeiitic suite. Fig. 6.4d also indicates that the higher Unit 4 $^{87}Sr/^{86}Sr$ ratios may have been produced by the assimilation of a contaminant with a $^{87}Sr/^{86}Sr$ ratio equal 0.75 (see the curve labelled by an "A" symbol).

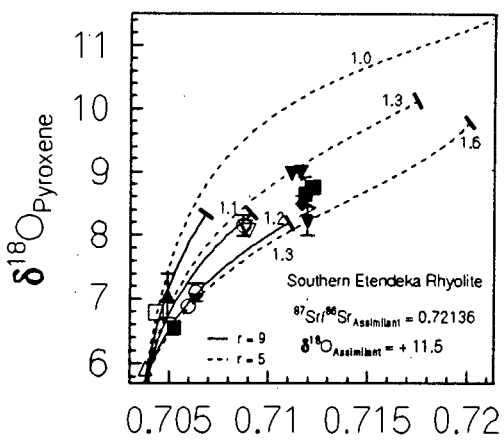

Fig. 6.4a

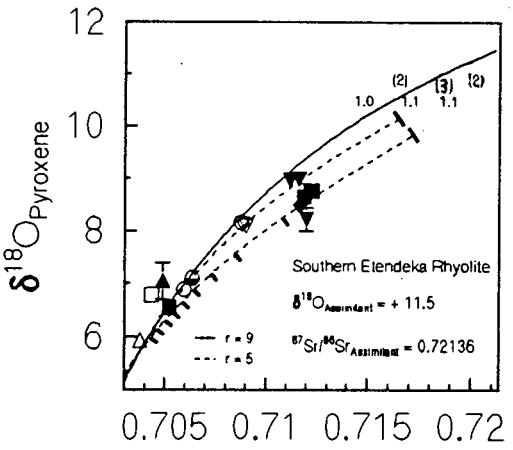

Fig. 6.4b

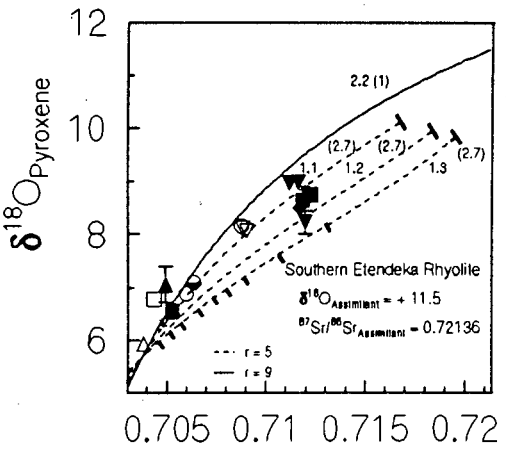

Fig. 6.4c

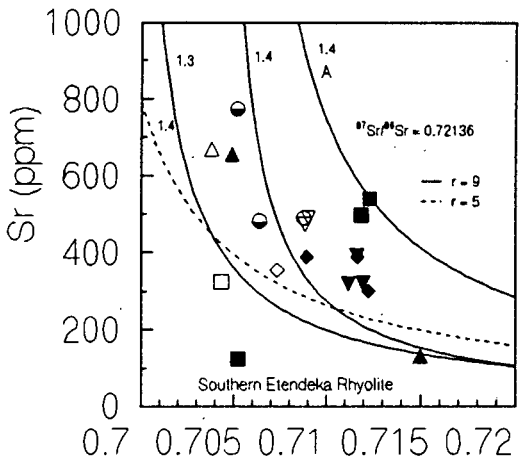

Fig. 6.4d

Fig. 6.4a - Fig. 6.4c Plots of $\delta^{18}O$ versus $^{87}Sr/^{86}Sr$, showing various trajectories that would be followed during combined assimilation-fractional crystallization (AFC) in a magma chamber. The $\delta^{18}O$ (+ 11.5 ‰) and $^{87}Sr/^{86}Sr$ (0.72136) values are selected for a southern Etendeka rhyolite assimilant. The β value for each curve is listed adjacent to the curve. The β = 1.0 lines are coincident with simple hyperbolic mixing curves. The end points of the curves are placed at 99 % crystallization (f = 0.01). The tick marks in Figs. 6.4b and 6.4c, indicate the percentage of magma crystallized at 10 % intervals from 10 to 90 %. The value of the initial ratio of ppm Sr in the magma to that in the country rocks (C°_m/C_a) is indicated in brackets for each curve, except for Fig. 6.4a, where it is assumed to equal a constant value of 10. The ratio of cumulates to assimilated rock is denoted by the r symbol, and is varied from 5 to 9. Other symbols used are: (1) tholeiitic suite units: 1 (○), 2 (◇), 3 (▽), 4 (■), 5 (◆) and 6 (▼), (2) alkaline gabbro (◒), (3) syenite (▲), (4) nepheline syenite (□) and (5) essexite dyke / oligoclase essexite (△). The β = 1.1 curves in Fig. 6.4b, for C°/C_m values equal to 3 and 2, indicate that steeper curves may be generated by increasing the C°_m/C_m ratio.
(Note that where errors are not shown, the magnitude of the error is smaller than the symbol size.)
Fig. 6.4d Plot of the calculated Sr contents (ppm) of the magmas at each stage (C_m) versus the $^{87}Sr/^{86}Sr$ values. Curves are shown for C°_m/C_m = 10, β = 1.3 - 1.4, C_a = 450 ppm, and C°_m = 450 ppm. The curve labelled by the "A" symbol has been calculated for an assimilant $^{87}Sr/^{86}Sr$ value = 0.75.

The curve for a metasedimentary granulite contaminant, which best fits the inner units (1 - 3) and outer Unit 6, has C^{o}_{m}, β and r values of 1.3, 1.0 and 9 respectively (Fig. 6.5). The higher amounts of assimilated material (ie. r > 5) required to generate the $\delta^{18}O$ values of the outer units (4 - 6) indicates the lower likelihood of a metasedimentary granulite contaminant.

Simple mixing hyperbolae for the Sorris-Sorris granite indicate that the inner and outer units of the tholeiitic suite require C^{o}_{m}/C_{a} values in the range of 8 to 3.8 and 8 to 3.1 respectively (Fig. 6.6). The C_{a} value (118 ppm) for the Sorris-Sorris granite, produces C^{o}_{m} values in the range of 944 - 590 ppm and 944 - 448 ppm for the inner and outer units respectively. This model requires unrealistically high initial magma Sr concentrations (C^{o}_{m}), which by far exceed the maximum C^{o}_{m} value calculated for the tholeiitic gabbros (361 ppm) (Table 6.2).

The best fit curve for a Kuiseb mica schist contaminant (C^{o}_{m}/C_{m} = 3.5, β = 1.1 and R = 9) indicates that tholeiitic suite was produced while 40 % - 70 % of the magma crystallized (Fig. 6.7). Such a contaminant would unrealistically require that the r values were higher than 9 for the entire suite.

6.7 AFC models for magma recharge and non-recharge

6.7.1 AFC without magma recharge

Aitcheson & Forrest (1994) derived the following formula for the crust / magma ratio, ρ, for the AFC situation which does not involve magma recharge:

$$\rho = r / (r-1) \left\{ \left[1 + \lambda (r + D - 1) / (r \gamma) \right]^{(r-1)/(r+D-1)} - 1 \right\} \text{ for } r + D \neq 1, r \neq 1 \qquad (7)$$

where r, λ, γ and D are as defined in the Notation (see Table 6.3). The values of r and D are considered constant. This relation allows λ to be determined without estimates of the fraction of magma remaining or the concentration of the element in the contaminated magma. Independent estimates of the r and ρ values may be obtained by applying the graphical technique outlined by Aitcheson & Forrest (1994) to solve the set of multi-element simultaneous equations of the above form. The values r and ρ are best

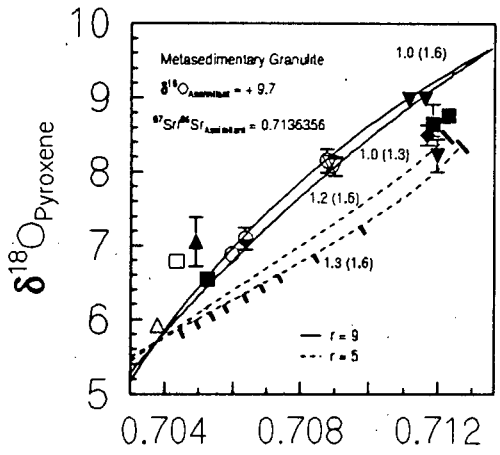

Fig. 6.5 $^{87}Sr/^{86}Sr_{initial}$

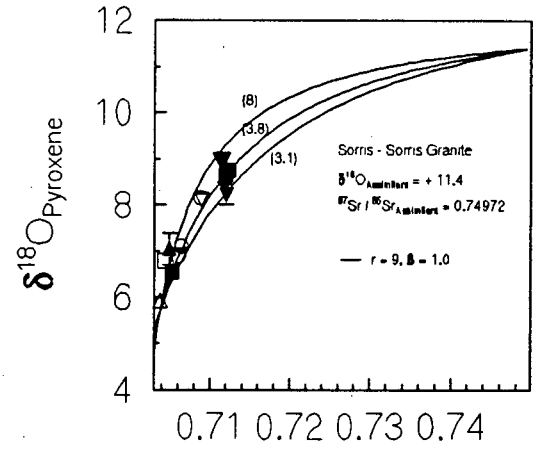

Fig. 6.6 $^{87}Sr/^{86}Sr_{initial}$

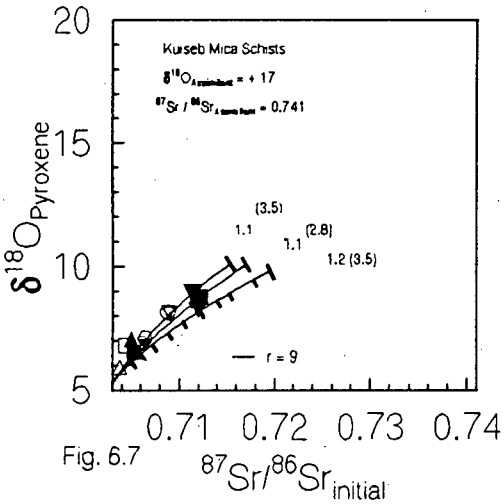

Fig. 6.7 $^{87}Sr/^{86}Sr_{initial}$

Fig. 6.5 - Fig. 6.7 Plots of $\delta^{18}O$ versus $^{87}Sr/^{86}Sr$, showing various trajectories that would be followed during combined assimilation-fractional crystallization (AFC) in a magma chamber. The $\delta^{18}O$ and $^{87}Sr/^{86}Sr$ values of the following possible assimilants: metasedimentary granulite (Fig. 6.5), Sorris-sorris granite (Fig. 6.6), and a Kuiseb mica schists (Fig. 6.7), are listed within each diagram. The β value for each curve is listed adjacent to the curve, except in Fig. 6.6, where it equals a constant value of 1.0. The end points of the curves are placed at 99 % crystallization (f = 0.01). The tick marks in Figs. 6.5 and 6.7, indicate the percentage of magma crystallized at 10 % intervals from 10 to 90 %. The value of the initial ratio of ppm Sr in the magma to that in the country rocks (C°_m/C_a) is indicated in brackets for each curve in all the diagrams. The ratio of cumulates to assimilated rock is denoted by the r symbol, and is varied from 5 to 9. Other symbols used are: (1) tholeiitic suite units: 1 (○), 2 (◇), 3 (▽), 4 (■), 5 (♦) and 6 (▾), (2) alkaline gabbro (◒), (3) syenite (▲), (4) nepheline syenite (□) and (5) essexite dyke / oligoclase essexite (△).

Table 6.3 This dissertation follows the notation of DePaolo (1981), Taylor & Sheppard (1986) and Aitcheson & Forrest (1994).

- Notation -	
M_m	mass of magma remaining (including neutrally buoyant crystals)
M^o_m	mass of original magma
M_a	mass of crust assimilated
M_c	mass of crystals effectively separated from the magma
M_r	total mass of recharge magma added to the system
$F = M_m/M^o_m$	fraction of magma remaining in non-recharge situations
r	(rate of assimilation of crust)/(rate of fractional crystallization)
D	bulk distribution coefficient of the element
C_m	element concentration in the contaminated magma
ε_m	isotopic ratio in the contaminated magma
C_a	element concentration in wall-rock melt
ε_a	isotopic ratio in the wall-rock melt
C^o_m	element concentration in the original magma
ε^o_m	isotopic ratio in the original magma
$\rho = M_a/M^o_m$	crust / magma ratio in non-recharge situations
or $M_a/(M^o_m + M_r)$	crust / magma ratio in situations involving magma recharge or replenishment
$\beta = M_r/M_a$	(rate of magma replenishment)/(rate of assimilation)
or	
β	bulk distribution coefficient for element ($\delta^{18}O$-$^{87}Sr/^{86}Sr$ plots)
$\lambda = (\varepsilon^o_m - \varepsilon_m)/(\varepsilon_m - \varepsilon_a)$	
$\gamma = C_a / C^o_m$	
C_r	element concentration in the recharge magma
ε_r	isotopic ratio in the recharge magma

constrained by high curve intersection angles which are observed for elements with widely differing D values. The technique is thus well suited to model Sr (D = 2.19), Nd (D = 0.66) (these are the average D values for the tholeiitic suite; see Table 6.2), and O (D assumed as 1) (Aitcheson & Forrest, 1994) isotope data.

The value of r is strictly greater than 0. This may result in incomplete graphs for elements with D values less than unity. A further restriction on the minimum value of r may be obtained by applying the following inequality for values of D < 1:

$$r \geq \lambda (1 - D) / (\gamma + \lambda) \qquad (8)$$

6.7.2 Values of the parameters used in the calculation of ρ

The values of the parameters used in the calculation of the crust / magma ratio (ρ) in the tholeiitic suite are listed in Table 6.4 . Aitcheson & Forrest (1994) illustrate that the largest error contributions are from C^{o}_{m}, ε_a and C_a, whereas contributions by uncertainties in D are trivial. The D values, which may be calculated by the denominator of equation (5), are listed in Table 6.2 . The values of D, C_a and C^{o}_{m} for oxygen may be assumed to be 1, 50 and 50 respectively (Aitcheson & Forrest; 1994). The D values for Sr (2.19) and Nd (0.66) are the average values for the tholeiitic suite. The C_a and ε_a values are estimated for a southern Etendeka rhyolite assimilant. The initial Sr and Nd magma compositions have been estimated by equation (5). The $^{87}Sr/^{86}Sr$ initial ratios have been recalculated to t = 130 Ma by equation (6) (see Section 6.6.2). Similarly, the initial $^{143}Nd/^{144}Nd$ values have been recalculated using:

$$^{143}Nd/^{144}Nd_t = {}^{143}Nd/^{144}Nd_{present} - {}^{147}Sm/^{144}Nd\ (e^{\lambda t} - 1) \qquad (9)$$

where $\lambda = 6.54 \times 10^{-12}$. The ε_{Nd} value has been calculated by:

$$\varepsilon_{Nd} = ((^{143}Nd/^{144}Nd_{sample(t)})/(^{143}Nd/^{144}Nd_{CHUR(t)}) - 1) \times 10^4 \qquad (10)$$

where $^{147}Sm/^{144}Nd = 0.1967$ for CHUR and the present-day $^{143}Nd/^{144}Nd = 0.51262$.

The values of C_a and ε_a have been estimated for a southern Etendeka rhyolite assimilant (see Table 6.4). The ε_m values are estimated from the tholeiitic suite samples with the

Table 6.4 Parameters used for calculation of the crust / magma ratio in the tholeiitic olivine gabbro - quartz monzodiorite suite.

	Sr	*O*	*Nd*
Parameter values			
D	2.19_1	1.0_3	0.66_1
C_a	153_2	50_3	40.4_6
C^o_m	380_1	50_3	60_1
ε_a	0.71705_2	$+10_2$	-8.8535_6
ε^o_m	0.70378_1	$+5.7_4$	4.6384_1
ε_m	0.70559_1	$+6.7_5$	0.284785_1
Ranges			
D	(1.33 - 3.05)	(0.99 - 1.01)	(0.14 - 1.17)
C_a	139 - 167	45 - 55	34.5 - 46.2
C^o_m	360 - 450	45 - 55	62.1 - 58.5
ε_a	0.71274 - 0.72136	+9.00 - +11.5	-9.42 - -8.29
ε^o_m	0.70328 - 0.70428	+5.4 - +6.0	4.6384 - 8.5
ε_m	0.70523 - 0.70595	+6.5 - +6.9	-0.6387 - 1.20831

Note: The best estimate for the value of each parameter is illustrated in the top half of the table. The ranges of possible values assumed for each parameter are shown in the lower half. Concentrations are in ppm, except for oxygen, which is in per cent. The isotope ratios are given as $^{87}Sr/^{86}Sr$, ε_{Nd}, and $\delta^{18}O$. The parameter values have been estimated from the following data sources: (1) Milner *et al.* (1994); (2) Harris *et al.* (1990); Harris (1995); (3) Aitcheson & Forrest (1994); (4) Ito *et al.* (1987); Harmon & Kempton (1990); (5) this work; (6) Hawkesworth *et al.*(1984). See Section 6.7.2 for further details.

most primitive whole-rock $^{87}Sr/^{86}Sr$ ratios (OKJ-004 and OKJ-068) (ie. the lowest $^{87}Sr/^{86}Sr$ ratios, which most closely resemble the ratio for a mantle-derived magma ($^{87}Sr/^{86}Sr \approx$

0.704)) (Table 5.1). A primary mantle value of + 5.7 ‰ is assumed for the initial $\delta^{18}O$ of the magma (Ito *et al.*, 1987; Harmon & Kempton, 1990). The initial $^{87}Sr/^{86}Sr$ ratio (0.70378) and ε_{Nd} value (4.6384) of the magma are estimated from the sample with the most primitive (ie. lowest and most mantle-like value, which assumed to represent the minimum value of the uncontaminated magma) initial $^{87}Sr/^{86}Sr$ ratio measured throughout the complex (OKJ-018) (Table 5.1). The C^o_m values for Sr and Nd are calculated by equation (5) (Table 6.2). The average C^o_m value for Sr (360 ppm) is calculated from average the samples with the most primitive $^{87}Sr/^{86}Sr$ ratios measured throughout the complex (OKJ-018) (450 ppm), and within the tholeiitic gabbro transect (OKJ-068) (270 ppm) . The average C^o_m value for Nd (60 ppm), is calculated from OKJ-018 (58.5 ppm), and the tholeiitic gabbro sample OKJ-068 (62.1 ppm), which is derived from Unit 1. Estimates of the C^o_m Sr (380 ppm) and Nd (60 ppm) are calculated by equation (5) for the average concentrations of these elements in the tholeiitic suite unit 1 (OKJ-062) and the essexite dyke.

6.7.3 Results for AFC without magma recharge

The value of r indicated by the Sr - O intersection in Fig. 6.8a is 0.2 . The minimum r value indicated by applying the above inequality (equation (7)) for the Nd D value (0.66), is 0.141. The rate of assimilation was thus about 5 to 7 times slower than the rate of fractional crystallization. The value of ρ lies at 0.133 and indicates that the amount of crustal contamination was in the order of 13 %. The ranges in the possible values of ρ (0.13 - 0.21) and r (0.18 - 0.5) have been calculated by the parameter replacement scheme outlined by Aitcheson & Forrest (1994), and are shown in Fig. 6.8b . The upper limits of these ranges place the maximum amount of crustal contamination at 21 %, for an unrealistically high rate of assimilation (ie. half the rate of fractional crystallization). Making no assumption about the value of r, the value of ρ lies in the range of 0.13 to 0.21, ie., the tholeiitic suite as a whole forms 11 - 17 % crust in the system [as the percentage of crust in the system is given by ρ / (1 + ρ) x 100]. These results compare favourably with the results of analogous calculations for the upper zone of the Lille Kufjord layered gabbro intrusion (Aitcheson & Forrest, 1994), which as a whole forms 2 - 14 % crust. The absence of intersections involving Nd may be attributed to the low Nd D value (0.66).

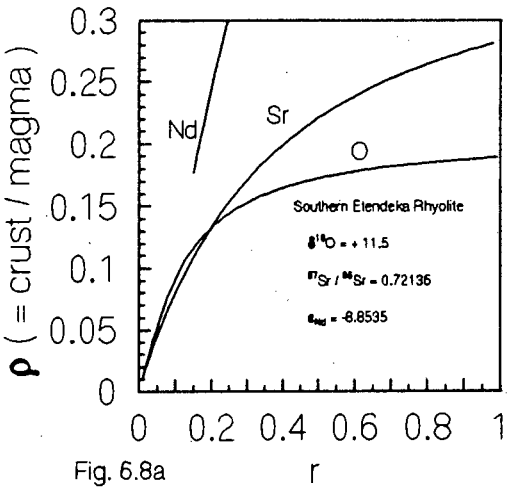

Fig. 6.8a

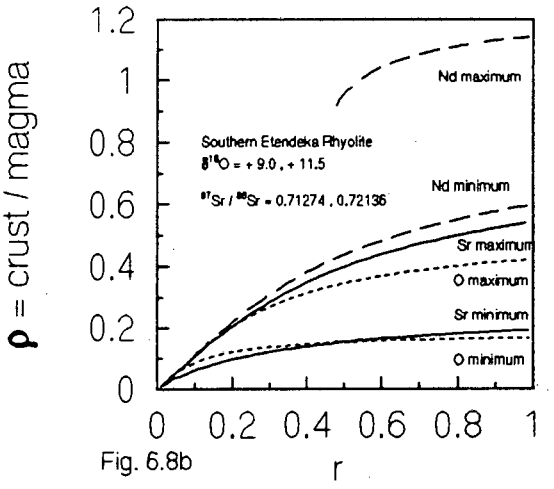

Fig. 6.8b

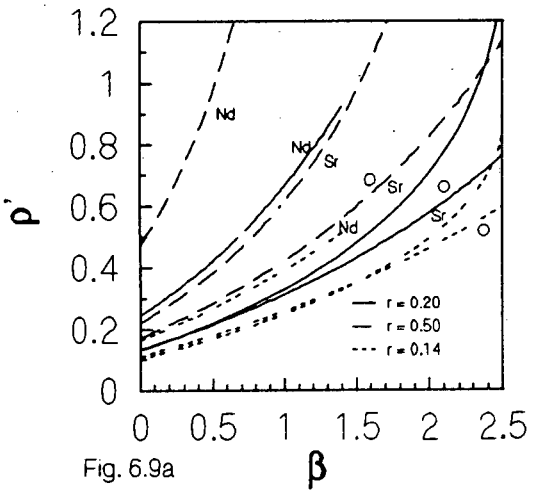

Fig. 6.9a

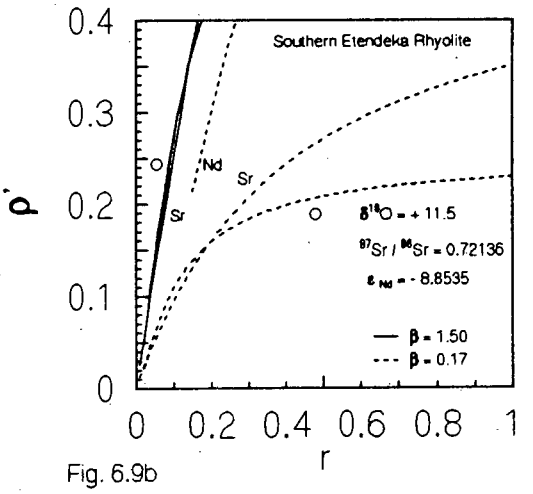

Fig. 6.9b

Fig. 6.8a Sr, O and Nd ρ-r curves for the case of AFC without recharge. The curves were calculated using equation (6) and the parameter values given in Table 6.3 , and do not take errors into account. The intersecton of the curves gives a best estimate of the values of r (= rate of assimilation / rate of fractional crystallization) and ρ (crust / magma). The $\delta^{18}O$ (+ 11.5 ‰), $^{87}Sr/^{86}Sr$ (0.72136) and ε_{Nd} (-8.8535) values are selected for a southern Etendeka rhyolite assimilant.

Fig. 6.8b Sr, O and Nd ρ-r curves for the maximum and minimum possible values of ρ, for the case of AFC without recharge. The curves were drawn using equation (6) and the maximum and minimum possible values of the parameter ranges in Table 6.3 . The possible values of ρ and r are defined by the area common to both pairs of maximum -minimum curves. The ranges indicated for the possible values of ρ and r, are (0.13 - 0.21) and (0.18 - 0.5) respectively.

Fig. 6.9a Cross-sections through the ρ-β surfaces calculated for the tholeiitic olivine gabbro - quartz monzodiorite suite for the case of AFC with magma recharge. The cross-sections were chosen for possible r values of 0.141, 0.2 and 0.5 . The Sr and O curves for r values greater than 0.21 intersect at β values which are less than or equal to 0 (ie. the case of no magma recharge). The r = 0.2 set of curves thus represent an estimate of the minimum β value.

Fig. 6.9b Cross-sections through the ρ-r surfaces for the β values of 1.5 and 0.17, which have been determined for r values of 0.141 and 0.2 respectively (see Fig. 6.9a). Both of the above figures indicate ρ' values of 0.16 and 0.36.

6.7.4 AFC with magma recharge

A false assumption of zero recharge leads to increasing overestimates of ρ with increasing D values. Aitcheson & Forrest (1994) derive formulae for the calculation of the (crust / magma) ratio for the case of AFC with periodic or continuous magma replenishment. By assuming that: 1) the recharge magma composition is identical to that of the original magma and 2) the values of D, r and β remain constant during magma crystallization, the ρ value may be estimated by:

$$\rho \text{ (recharge)} = M_a / (M^\circ_m + M_r) = \rho' / (\beta (1 + \rho') + 1) \quad (11)$$

$$\text{where: } \rho' = \frac{(1+\beta)r}{((1+\beta)r-1)} \cdot \frac{\left\{\left(1 + C^\circ_m(\varepsilon^\circ_m-\varepsilon_m)[(1+\beta)r+D-1]\right)^{((\beta+1)r-1)/((\beta+1)r+D-1)} - 1\right\}}{r[C_a(\varepsilon_m-\varepsilon_a)-\beta C_r(\varepsilon_r-\varepsilon_m)]} \quad (12)$$

The values of ρ, r, ρ' may be estimated independently from the surface intersections if three or more elements are considered. For the case of $C_r = C^\circ_m$ and $\varepsilon_r = \varepsilon^\circ_m$, the following inequalities may be used to determine the minimum and maximum r values:

$$r \geq \lambda (1-D) / (\lambda + \gamma) \quad \text{if } \gamma > \beta \lambda \quad (13)$$

and

$$r \leq \lambda (1-D) / (\lambda + \gamma) \quad \text{if } \gamma < \beta \lambda \quad (14)$$

6.7.5 Results for AFC with magma recharge

For the inequality equation (8), the λ and γ values for Sr and O indicate that the r value exceeds - 0.335 and 0 respectively. The Nd λ (0.476415) and γ (0.67333) values indicate that for β greater than 1.413 (γ / λ), r is less than or equal to 0.141 (equation (14)), and for β less than 1.413, r is greater than or equal to 0.141 (equation (13)).

Curves of ρ' versus β values have been calculated by equation (12) for r values of: 0.141, 0.2 and 0.5 (Fig. 6.9a). The values of ρ are calculated from equation (11). Figure 6.9a indicates that the r value was less than 0.5 for the magma recharge situation. Not shown are curves for r values of 0.4 and 0.3 which have Sr - O intersections at β values less than or equal to 0 (ie. non-recharge situation). For r = 0.2, β = 0.17 and ρ = 0.2 (ρ' = 0.16).

For r = 0.141, β = 1.5 and ρ = 0.12 (ρ' = 0.36). The lower value of ρ, suggests that the true r value may have been closer to 0.141 than 0.2 .

For an r value of 0.2, r β = M_r / M_c = 0.2 X 0.17 = 0.034 and the relative sizes of M_a : M_c : M_r are 20 : 100 : 3.4 . Thus the rate of fractional crystallization was five times the rate of assimilation and about 30 times the magma recharge rate. For a r value of 0.141, r β = M_r / M_c = 0.141 X 1.5 = 0.21 and the relative sizes of M_a : M_c : M_r are 14 : 100 : 21. This suggests a crystallization rate seven times the assimilation rate and five times the recharge rate. The crust / magma budget for both r value possibilities are illustrated schematically in Fig. 6.10 . These results compare favourably with analogous calculations for lavas of the Andean Central Volcanic Zone (CVZ), for which the rate of fractional crystallization was about double the rate of recharge and six times the rate of assimilation of the wall rocks (Aitcheson & Forrest, 1994). In contrast, however, the magma recharge rate appears to have been much slower relative to the CVZ lavas, for which the rate of fractional crystallization was double that of the recharge rate.

6.8 Summary

Assuming that the most likely contaminant is that which requires the least amount of contamination, the simple mixing models for the oxygen and strontium isotope data are consistent with contamination of the tholeiitic suite by crustal material derived from the same source as the southern Etendeka rhyolite. The $\delta^{18}O$-$^{87}Sr/^{86}Sr$ curves calculated for a Kuiseb mica schist assimilant ($\delta^{18}O$ = + 17 ‰), require less than 11 % contamination for the entire tholeiitic suite. It should be noted, however, that the $\delta^{18}O$ value selected for the Kuiseb mica schist is an extreme value, and that the typical Kuiseb schist $\delta^{18}O$ compositions lie well below this value. The maximum amounts of crustal contaminant assimilated, have been calculated by assuming a mantle-like $\delta^{18}O$ value, equal to the value of 5.7 ‰ of MORB, and an initial $^{87}Sr/^{86}Sr$ ratio equal to the lowest ratio (least contaminated) measured throughout the complex (0.70378), for the uncontaminated magma. The maximum amounts of assimilation (%) required by the $\delta^{18}O$ and initial $^{87}Sr/^{86}Sr$ simple mixing models, for an assimilant derived from the same source as the southern Etendeka rhyolite, are: 14 - 57 % and 19.5 to 71.6 % respectively. Lower degrees of contamination would be required if more evolved oxygen and strontium

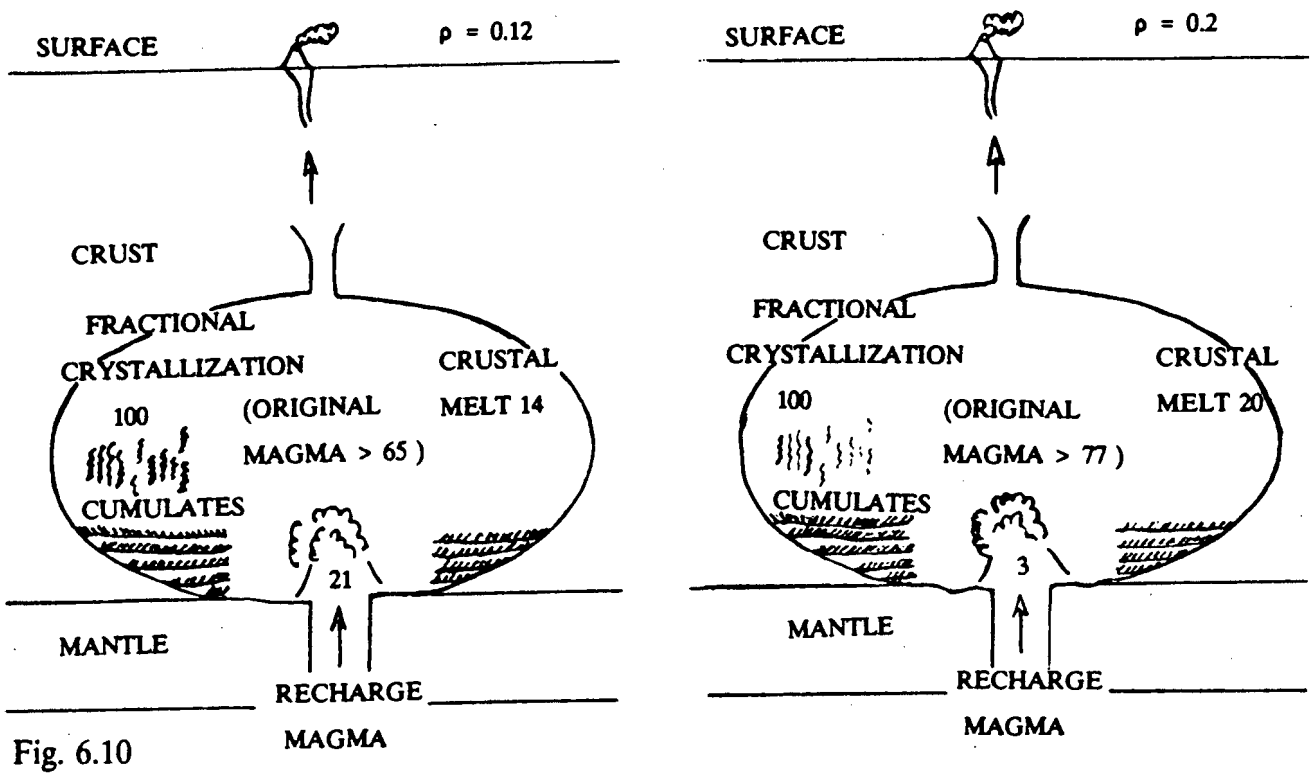

Fig. 6.10

Fig. 6.10 Schematic illustration of the crust / magma budget for the tholeiitic suite based on the calculated values for r, ρ and β. The two cases for r = 0.2 and r = 0.141 are shown. The number after each component is its mass relative to the other components in the system. The diagram illustrates two AFC models with distinctly different magma recharge rates, which may be applied to the tholeiitic suite. For a constant rate of fractional crystallization, a system with a crust to magma ratio (ρ) equal to 0.12, requires a magma recharge rate seven times that of a system with a ρ value equal to 0.2.

isotope compositions (ie. higher $\delta^{18}O$ and $^{87}Sr/^{86}Sr$ values), were assumed for the uncontaminated magma. The $\delta^{18}O$-$^{87}Sr/^{86}Sr$ curves calculated for the various possible assimilants and parameter estimates, are reconcilable with the crystallization of cumulus plagioclase in a moderate to shallow plutonic environment. The effects of magma mixing on the oxygen isotope geochemistry of outer units may be further considered by construction of models with values for the ratio of cumulates to assimilated rock in the range of 7 to 5.

The presence of O - Sr isotope curve intersections on the ρ-β-r plots illustrate that the observed variations in the oxygen and strontium isotope data (see Chapter 5) for the tholeiitic suite may be attributed to an AFC process with / without magma recharge. For the case of magma recharge, if r = 0.141 and β = 1.5, the crust / magma ratio is 0.12 . Alternatively, for r = 0.2 and β = 0.17, a crust / magma ratio of 0.2 is indicated.

Chapter 7 - Water-rock interactions -

7.1 Introduction

The petrographic observations and oxygen isotope disequilibria of the feldspar-clinopyroxene and feldspar-olivine mineral-pairs in the nepheline syenite, monzodiorite (Units 5 & 6), tholeiitic gabbro (Unit 2) and alkaline gabbro, which are indicative of minor hydrothermal alteration, have been discussed previously. The petrographic observations do not reveal whether the biotite present is primary (ie. crystallized from a magma) or secondary (ie. formed by subsolidus alteration of a pre-existing primary mineral) in origin. This section aims to 1) determine the primary or secondary nature of the biotite, 2) quantify the water/rock (W/R) ratios during alteration of the tholeiitic suite and the alkaline gabbro, 3) determine possible alteration temperature ranges and initial fluid $\delta^{18}O$ values, and 4) consider possible sources for the alteration fluids.

7.2 Origin of biotite

The petrographic observations indicate that biotite is present both as an interstitial phase and as large, possibly primary, flakes which rim Fe-Ti oxide minerals in the tholeiitic suite. A plot of the value of $\Delta_{plagioclase\text{ - }pyroxene}$ (‰) versus the biotite modal abundance (%) shows no systematic variation (Fig. 7.1). As discussed previously, $\Delta_{plagioclase\text{ - }pyroxene}$ changes with increased amount of exchange with fluid. The absence of a correlation indicates that the biotite is not related to the influx of an external fluid, but could be derived from a deuteric fluid at subsolidus temperatures (ie. by the interaction of a residual magmatic fluid with the primary minerals).

7.3 Deviations from isotopic equilibrium

A plot of the biotite $\delta^{18}O$ (‰) versus $\Delta_{Plagioclase\text{ - }Pyroxene}$ value (‰) is shown in Fig. 7.2. The absence of a statistically significant correlation ($r = 0.49$, $n = 7$) for the tholeiitic suite data in Fig. 7.2, is consistent with a deuteric origin for the biotite within the tholeiitic gabbro. In contrast, the occurrence of biotite as coronas around Fe-Ti oxides and amphibole, suggests a secondary, rather than primary origin for the biotite within the

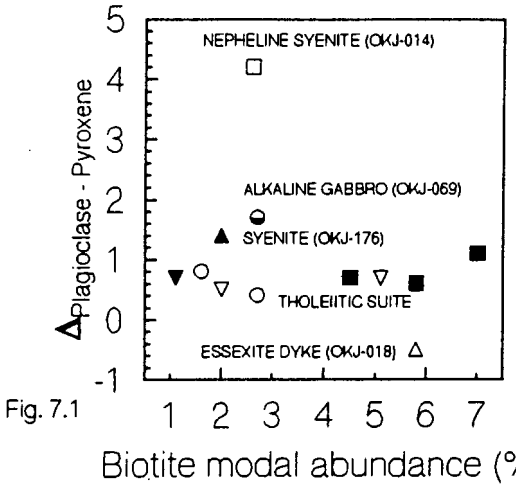

Fig. 7.1

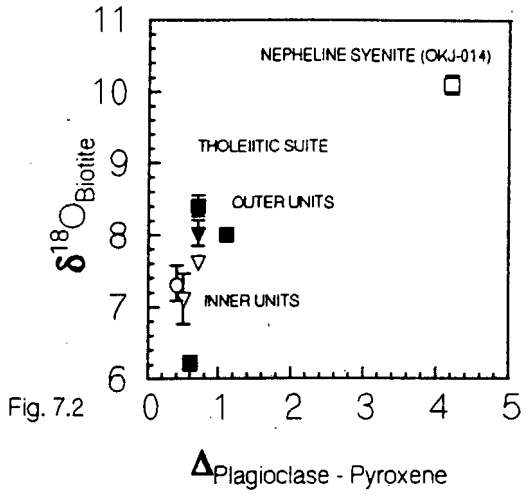

Fig. 7.2

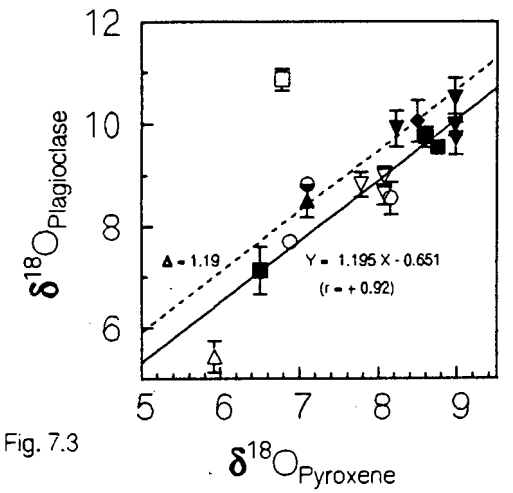

Fig. 7.3

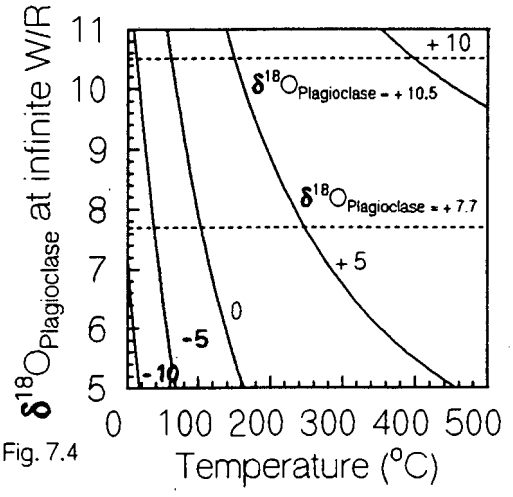

Fig. 7.4

Fig. 7.1 Plot of the plagioclase-clinopyroxene fractionation factor ($\Delta_{plagioclase - clinopyroxene}$) (‰) versus the biotite modal abundance (%). Symbols used are: (1) tholeiitic suite units: 1 (○), 2 (◇), 3 (▽), 4 (■), 5 (♦) and 6 (▾), (2) alkaline gabbro (◒), (3) syenite (▲), (4) nepheline syenite (□) and (5) essexite dyke / oligoclase essexite (△).

Fig. 7.2 Plot of the biotite $\delta^{18}O$ (‰) versus the $\Delta_{plagioclase - clinopyroxene}$ value (‰). Note that where errors are not shown, the magnitude of the error is smaller than the symbol size.)

Fig. 7.3 Plot of the plagioclase $\delta^{18}O$ (‰) versus the pyroxene $\delta^{18}O$ (‰) value. Also shown are the $\Delta_{Plagioclase - Pyroxene}$ fractionation factor lines for: 1) $\Delta_{Albite-Diopside}$ = 1.58 (Mathews *et al.*, 1983), 2) $\Delta_{Plagioclase-Pyroxene}$ = 1.186 (calculated from: $\Delta = 1.70 - 1.04\,\beta$, where β = 0.494 represents the average anorthite mole fraction for the tholeiitic suite) (Bottinga & Javoy, 1975), and 3) the linear regression through the tholeiitic suite data: Y = 1.195 X + 0.651 (r = + 0.922). (See section 7.3 for further details.) Symbols used are: (1) tholeiitic suite units: 1 (○), 2 (◇), 3 (▽), 4 (■), 5 (♦) and 6 (▾), (2) alkaline gabbro (◒), (3) syenite (▲), (4) nepheline syenite (□) and (5) essexite dyke / oligoclase essexite (△).

Fig. 7.4 Plot of the final $\delta^{18}O$ value (‰) in the gabbro altered at an infinite W/R ratio versus the temperature (°C). The curves shown were calculated by: $\delta^{f}_{r} = \Delta + \delta^{i}_{w}$ where δ^{i}_{w} is the initial water $\delta^{18}O$ value (+10 ‰, +5 ‰, 0 ‰, -5 ‰, -10 ‰) and $\Delta = 1.49\,(10^{6}\,T^{-2}) - 2.81$ (Matsuhisa *et al.*, 1979). The horizontal lines enclose the range in the observed tholeiitic suite gabbro $\delta^{18}O$ values (7.7 - 10.5 ‰).

nepheline syenite (OKJ-014). The higher $\Delta_{plagioclase\ -\ pyroxene}$ value (+ 4.2 ‰), may be attributed to the interaction with an external fluid, which had a higher initial $\delta^{18}O$ value than the rock. The reverse fractionation indicated by the $\Delta_{plagioclase\ -\ pyroxene}$ value observed for the essexite dyke (-0.5 ‰), may be attributed to a disequilibrium process which caused the plagioclase to shift to a lower $\delta^{18}O$ value (eg. the interaction with an external fluid characterized by a lower initial $\delta^{18}O$ value than the rock).

The plagioclase $\delta^{18}O$ (‰) versus pyroxene $\delta^{18}O$ (‰) values are plotted in Fig. 7.3 . Also shown are the $\Delta_{Plagioclase\ -\ Pyroxene}$ fractionation lines for: 1) $\Delta = 1.2$ (calculated from: $\Delta = 1.7 - 1.0\ \beta$, where $\beta = 0.5$ represents the average anorthite mole fraction for the tholeiitic suite (see Table 5.3.1) (Bottinga & Javoy, 1975), and 2) the linear regression through the tholeiitic suite data: $Y = 1.195\ X + 0.651$ ($r = + 0.92$). As a result of its greater resistance to hydrothermal alteration, pyroxene is characterized by $\delta^{18}O$ values, which are more likely to reflect changes in the magma $\delta^{18}O$ value than plagioclase. The deviation in the measured plagioclase $\delta^{18}O$ value from the best-fit line may be used to estimate the relative degrees of alteration. The most altered sample will show the maximum value for:

$$f = \left| \delta^{18}O_{plagioclase} - 1.195\ \delta^{18}O_{pyroxene} - 0.651 \right| \qquad (1)$$

The Bottinga & Javoy (1975) fractionation factor equation ($\Delta = 1.7 - 1.0\ \beta$), indicates that an increase in the anorthite mole fraction of plagioclase will result in a decrease in the plagioclase-pyroxene fractionation factor. The largest deviations from the best-fit line are displayed by the essexite dyke and nepheline syenite samples (f = 2.3 and 2.2 respectively). This is in accordance with the greater degree of alteration in these samples, as indicated by the higher L.O.I. values (see Chapter 3).

The largest deviations from the best-fit line (f values range from 1.2 to 1.9) displayed by the tholeiitic gabbro, occur in the inner Units 1 and 3 (OKJ-033, -062 and -068), which are characterized by schillerized clinopyroxene, clouded plagioclase, and L.O.I. values in the range of 0.9 % to 1.2 % (Table 3.1). The smallest deviations (f = 0.6 to 0.9) are observed for the outer Units 5 and 6 (OKJ-044, -045 and -047), which are characterized by sericitized plagioclase, chloritization, and altered clinopyroxene

phenocrysts mantled by hornblende, and L.O.I. values ranging from 1.0 % to 2.3 %. These characteristics are in accordance with a greater degree of alteration by a magmatic deuteric fluid at subsolidus temperatures (see sections 7.4 - 7.6 below), for the inner units with respect to the outer units. The sericitization, chloritization, clinopyroxene alteration, amphibole mantles, and higher L.O.I. values observed for the outer units, may be attributed to a greater degree of recent low temperature hydrothermal alteration (by meteoric fluids probably).

7.4 Possible alteration temperature ranges

The water/rock (W/R) ratio may be calculated from the plagioclase $\delta^{18}O$ data by the following relation derived from mass-balance considerations (Taylor, 1977):

$$W/R = (\delta^{f}_{r} - \delta^{i}_{r)}) / (\delta^{i}_{w} - \delta^{f}_{r} + \Delta) \qquad (2)$$

where δ^{i} and δ^{f} are the initial and final $\delta^{18}O$ values (‰), W and R are the atom percentages of the element of interest in the water (w) and rock (r) relative to the entire water/rock system, and Δ is the per mil difference between the isotope composition of the rock and water. The average anorthite mole fraction for the tholeiitic suite (0.494) allows the fractionation factor (Δ) between gabbro - water to be approximated by the equation for Δ of plagioclase (An_{50}) of Matsuhisa *et al.* (1979):

$$10^{3} \ln \alpha_{\text{anorthite-water}} \approx \delta^{18}O_{\text{anorthite}} - \delta^{18}O_{\text{water}} \qquad (3)$$
$$= 1.49\ (10^{6}\ T^{-2}) - 2.81 \quad (400\ ^{\circ}C - 500\ ^{\circ}C)$$

The plagioclase versus pyroxene δ-δ plot, and the petrographic observations indicative of minor hydrothermal alteration, suggest that the above relation, which is for a closed system, may be applied to model the water/rock ratio for the tholeiitic suite.

For an infinite W/R ratio, the denominator of equation (2) must equal zero:

$$(\Delta + \delta^{i}_{w} - \delta^{f}_{r}) = 0 \qquad (4)$$

By substituting the Matsuhisa *et al.* (1979) fractionation factor (equation (3)) for $\Delta_{anorthite\text{-}water}$ equation (4) may be rearranged as follows:

$$\delta^{f}_{r} = 1.49\ (10^{6}\ T^{-2}) - 2.81 + \delta^{i}_{w} \qquad (5)$$

where δ^{i}_{w} is the initial water $\delta^{18}O$ value. The final $\delta^{18}O$ value (‰) in the gabbro, for a maximum W/R ratio value of infinity, is illustrated in Fig. 7.4 as a function of the set of possible initial $\delta^{18}O$ compositions and temperatures (< 500 °C) of the alteration fluid. Curves have been calculated for δ^{i}_{w} values of + 10 ‰, + 5 ‰, 0 ‰, -5 ‰ and -10 ‰. The diagram indicates that the range of δ^{f}_{r} values observed for the tholeiitic gabbros, estimated from the range of plagioclase $\delta^{18}O$ values (7.7 - 10.5 ‰), may have been produced by a fluid with a magmatic initial δ^{i}_{w} value of + 5 ‰, at temperatures in the range of 150 °C to 250 ° C. A water/rock ratio below the maximum W/R, and a higher δ^{i}_{w} value, would require a higher temperature range. An initial $\delta^{18}O$ fluid composition of sea water (0 ‰), or meteoric water (- 5 ‰), would require alteration temperatures below 110 °C. The general absence of highly sericitized plagioclase for most of the tholeiitic gabbro samples (Chapter 3), suggests that the alteration was probably not due to a low temperature, low $\delta^{18}O$ (≤ 0 ‰) value fluid.

7.5 Water/rock ratios

Plots of the atomic water/rock ratio versus the final $\delta^{18}O$ (δ^{f}_{r}) of the altered rock for the tholeiitic suite are shown in Fig. 7.5a - d . As previously noted, plagioclase is more easily altered than pyroxene. Consequently, the maximum water/rock ratio may be determined, by allowing the δ^{f}_{r} value to equal the $\delta^{18}O$ value of plagioclase, and the δ^{i}_{r} value to be calculated from the pyroxene $\delta^{18}O$ value (by equation (6)), of the most altered tholeiitic gabbro sample. The δ^{f}_{r} value is estimated from the plagioclase $\delta^{18}O$ value (8.6 ‰) for the olivine gabbro (Unit 1) (OKJ-062), which shows the largest deviation from the best-fit $\Delta_{plagioclase\text{ - }clinopyroxene}$ line regressed through the tholeiitic suite. The initial $\delta^{18}O$ value of the gabbro is assumed to be + 9.14 ‰ in all cases. This value is calculated from the pyroxene $\delta^{18}O$ value for OKJ-062 (8.2 ‰), by the best-fit line equation:

$$\delta^{i}_{r} \approx \delta^{i}_{plagioclase} \approx \delta_{clinopyroxene} \times 1.1945 + 0.651 \qquad (6)$$

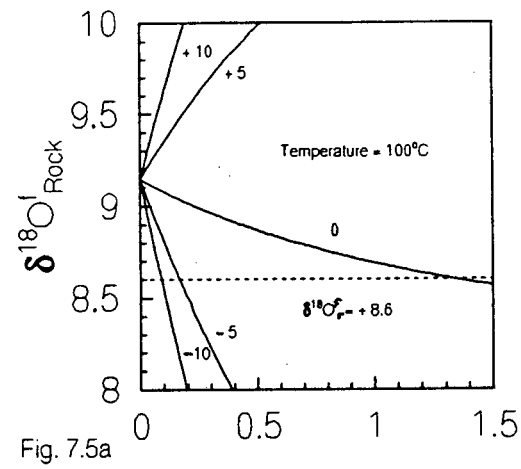

Fig. 7.5a

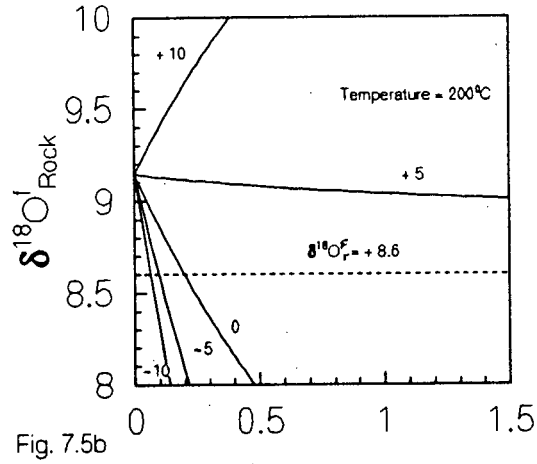

Fig. 7.5b

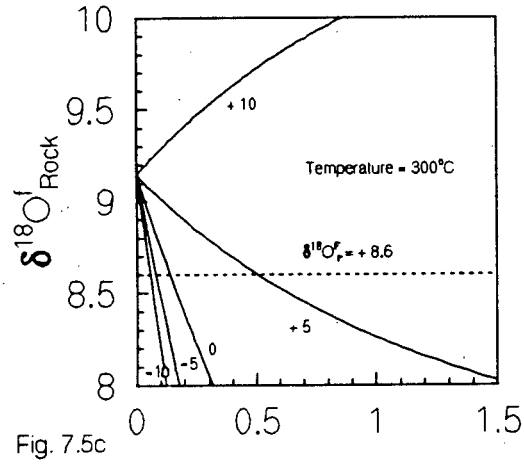

Fig. 7.5c

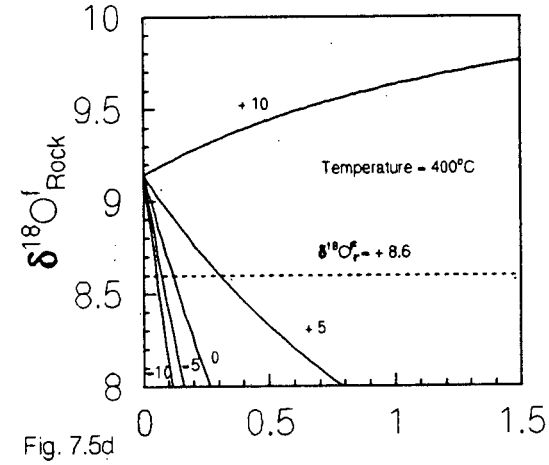

Fig. 7.5d

Fig. 7.5a - d Plots of the atomic water/rock ratio versus the final $\delta^{18}O$ (δ^{f}_{r}) of the rock, for tholeiitic gabbro. The δ^{f}_{r} value is estimated from the plagioclase ^{18}O value (8.6 ‰) for the olivine gabbro (Unit 1) (OKJ-062). The initial $\delta^{18}O$ value of the gabbro is assumed to be + 9.14 ‰ in all cases. This value is calculated from the best-fit $\Delta_{plagioclase\text{ - }clinopyroxene}$ line regressed through the tholeiitic suite: $\delta^{i}_{r} = \delta_{clinopyroxene} \times 1.2 - 0.7$. Families of curves, for a series of possible initial fluid $\delta^{18}O$ values (+10 ‰, +5 ‰, 0 ‰, -5 ‰, -10 ‰), have been plotted for constant temperature values of: 100 °C, 200 °C, 300 °C and 400 °C. The gabbro - water fractionation factor (Δ) is taken to be that of anorthite (An_{100}) - water:
$\Delta = 1.49\ (10^{6}\ T^{-2}) - 2.81$ (Matsuhisa *et al.*, 1979) (see text). (Note: The average anorthite mole fraction for the tholeiitic suite is 0.494 .) This diagram illustrates that high temperatures are required for any shift to lower $\delta^{18}O$ values for any magmatic fluid ($\geq$ + 5 ‰).

The water/rock ratio has been reduced by multiplying by a factor equal to the average modal abundance of plagioclase within the tholeiitic suite (0.576). The fractionation factor (Δ) is taken to be that of anorthite - water (Matsuhisa *et al.*, 1979) (equation (3) above). Families of curves, for a series of possible initial fluid $\delta^{18}O$ values (+10 ‰, +5 ‰, 0 ‰, -5 ‰, -10 ‰), have been plotted for constant temperature values of: 100 °C, 200 °C, 300 °C and 400 °C. The maximum water/rock ratio may be determined from the intersections of the line representing the most altered tholeiitic gabbro ($\delta^{18}O$ = + 8.6 ‰), with the curves for the various possible initial fluids.

Similar plots have been generated for the alkaline gabbro (Fig. 7.6a - d). The δ^{f}_{r} value (for the maximum w/r ratio of the alkaline gabbro), is estimated from the plagioclase ^{18}O value (+ 8.8 ‰) for the most altered alkaline gabbro sample (OKJ-069), which has the largest $\Delta_{\text{plagioclase - clinopyroxene}}$ value. A relation analogous to equation (3) could not be determined for the alkaline gabbro, as a result of the highly limited $\delta^{18}O$ data available (Table 5.1). Nevertheless, the initial $\delta^{18}O$ value of the alkaline gabbro was estimated as + 7.83 ‰, by substituting the pyroxene $\delta^{18}O$ value for OKJ-069 (+ 7.1 ‰) into equation (3). The alkaline gabbro water/rock ratio curves have been reduced by a plagioclase modal abundance correction factor of 0.504, as determined from OKJ-069.

The plots for the olivine gabbro (Unit 1) (δ^{f}_{r} = + 8.6 ‰), show that for a magmatic initial fluid of + 5 ‰, high (> 300 °C) temperatures are required for any shift to lower the $\delta^{18}O$ value of the rock. The maximum W/R ratios for such a fluid range from 0.5 (300 °C) to 0.3 (400 °C).

The plots for the alkaline gabbro (δ^{f}_{r} = + 8.8 ‰) (Fig.7.6a - d) indicate a maximum W/R ratio in the range of 0.22 (100 °C) to 1.14 (400 °C) for a magmatic initial $\delta^{18}O$ water value of + 10 ‰. A W/R of 0.47 is required for a lower $\delta^{18}O$ value of + 5 ‰ at 100 °C. Figure 7.5 reveals that $\delta^{18}O$ values less than or equal to 0 ‰ for the initial fluid were highly unlikely for temperatures equal to or exceeding 100 °C. Instead, the alteration of the alkaline gabbro may have involved a low temperature (100 °C) deuteric fluid with a W/R ratio in the range of 0.22 to 0.47 and a $\delta^{18}O$ value in the range of 5 to 10 ‰. An initial $\delta^{18}O$ value greater than + 5 ‰ would require temperatures exceeding 100 °C.

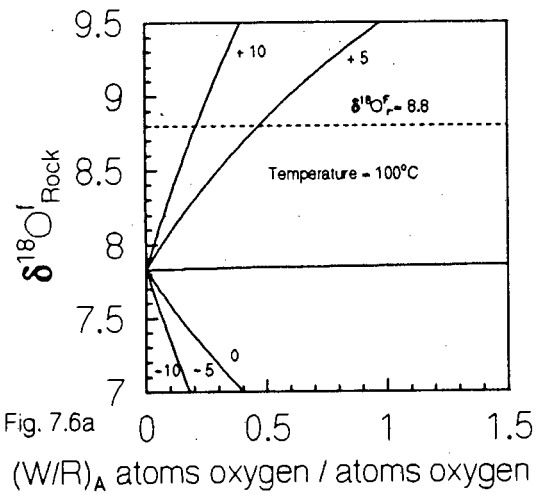

Fig. 7.6a

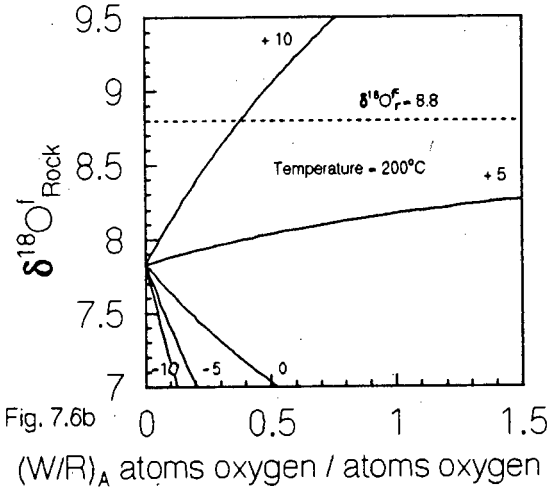

Fig. 7.6b

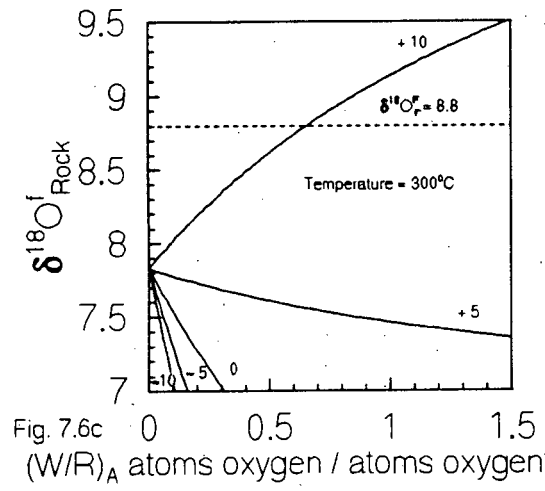

Fig. 7.6c

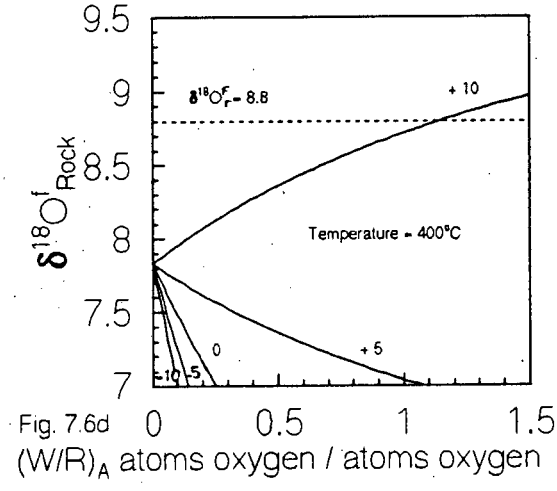

Fig. 7.6d

Fig. 7.6a - d Plots of the atomic water/rock ratio versus the final $\delta^{18}O$ (δ^{f}_{r}) of the rock. The δ^{f}_{r} value is be estimated from the plagioclase ^{18}O value (8.8 ‰) for the most altered alkaline gabbro (OKJ-069), and may be used to estimate the maximum w/r ratio. The calculated initial $\delta^{18}O$ value of the gabbro is assumed to be + 7.83 ‰ in all cases. Families of curves, for a series of possible initial fluid $\delta^{18}O$ values (+10 ‰, +5 ‰, 0 ‰, -5 ‰, -10 ‰), have been plotted for constant temperature values of: 100 °C, 200 °C, 300 °C and 400 °C. The gabbro - water fractionation factor (Δ) is taken to be that of anorthite (An_{100}) - water: $\Delta = 1.49\ (10^{6}\ T^{-2}) - 2.81$ (Matsuhisa *et al.*, 1979) (see text). (Note: The anorthite mole fraction for the alkaline gabbro is assumed to be similar to that of the tholeiitic suite average.) The diagram illustrates that unrealistically low temperatures (well below 100 °C) would be required for a meteoric initial fluid.

7.6 Possible sources of fluid

The final $\delta^{18}O$ values for the most altered tholeiitic and alkaline gabbro samples, indicate a magmatic ($\delta^{18}O = \geq + 5$ ‰) initial fluid, and w/r ratios in the range of 0.2 to 0.5 for both rock types. In addition, the tholeiitic gabbros may have been altered at higher temperatures (300 °C - 400 °C) than the alkaline gabbro (≥ 100 °C). In other words, the alteration in both the tholeiitic and alkaline gabbro may have been produced by a dominantly magmatic deuteric fluid at subsolidus temperatures.

Taylor (1986) attributes depletions in the $\delta^{18}O$ value of quartz (derived from the Yellowstone rhyolite), on a plot of the quartz $\delta^{18}O$ value versus age, to caldera collapse. The variation in the $\Delta_{plagioclase\ -\ clinopyroxene}$ value versus the distance along the transect through the tholeiitic gabbro is plotted in Fig. 7.7. Relative to the $\delta^{18}O$ value depletions (3 - 6 ‰) in the Yellowstone volcanic field, Fig. 7.7 reveals only very minor depletions in the $\Delta_{plagioclase\ -\ clinopyroxene}$ values for Unit 1 (0.4 ‰), Unit 3 (0.2 ‰), Unit 4 (0.4 ‰) and Unit 6 (1 ‰). Other than for Unit 6, these variations lie within the analytical error for the data (see Table 5.1). This suggests that the alteration effects related to possible caldera collapse were minimal, but possibly significant. This is consistent with the minor alteration, as indicated by the low W/R ratios and petrographic observations.

7.7 Summary

The biotite present in the tholeiitic gabbro is probably primary and derived from a deuteric fluid at subsolidus temperatures. Both the tholeiitic and alkaline gabbro experienced minor alteration (w/r ratios in the range of 0.2 to 0.5), by dominantly magmatic deuteric fluids ($\delta^{18}O \geq + 5$ ‰) at subsolidus temperatures, in the range of 300 °C to 400 °C, and 100 °C to 400 °C, respectively.

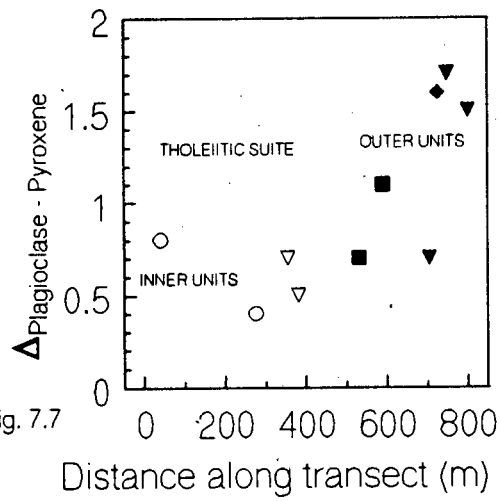

Fig. 7.7

Fig. 7.7 Plot of the plagioclase-clinopyroxene fractionation factor ($\Delta_{plagioclase\text{ - }clinopyroxene}$) (‰) versus the distance along the transect through the tholeiitic gabbro (m). (Symbols used for the tholeiitic suite units are as follows: 1 (○), 2 (◇), 3 (▽), 4 (■), 5 (♦) and 6 (▾). This plot illustrates that intra-unit depletions in the $\Delta_{plagioclase\text{ - }clinopyroxene}$ value, which may be related to caldera collapse (Taylor, 1986), are minimal.

-Chapter 8 - Conclusions -

8.1 Introduction

The major points covered in this dissertation are listed below. In addition, future work which may serve to further the understanding of the petrogenetic history of the Okenyenya complex is also discussed.

8.2 Origin of carbonates

The carbonate within the syenite, alkaline gabbro and monzodiorite is secondary. In contrast, the essexite dyke may represent a sample of primary mantle carbonate. The replacement of plagioclase by calcite indicates that the carbonate was probably produced by the infiltration of a late stage mantle CO_2-bearing fluid related to the intrusion of the essexite dyke.

The calcite probably equilibrated at about 270 °C with a final CO_2 gas component, characterized by the average $\delta^{18}O$ and $\delta^{13}C$ values of + 22.9 ‰ and - 2.7 ‰ respectively. Alternatively, the calcite may have equilibrated with a dissolved bicarbonate ($\delta^{13}C$: - 8.7 ‰) or carbonate ($\delta^{13}C$: - 9 ‰) species. The essexite dyke carbonate data are consistent with a mantle source for the carbon. The carbonate within the essexite dyke, alkaline gabbro, syenite, and in particular the quartz monzodiorite transect sample, may have equilibrated with a fluid related to the intrusion of the ultramafic lamprophyres. Alternatively, the carbonates may have equilibrated with a fluid related to the intrusion of the essexite dyke.

8.3 Mineral - pair thermometry

The majority of the temperatures (Table 5.3.1) calculated for the various plagioclase, pyroxene, olivine, and biotite based mineral-pair thermometers (Mathews *et al.*, 1983; Bottinga & Javoy, 1974; 1975), yield neither crystallization nor closure temperatures, as a result of oxygen isotope diffusion during slow cooling. The variability in the calculated temperatures may also be attributed to alteration and crustal contamination. The tholeiitic leucogabbro (OKJ-033) indicates closure temperatures of 560 °C and 540 °C for the anorthite-clinopyroxene (Mathews *et al.*; 1983) and plagioclase-biotite (Bottinga

& Javoy, 1975) mineral-pairs respectively.

8.4 Closed- and open-system equilibria

The absence of disequilibrium arrays in the silicate oxygen isotope δ - δ diagrams is consistent with isotopically equilibrated closed system behaviour (Gregory & Taylor, 1986). The low average for the plagioclase-biotite (Bottinga & Javoy, 1975) equilibration temperatures (600 °C), is typical for closed system closure temperatures (about 570 °C) (eg. Vennemann, 1989). The δ-δ plots therefore suggest minimal open system exchange for the tholeiitic suite.

8.5 Crustal contamination

The high silicate $\delta^{18}O$ values, and the correlation of the pyroxene $\delta^{18}O$ value with the whole rock initial $^{87}Sr/^{86}Sr$ ratio and other geochemical parameters, provide clear evidence for crustal contamination within the tholeiitic suite. The variation in the $\delta^{18}O$ value of the magma (approximated from the pyroxene value) with respect to the percentage of magma crystallized, indicates that the assimilant may have been derived from the same source as the southern Etendeka rhyolite ($\delta^{18}O$ = + 11.5 ‰), if one assumes a cumulates / assimilated rock ratio (r) value equal to 9.

The $\delta^{18}O$ value of 5.7 ‰ of MORB (Ito *et al.*, 1987; Harmon & Kempton, 1990), and the most primitive mantle-like $^{87}Sr/^{86}Sr$ ratio of 0.70378 (ie. lowest ratio measured throughout the complex), have been selected for the uncontaminated magma to determine the maximum amounts of assimilation for the tholeiitic suite. Simple oxygen and strontium isotope mass balance calculations are consistent with a southern Etendeka rhyolite type contaminant, and constrain the lower (14 % and 19.5 % respectively) and upper (57 % and 71.6 % respectively) limits of the amount of contamination. Lower degrees of contamination would be required if more evolved uncontaminated magma isotope compositions (ie. higher $\delta^{18}O$ and $^{87}Sr/^{86}Sr$ values) were assumed.

The $\delta^{18}O$ - $^{87}Sr/^{86}Sr$ curves for a constant initial magma / assimilant Sr concentration ratio (C^o_m/C_a) equal to 10, suggest that the outer units (4 to 6) require lower cumulates / assimilated rock (r) values ($9 > r > 5$) and higher bulk distribution coefficients (β)

values (1.3 - 1.6), than the inner units (1 - 3) ($r = 9$; $\beta = 1.2$). A plot of the Sr concentration versus the initial $^{87}Sr/^{86}Sr$ ratio indicates that a southern Etendeka rhyolite type assimilant may be reconciled with the measured Sr concentrations, and that the outer units may have assimilated higher $^{87}Sr/^{86}Sr$ material than the inner units. The higher $\delta^{18}O$ values of the outer units may be explained by an increase in the percentage of magma crystallized or an increase in the bulk distribution coefficient (β) value. Alternatively, it may be ascribed to the intrusion of these units into higher temperature country rocks, which would have facilitated an increase in the amount of material assimilated. This is consistent with a possible origin of the outer units by magma mixing, instead of AFC, processes.

Within the tholeiitic suite, for the case of AFC without magma recharge, the rate of assimilation is estimated to have been about 5 to 7 times slower than the rate of fractional crystallization and the ratio (total mass of crust assimilated) / (mass of original magma) (ρ) could have been 0.133 . Models for the case of AFC with magma recharge suggest that for a ρ value of 0.2, the rate of fractional crystallization was five times the rate of assimilation and about 30 times the magma recharge rate. For an ρ value of 0.12, the crystallization rate was seven times the assimilation rate and five times the recharge rate.

8.6 Origin of the biotite

Plots of the plagioclase-pyroxene fractionation factor ($\Delta_{plagioclase - pyroxene}$) value with respect to the biotite modal abundance and the biotite $\delta^{18}O$ value show no systematic variations. This is consistent with the origin of the biotite from a deuteric fluid at subsolidus temperatures. The $\Delta_{plagioclase - pyroxene}$ values observed for the nepheline syenite and essexite dyke indicate that the biotite within these rocks may be derived from external fluids. These fluids may have been respectively characterized by higher and lower initial $\delta^{18}O$ fluid values than the fluid which altered the tholeiitic suite.

8.7 Alteration

The calculated deviations from the best-fit line regressed through the tholeiitic suite data, on a plot of the plagioclase $\delta^{18}O$ (‰) versus pyroxene $\delta^{18}O$ (‰) values, are in accordance

with a greater degree of alteration for the inner units with respect to the outer units. Maximum water/rock ratios have been calculated for the most altered tholeiitic and alkaline gabbro samples. Both the tholeiitic and alkaline gabbro experienced minor alteration (w/r ratios in the range of 0.2 to 0.5), by dominantly magmatic deuteric fluids ($\delta^{18}O \geq + 5$ ‰) at subsolidus temperatures, in the range of 300 °C to 400 °C, and 100 °C to 400 °C, respectively. It should be noted that these values are not universal throughout the complex, and are only appropriate for rocks where shifts in the $\delta^{18}O$ value of the plagioclase occurred.

The variation in the $\Delta_{plagioclase - pyroxene}$ value with the sample distance along the transect through the tholeiitic suite, does not reveal any significant "depletion" or "recovery" in the $\delta^{18}O$ value of the magma. This suggests that the alteration effects related to possible caldera collapse were minimal, and is consistent with the general absence of meteoric alteration in the tholeiitic suite, as indicated by the petrographic observations and water/rock ratio calculations.

8.8 Future work

Interdiffusion between coexisting minerals may result in the calculation of reset or discordant apparent temperatures when stable isotope thermometers are applied to slowly cooling rocks (Deines, 1977; Javoy, 1977; Cole & Ohomoto, 1986; Valley, 1986). The effects of diffusional exchange on the recorded stable isotope signatures are considered in the Giletti (1986) model (Jenkin *et al.*; 1989; Farver, 1989; Coghlan, 1990; Ehlers. *et al*, 1994); single and multiple isotope exchange trajectory (IET) models (Farquhar *et. al*, 1993) and in the Fast Grain Boundary (FGB) model (Eiler *et. al*, 1991; 1992; 1993). Such models also allow for the calculation of: closure temperatures, the $\delta^{18}O$ value of each phase, apparent equilibrium temperatures and cooling rate estimates.

The application of these models, which are based on whole-rock $\delta^{18}O$ values, requires the collection of further olivine, biotite, amphibole, magnetite and quartz oxygen isotope data. A determination of the cooling rate for the tholeiitic suite may be considered in terms of: 1) the rate, depth, and possibly other variables related to the emplacement mechanics of the intrusion (rapid and slow cooling rates may be indicative of shallow and

deep intrusions respectively), 2) the feasilibity of magma mixing for the outer units, 3) the relative rates of assimilation and fractional crystallization calculated in this study, and 4) the variation in other temperature dependant geochemical variables. The data should allow for a verification of the "high level sub-volcanic" nature of the intrusion, and the "structurally controlled emplacement mechanism" discussed by Milner *et al.* (1993; 1994). In short, the data may facilitate the construction of a dynamic model for the system by allowing variations in the geochemical parameters to be related in space and time.

More realistic estimates of the amounts of assimilation may be obtained by recalculating the contamination models for a less primitive parental magma (see section 8.5). Since the assimilation of crustal material results in an increase in the $\delta^{18}O$ and $^{87}Sr/^{86}Sr$ values, estimates of these values for the uncontaminated magma should lie below the $\delta^{18}O$ (+ 6.9 ‰ ± 0.02) and $^{87}Sr/^{86}Sr$ (0.70595) values of the most primitive tholeiitic gabbro transect sample (OKJ-068).

More pyroxene $\delta^{18}O$ data are required for units 2 and 5 to verify whether the effects of caldera collapse were also minor for these units. The analysis of xenoliths of upper mantle composition and megacryst phases in the highly alkaline lamprophyric suite would allow 1) a test of whether the observed geochemical variations may be related to a possible sub-lithoshperic mantle heterogeneity, and 2) better constraints to be placed on the initial magma oxygen and strontium geochemistry. The collection of neodymium and lead isotope data, for the samples analysed in this study, may enable the parameters associated with the Aitcheson & Forrest (1994) AFC models to be better constrained.

This dissertation was financially supported by the Foundation for Research and Development. In particular, I would like to thank Chris Harris (CH) and Anton le Roex (ALR) for extensive and extremely useful discussions. I would also like to thank ALR, R. T. Watkins (RTW) and S. Milner for the use of unpublished major and trace element, and isotope data; ALR and RTW for collecting most of the samples; Neville, David, Ernest, Ivan, Patrick, Nikki, Isobel, Veronica, Anita, Ann and Gene: for all kinds of small, but essential, assistance throughout the duration of this project; Charlie for the photographs; and anybody else not mentioned above, who contibuted materially to my dissertation.

Off-campus support, without which this dissertation would never have materialised, came from my ever loving family: Peter, Roux, Mom (♥) & Dad (♥) (!....did I *actually* write that???....), tolerant friends: Erminia, Russel, Charl & Alf, & my second home: Monique (♥), Tammy (♥), Sue, Annie, Jane, Jodie, *et al.* (a subset of the union of the Sea Point - Campsbay Jewish, musician and *happy people* communities)...& others too painful to recall. Finally, I have to mention MLVC (♥) of course.....

Al-aasm, I.S., Taylor, B.E. & South,B. (1990) Stable isotope analysis of multiple carbonate samples using selective acid extraction. *Chem. Geol.*, **80**, 119 - 125.

Aitcheson, S.J. & Forrest, A.H. (1994) Quantification of crustal contamination in open magmatic systems. *Jour. Petrol.*, **35**. 461 - 488.

Baumgartner, M. (1994) The xenoliths of the Okenyenya volcanic breccia. University of Cape Town, Unpub. MSc. dissertation, 144 p

Borthwick, J. & Harmon, R.S. (1982) A note regarding ClF_3 as an alternative to BrF_5 for oxygen isotope analysis. *Geochim. Cosmochim. Acta*, **46**, 1665 - 1668.

Bottinga, Y. (1968 a) Isotopic fractionation in the system, Calcite - graphite - carbon dioxide - methane - hydrogen - water: California University at San Diego, Ph.D. dissertation, 126p

Bottinga, Y. (1968 b) Calculation of fractionation factors for carbon and oxygen exchange in the system calcite - carbon dioxide - water: *Jour. Phys. Chem.*, **72**, 800 - 808.

Bottinga, Y. & Javoy, M. (1974) Comments on oxygen isotope thermometry. *Earth Planet. Sci. Lett.*, **20**, 250 - 265.

Bottinga, Y. & Javoy, M. (1975) Oxygen isotope partitioning among the minerals in igneous and metamorphic rocks. *Rev. Geophys. Space Phys.*, **13**, 401 - 418.

Bristow, J.W., Allsopp, H.L., Erlank, A.J., Marsh, J.S. & Armstrong, R.A. (1984) Strontium isotope characterization of Karoo volcanic rocks. *Geol. Soc. Afr. Spec. Publ.*, **13**, 295 - 329.

Clague, D.A. (1987) Hawaiian alkaline volcanism. In: *Alkaline rocks*. Eds. Fitton J.G. & Upton B.G.J. *Geol. Soc. Afr. Spec. Publ.*, **30**, 227 - 252.

Coghlan, R.A. (1990) Studies in diffusional transport: grain boundary transport of oxygen in feldspars, diffusion of oxygen, strontium and the REE's in garnet, and thermal histories of granitic intrusions in south-central Maine using oxygen isotopes. Brown University, Ph.D. dissertation.

Cole, D. R. & Ohomoto, H. (1986) Kinetics of isotopic exchange at elevated temperatures and pressures. In: *Stable Isotopes in High Temperature Geological Processes* (Ed. Valley, J.W., Taylor, H.P.Jr & O'Neil, J.R.); *Rev. Mineral.*, **16**, 41 - 87.

Cortecci, G., Del Moro, A., Leone, G. & Pardini, G.C. (1979) Correlation between strontium and oxygen isotopic compositions of rocks from the Adamello Massif

(northern Italy). *Contrib. Mineral. Petrol.*, **68**, 421 - 427.

Cox, K.G., Bell, J.D. & Pankhurst, R.J. (1979) *The interpretation of igneous rocks.* George Allen & Unwin, 450 p

Davidson, J.P. & Harmon,R.S. (1989) Oxygen isotope constraints on the petrogenesis of volcanic arc magmas from Martinique, Lesser Antilles. *Earth Planet. Sci. Lett.*, **95**, 255 - 270.

Deines, P. (1977) On the oxygen isotope distribution among mineral triplets in igneous and metamorphic rocks. *Geochim. Cosmochim. Acta*, **41**, 1709 - 1730.

Deines, P., Harris, J.W., Robinson, D.N., Gurney, J.J. & Shee, S.R. (1991) Carbon and oxygen isotope variations in diamond and graphite eclogites from Orapa, Botswana, and the nitrogen content of their diamonds. *Geochim. Cosmochim. Acta*, **55**, 515 - 524.

DePaolo, D. (1981) Trace element and isotopic effects of combined wall rock assimilation and fractional crystallization. *Earth Planet. Sci. Lett.*, **53**, 189 - 202.

Dodson, M.H. (1973) Closure temperature in cooling geochronological and petrological systems. *Contrib. Mineral. Petrol.*, **40**, 259 - 274.

Downes, H., Dupuy, C. & Leyreloup, A.F. (1990) Crustal evolution of the Hercynian belt of Western Europe: Evidence from lower - crustal granulitic xenoliths (French Massif Central). *Chem. Geol.*, **83**, 209 - 231.

Eiler, J.M. (1991) Oxygen isotope studies of Adirondack orthogneiss. University of Wisconsin, M.Sc. dissertation.

Eiler, J.M., Baumgartner, L.P. & Valley, J.W. (1992) Intercrystalline stable isotope diffusion: a fast grain boundary model. *Contrib. Mineral. Petrol.*, **112**, 543 - 557.

Eiler, J.M., Valley, J.W., Baumgartner, L.P. (1993) A new look at stable isotope thermometry. *Geochim. Cosmochim. Acta*, **57**, 2571 - 2583.

Ehlers, K. & Powell, R. (1994) An empirical modification of Dodson's equation for closure temperature in binary systems. *Geochim. Cosmochim. Acta*, **58**, 241 - 248.

Farquhar, J., Chacko, T. & Frost, B.R. (1993) Strategies for high-temperature oxygen isotope thermometry: a worked example from the Laramie Anorthosite Complex, Wyoming, U.S.A. *Earth Planet. Sci. Lett.*, **117**, 407 - 422.

Faure, G., Bowman, J.R. , & Elliot, D.H. (1979) The initial $^{87}Sr/^{86}Sr$ ratios of the Kir wan volcanics of Dronning Maud Land: comparison with the Kirhpatrick volcanics, Trans-antarctic Mountains. *Chem. Geol.*, **26**, 77 - 90.

Faure, G. (1986) *Principles of isotope geology.* (2nd Ed.) John Wiley & Sons, 589 p.

Faure, K. (1989) A stable isotope study of the Kaap Valley Tonalite, Barberton Mountain Land, South Africa. University of Cape Town, Unpub. M.Sc. dissertation, 148 pp.

Faure, K. & Harris, C. (1991) Oxygen and carbon isotope geochemistry of the 3.2 Ga Kaap Valley tonalite, Barberton greenstone belt, South Africa. *Pre. Res.*, **52**, 301 - 319.

Farver, J.R. (1989) Oxygen self diffusion in diopside with application to cooling rate determinations. *Earth Planet. Sci. Lett.*, **92**, 386 - 396.

Fitch, F.J. & Miller, J.A. (1984) Dating Karoo igneous rocks by the conventional K - Ar and $^{40}Ar/^{39}Ar$ age spectrum methods. *Geol. Soc. S. Afr. Spec. Publ.*, **13**, 247 - 266.

Forester, R.W. & Taylor, H.P. (1977) $^{18}O/^{16}O$, D/H and $^{13}C/^{12}C$ studies of the Tertiary igneous complex of Skye Scotland. *Am. Jour. Sci.*, **277.**, 136 - 177.

Fourcade, S., Maury, R.C., Defant, M.J. & Dermott, F. (1994) Mantle metasomatic enrichment versus arc crust contamination in the Philippines: Oxygen isotope study of Batan ultramafic nodules and northern Luzon arc lavas. *Chem. Geol.*, **114**, 199 - 215.

Fowler, M.B. & Harmon, R.S. (1990) The oxygen isotope composition of lower crustal granulite xenoliths. In: *Granulites and Crustal Evolution* (Ed. D. Vielzeuf & P. Vidal), 493 - 506, Kluwer.

Friedman, I., & O'Neil, J.R. (1977) Compilation of stable isotope fractionation factors of geochemical interest. In: M. Fleischer, ed., *Data of Geochemistry, sixth ed., Chapter KK, US. Geol. Surv. Prof. Paper 440-KK*, 12 p. and 49 figures.

Gevers, T.W. (1936) The Etjo beds of northern Hereroland. *Trans. Geol. Soc. S. Afr.*, **39**, 317 - 329.

Giletti, B.J. (1986) Diffusion effects on oxygen isotope temperatures of slowly cooled igneous and metamorphic rocks. *Earth Planet. Sci. Lett.*, **77**, 218 - 229.

Graham, C.M. & Harmon, R.S. (1983) Stable isotope evidence on the nature of crust-mantle interactions, In: *Continental basalts and mantle xenoliths.* (Hawkesworth, C.J., & Norry, M.J., Eds.), Cheshier, UK., Shiva Publishing Limited, 20 - 45.

Gregory, R.T. & Criss, R.E. (1986) Isotopic exchange in open and closed systems. In: *Stable Isotopes in High Temperature Geological Processes* (Ed. Valley, J.W., Taylor, H.P.Jr & O'Neil, J.R.); *Rev. Mineral.*, **16**, 91 - 127.

Gregory, R.T. & Taylor, H.P. (1981) An oxygen isotope profile in a section of Cretaceous oceanic crust, Samail ophiolite, Oman: evidence for $\delta^{18}O$ buffering of the oceans by deep (>5km) seawater-hydrothermal circulation at mid-ocean ridges. *Jour. Geophys. Res.*, **86**, 2737 - 2755.

Gregory, R.T. & Taylor, H.P. (1986) Possible non-equilibrium oxygen isotope effects in mantle nodules, an alternative to the Kyser-O'Neil-Carmichael $^{18}O/^{16}O$ geothermometer. *Contrib. Mineral. Petrol.*, **93**, 114 - 119.

Gregory, R.T., Criss, R.E. & Taylor, H.P. Jr. (1989) Oxygen isotope exchange kinetics of mineral pairs in closed and open systems: applications to problems of hydrothermal alteration of igneous rocks and Precambrian iron formations. *Chem. Geol.*, **75**, 1 - 42.

Haack, U., Hoefs, J. & Gohn, E. (1982) Constraints on the origin of Damaran granites in the light of Rb/Sr and $\delta^{18}O$ data: Contributions to Mineralogy and Petrology, **79**, 279 - 289.

Harmon, R.S. & Kempton, P.D. (1990) ^{18}O character of lower crustal xenoliths: The global story. S.R. Taylor Symposium, Australian Natl. Univ. (abstr. vol.), 11 - 12.

Harris, C., Whittingham, A. M., Milner, S.C., & Armstrong, R.A. (1990) Oxygen isotope geochemistry of the silicic volcanic rocks of the Etendeka / Paraná province: Source constraints. *Geology,* **18**, 1119 - 1121.

Harris, C. & Watkins, R.T. (1990) Fluid interaction in the Witwatersrand goldfields: oxygen isotope geochemistry of Ventersdorp-age dolerite intrusions. *S. Afr. Jour. Geol.*, **4**, 611 - 615.

Harris, C. (1995) The oxygen isotope geochemisrty of the Karoo and Etendeka volcanic provinces of Southern Africa. *S. Afr. Jour. Geol.,(Submitted)*

Harris, C. (1995) The oxygen isotope geochemistry of the Karoo and Etendeka volcanic provinces of southern Africa. University of Cape Town Geological Sciences Centenary Proceedings (1 - 3 February 1995).

Hart, S.R. & Dunn,T. (1993) Experimental cpx/melt partitioning of 24 trace elements. *Contrib. Mineral. Petrol.*, **113**, 1 - 8.

Hawkesworth, C.J., Kramers, J.D. & Miller, R. McG. (1981) Old model Nd ages in Namibian Pan-African rocks. *Nature,* **289**, 278 - 282.

Hawkesworth, C.J. & Marlow, A.G. (1983) Isotope evolution of the Damara orogenic belt. *Geol. Soc. S. Afr. Spec. Publ.*, **11**, 397 - 407.

Hawkesworth, C.J., Marsh, J.S., Duncan, A.R., Erlank, A.J., & Norry, M.J. (1984) The role of continental lithosphere in the generation of the Karoo volcanic rocks: Evidence from combined Nd- and Sr-isotope studies. *Geol. Soc. S. Afr. Spec. Publ.*, **13**, 341 - 354.

Hoernes, S. & Hoffer, E. (1979) Equilibrium relations of prograde metamorphic mineral assemblages. *Contrib. Mineral. Petrol.*, **68.**, 377 - 389.

Ito, E., White, W.M. & Gopel, C. (1987) The O, Sr, Nd, and Pb isotope geochemistry of MORB. *Chem. Geol.*, **62**, 157 - 176.

James, D.E. (1981) The combined use of oxygen and radiogenic isotopes as indicators of crustal contamination: *Ann. Rev. Earth Planet. Sci.*, **9**, 311 - 344.

Javoy, M. (1977) Stable isotopes and geothermometry. *Jour. Geol. Soc. Lond.*, **133**, 609 - 636.

Javoy, M., Pineau, F. & Delorme, H. (1986) Carbon and nitrogen isotopes in the mantle. *Chem. Geol.*, **57**, 41 - 62.

Jenkin, G.R.T., Fallick, A.E. & Farrow, C.M. (1989) *COOL: Computer program for modelling stable isotopes in cooling closed systems. User manual and documentation.* Scottish Universities Research & Reactor Centre (SURRC), 113p.

Jenkin, G.R.T., Linklater, C., Fallick, A.E. (1991) Modeling of mineral $\delta^{18}O$ values in an igneous aureole: Closed-system model predicts apparent open-system $\delta^{18}O$ values. *Geology*, **19**, 1185 - 1188.

Jenkin, G.R.T., Farrow, C.M., Fallick, A.E. & Higgins, D. (1994) Oxygen isotope exchange and closure temperatures in cooling rocks. *Jour. Meta. Geol.*, **12**, 221 - 235.

Kalamarides, R.I. (1984) Kiglapait geochemistry VI: oxygen isotopes. *Geochim. Cosmochim. Acta*, **48**, 1827 - 1836.

Kempton, P.D. & Harmon, R.S. (1992) Oxygen isotope evidence for large-scale hybridization of the lower crust during magmatic underplating. *Geochim. Cosmochim. Acta*, **56**, 971 - 986.

Kirkley, M.B., Gurney, J.J., Otter, M.L., Hill, S.J. & Daniels, L.R. (1991) The application of C isotope measurements to the identification of the sources of C in diamonds: a review. *App. Geochem.*, **6**, 477 - 494.

Korn, H. & Martin, H. (1939) Junge vulkano-plutone in Sudwestafrika. *Geol. Rdsch.*, **30**, 631 - 636.

Korringa, M.K. & Noble,D.C. (1971) Distribution of Sr and Ba between natural feldspar and igneous melt. *Earth Planet. Sci. Lett.*, **11**, 147 - 151, North-Holland publishing company.

Kyser, T.K. (1986) Stable isotope variations in the mantle. In: *Stable Isotopes in High Temperature Geological Processes* (Ed. Valley, J.W., Taylor, H.P.Jr & O'Neil, J.R.); *Rev. Mineral.*, **16**, 141 - 164.

Kyser, T.K., O'Neil, J.R. & Carmichael, I.S.E. (1981) Oxygen isotope thermometry of basic lavas and mantle nodules. *Contrib. Mineral. Petrol.* **77**, 11 - 23.

Lanyon, R. & le Roex, A.P. (1995) Petrography, mineralogy and geochemistry of lamprophyric intrusives, Okenyenya Igneous Complex, northwestern Namibia. University of Cape Town Geological Sciences Centenary Proceedings (1 - 3 February 1995).

Le Maitre, R.W. (1989) *A classification of igneous rocks and glossary of terms.* Blackwell, Oxford, 193 pp.

le Roex, A.P. (1985) Geochemistry, mineralogy & magmatic evolution of the basaltic and trachytic lavas from Gough Island, South Atlantic. *Jour. Petrol.*, **26**, 149 - 186.

le Roex, A.P., Cliff, R.A. & Adair, B.J.I. (1990) Tristan da Cunha, South Atlantic: Geochemisrty and petrogenesis of a Basanite-phonolite lava series. *Jour. Petrol.*, **31**, 779 - 812.

le Roex, A.P., Watkins, R.T. & Reid, A.M. (1995) Geochemical evolution of the Okenyenya sub-volcanic ring complex, northwestern Namibia.(*in prep.*)

Malinin, S.D., Kropotova, O.I. & Grinenko, V.A. (1967) Experimental determination of C^{13} exchange constants in $CO_2(g)$-HCO_3 (Soln.) system under hydrothermal conditions: *Geochimiya*, **8**, 927 - 935 [in Russian].

Martin, H., Mathias, M. & Simpson, E.W.S. (1960) The Damaraland sub-volcanic ring complexes in South West Africa. *Rep. Int. geol. Cong. XXI sess.*, **13**, 156 - 174.

Mathews., A., Goldsmith, J.R., & Clayton, R.N. (1983) Oxygen isotope fractionations involving pyroxenes: the calibration of mineral-pair geothermometers. *Geochim. Cosmochim. Acta*, **47**, 631 - 644.

Matsuhisa, Y., Goldsmith, J.R., and Clayton, R.N. (1979) Oxygen isotopic fractionation in the system quartz-albite-anorthite-water. *Geochim. Cosmochim. Acta*, **43**, 1131 - 1140.

McCrea, J.M. (1950) On the isotopic chemistry of carbonates and a paleotemperature

scale. *Jour. Chem. Phys.*, **18**, 849 - 857.

McKenzie, D. & O'Nions, R.K. (1991) Partial melt distributions from inversion of rare earth element concentrations. *Jour. Petrol.*, **32**, 1021 - 1091.

Miller, R.McG. (1983) The pan-African Damaran orogen of South West Africa / Namibia - *Spec. Publ. geol. Soc. S. Afr.*, **11**, 431 - 515.

Milner, S.C. & Duncan, A.R. (1987) Geochemical characterization of quartz latite units in the Etendeka Formation: Geological Survey of South West Africa / Namibia Communications, **3**, 83 - 90.

Milner, S.C., le Roex, A.P. & Watkins, R.T. (1993) Rb-Sr determinations of rocks from the Okenyenya igneous complex, northwestern Namibia. *Geol. Mag.*, **130**, 335 - 343.

Milner, S.C., le Roex, A.P. & O'Connor, J.M. (1994) The age of Mesozoic igneous rocks in northwestern Namibia, and their relationship to continental breakup. *Jour. Geol. Soc. (in press)*

Milner, S.C. & le Roex, A.P. (1995) Mantle plume isotopic signature in rocks from sub-volcanic Mesozoic igneous intrusions, northwestern Namibia. University of Cape Town Geological Sciences Centenary Proceedings (1 - 3 February 1995).

Mitchell, R.H. (1986) *Kimberlites: mineralogy, geochemistry and petrology.* Plenum, New York, 442p.

Montel, J. M. & Weisbrod, A. (1986) Characteristics and evolution of "vaugneritic magmas": an analytical and experimental approach, on the examples of the Cevennes Medians (French Massif Central) *Bull. Mineral.*, **109**, 575 - 587

Mook, W.G., Boomerson, J.C., & Staverman, W.H. (1974) Carbon isotope fractionation between dissolved bicarbonate and gaseous carbon dioxide: *Earth Planet. Sci. Lett.*, **22**, 169 - 176.

Nemec, D. (1977) Differentiation of lamprophyre magma. *Kristalinikum*, **13**, 73 - 87.

Norton, D. (1984) Theory of hydrothermal systems. *Ann. Rev. Earth Planet. Sci.* **12**, 155 - 177.

Norton, D. & Taylor, H.P., Jr. (1979) Quantitative simulation of the hydrothermal systems of crystallizing magmas on the basis of transport theory and oxygen isotope data: An analysis of the Skaergaard intrusion. *Jour. Petrol.*, **20**, 421 - 486.

O'Neil, J. R., & Taylor, H. P., Jr. (1967) The oxygen isotope and cation exchange chemistry of feldspars: *Am. Mineral.*, **52**, 1414 - 1437.

O'Neil, J.R., Clayton, R.N., and Mayeda, T.K. (1969) Oxygen isotope fractionation in divalent metal carbonates: *Jour. Chem. Phys.*, **51**, 5547 - 5558.

Philpotts, J.A. & Schnetzler, C.C. (1970) Phenocryst-matrix partition coefficients for K, Rb, Sr and Ba, with applications to anorthosite and basalt genesis. *Geochim. Cosmochim. Acta*, **34**, 307 - 322.

Pirajno, F. & Schlögl, H.U. (1987) The alteration-mineralization of the Krantzberg tungsten deposit, South West Africa / Namibia. *S. Afr. Jour. Geol.*, **90**, 499 - 508.

Prins, P. (1981) The geochemical evolution of the alkaline and carbonatitic complexes of the Damaraland Igneous Province, South West Africa. *Ann. Univ. Stellenbosch, Series A1 (Geol.)*, **3**, 145 - 278.

Reid, D.L., Cawthorn, R.G., Kruger, F.J., Tredoux, M. (1993) Isotope and trace-element patterns below the Merensky Reef, Bushveld Complex, South Africa: evidence for fluids? *Chem. Geol.*, **106**, 171 - 186.

Rock, N.M.S. (1991) *Lamprophyres.*, Blackie & Son Ltd., 285 p

SACS (1980). Stratigraphy of South Africa. Part I. Lithostratigraphy of the Republic of S. A., South West Africa / Namibia and the Republics of Bophuthatswana, Transkei and Venda. *Handb. Geol. Surv. S. Afr.*, **8**.

Schiffries, C.M. & Rye, D.M. (1989) Stable isotopic systematics of the Bushveld complex: I. Constraints on magmatic processes in layered intrusions. *Am. Jour. Sci.*, **289**, 841 - 873.

Schiffries, C.M. & Rye, D.M. (1990) Stable isotopic systematics of the Bushveld complex: II. Constraints on hydrothermal processes in layered intrusions. *Am. Jour. Sci.*, **290**, 209 - 245.

Schnetzler, C.C. & Philpotts, J.A. (1968) Partition coefficients of rare-earth elements and barium between igneous matrix material and rock forming mineral phenocrysts. In: *Origin and Distribution of the Elements*, (Ed. L.H. Ahrens), 929 - 938, Pergamon.

Schnetzler, C.C. & Philpotts, J.A. (1970) Partition coefficients of rare-earth elements between igneous matrix material and rock forming mineral phenocrysts - II. *Geochim. Cosmochim. Acta*, **34**, 331 - 340.

Sharma, T. & Clayton, R.N. (1965) Measurement of O^{18}/O^{16} ratios of total oxygen of carbonates. *Geochim. Cosmochim. Acta*, **29**, 1347 - 1353.

Sheppard, S.M.F. (1986) Characterization and isotopic variations in natural waters. In:

Stable Isotopes in High Temperature Geological Processes (Ed. Valley, J.W., Taylor, H.P.Jr & O'Neil, J.R.); *Rev. Mineral.*, **16**, 165 - 183.

Sheppard, S.M.F. & Harris, C. (1985) Hydrogen and oxygen isotope geochemistry of Ascension Island lavas and granites: variation with crystal fractionation and interaction with sea water. *Contrib. Mineral. Petrol.*, **91**, 74 - 81.

Siedner, G. & Mitchell, J.G. (1968) Mesozoic volcanism in Namibia and Brazil: a K-Ar isochron study bearing on the opening of the South Atlantic. *Earth Planet. Sci. Lett.*, **30**, 292 - 302.

Simpson, E.S.W. (1950) Preliminary notes on the Okenjeje igneous complex, South West Africa. *Geol. Rdsch.*, **38**, 15 - 18.

Simpson, E.S.W. (1952) The Okonjeje Igneous Complex, South West Africa. University of Cambridge, Unpub. Ph.D. dissertation, 132 pp.

Simpson, E.S.W. (1954) The Okonjeje igneous complex, South West Africa. *Trans. Geol. Soc. S. Afr.*, **107**, 125 - 172.

Stakes, D.S. & O'Neil, J.R. (1982) Mineralogy and stable isotope geochemistry of hydrothermally altered oceanic rocks. *Earth Planet. Sci. Lett.*, **57**, 285 - 304.

Taylor, H.P., Frechen, J. & Degens, E.T. (1967) Oxygen and carbon isotope studies of carbonatites from the Laacher See district, West Germany, and the Alnö district, Sweden. *Geochim. Cosmochim. Acta*, **31**: 407-430.

Taylor, H.P., Jr. (1977) Water / rock interactions and the origin of H_2O in granite batholiths. *Jour. Geol. Soc. London*, **133**, 509 - 558.

Taylor, H.P., Jr. & Forester, R.W. (1979) An oxygen and hydrogen isotope study of the Skaergaard intrusion and its country rocks: a description of a 55-m.y. old fossil hydrothermal system. *Jour. Petrol.*, **20**, 355-419.

Taylor, H.P., Jr. (1980) The effects of assimilation of country rocks by magmas on $^{18}O/^{16}O$ and $^{87}Sr/^{86}Sr$ systematics in igneous rocks. *Earth Planet. Sci. Lett.* **47**, 243 - 254.

Taylor, H.P., Jr. (1987) Comparison of hydrothermal systems in layered gabbros and granites, and the origin of low-^{18}O magmas. In: *Magmatic processes: Physiochemical principles* (Ed. Mysen, B.O.); *Geochem. Soc. Spec. Publ.* **1** , 337 - 357.

Taylor, H.P., Jr. (1986) Igneous rocks: II. Isotopic case studies of circumpacific magmatism. In: *Stable Isotopes in High Temperature Geological Processes* (Ed. Valley, J.W., Taylor, H.P.Jr & O'Neil, J.R.); *Rev. Mineral.*, **16**, 273 - 318.

Taylor, H.P., Jr. & Sheppard, S.M.F. (1986) Igneous rocks: I. Processes of isotopic fractionation and isotope systematics. In: *Stable Isotopes in High Temperature Geological Processes* (Ed. Valley, J.W., Taylor, H.P.Jr & O'Neil, J.R.); *Rev. Mineral.*, **16**, 227 - 271.

Thode, H.G., Shima, M., Rees, C.E. & Krishnamurty, K.V. (1965) Carbon-13 isotope effects in systems containing carbon dioxide, bicarbonate, carbonate, and metal ions: *Canadian Jour. Chem.*, **43**, 582 - 595.

Valley, J.W. (1986) Stable isotope geochemistry of metamorphic rocks. In *Stable Isotopes in High-temperature Geological Processes* (Ed. J.W.Valley, H.P.Taylor,Jr., and J.R. O'Neil); *Rev. Mineral.*, **16**, 445 - 490.

Vennemann, T.W. (1989) A geochemical and stable isotope study of some rocks from the Bandelierkop formation, southern marginal zone of the Limpopo belt, South Africa. University of Cape Town, Unpub. Ph.D. dissertation, 236pp.

Wager, L.R. & Deer, W.A. (1939) Geological investigations in East Greenland. Part III - The petrology of the Skaergaard intrusion, Kangerdlugssuak, East Greenland. *Medd. om Gronland*, **105**, No. 4.

Watkins, R.T., McDougall, I. & le Roex, A.P. (1994) K-Ar ages of the Brandberg and Okenyenya igneous complexes, northwestern Namibia. *Geol. Rdsch.*, **83**, 348 - 356.

Watkins, R.T. & le Roex, A.P. (1991) Petrology and structure of syenite intrusions of the Okenyenya igneous complex. *Communs. Geol. Surv. Namibia.*, **7**, 55 - 70.

Watkins, R.T. & le Roex, A.P. (1995) A revised geology of the Okenyenya igneous complex: structure and history of emplacement. *Communs. Geol. Surv. Namibia.* (*in press*).

Watson, E.B., Othman,D.B., Luck,J. & Hofman, A.W. (1987) Partitioning of U, Pb, Cs, Yb, Hf, Re and Os between chromian diopsidic pyroxene and haplobasaltic liquid. *Chem. Geol.*, **62**, 191 - 208.

- Appendix 1 -

1.1 Petrographic descriptions:

Below is a summary of petrographic textural and alteration-related features for the samples analysed in this study. The descriptions are based on Milner *et al.* (1993), Simpson (1954), le Roex *et al.*(1995) and the author's observations. The abbreviations used in this section are as follows: Ab.: albite, Acc.: accessory, Akfsp.: alkali feldspar, Alter.: alteration minerals, Amph.: amphibole, An.: anorthite, Apt.: apatite, Bt.: biotite, Cpx.: clinopyroxene, En.: enstatite, Fe-Ti.: Iron-titanium, Fs.: ferrosalite, Fo.: fosterite, Ilm.: ilmenite, Mgt.: magnetite, MSc.: Muscovite, Ol.: olivine, Opx.: orthopyroxene, Ortho.: orthoclase, Plag.: plagioclase, Tr.: trace, Txt.: texture, W.R.T.: with respect to, Wo.: wollastonite

Descriptions

Tholeiitic gabbro: OKJ-004

Plag.: slight alteration along fractures; forms sub-parallel laths (< 5 mm) and intercumulus grains (0.25 - 1.0 mm) *Ol.:* altered along fractures and grain boundaries *Cpx.:* are schillerized and contain apatite, Fe-Ti oxide and biotite inclusions *Bt.:* occurs as primary subhedral flakes (1 mm) and as Fe-Ti oxide and olivine mantles (OKJ-004 represents an "off-transect" tholeiitic gabbro Unit 4 sample.)

Nepheline syenite: OKJ-014

Akfsp.: perthite forms variably altered large grains (< 8 mm) *Cpx.:* subhedral to anhedral grains (1-2 mm) *Amph.:* occurs as individual crystal (1-2 mm) and as pyroxene mantles *Bt.:* occurs as coronas on Fe-Ti oxides and as larger crystals mantled by amphibole.

Nepheline syenite: OKJ-018

Txt.: trachytoidal sodalite and nepheline form irregular crystals in groundmass *Ortho.:* large tabular perthitic (5 mm) phenocrysts occur in a groundmass of alkalifeldspar laths in fluxional arrangement *Plag.:* albite occurs as small twinned laths, interstially and as vein-like bodies in alkalifeldspar crystals *Cpx:* aegerine-augite forms allotriomorphic crystals and enclose titanaugite cores *Amph.:* ferrohastingsite forms irregular poikilitic crystals on groundmass feldspar *Acc.:* iron ore, sphene and apatite, with interstial

fluorite and calcite.

Leuco-gabbros: OKJ-033, OKJ-037, OKJ-061, OKJ-065

Txt.: Intergranular (OKJ-033), subophitic (OKJ-061 and OKJ-065) and ophitic (OKJ-037) textures occur *Plag.:* metamorphic clouding restricted to: OKJ-033, OKJ-061, OKJ-065; grain size varies from 3-7mm (OKJ-033 and OKJ-037) to 1-2 mm (OKJ-065); laths display concentric zoning & poor twinning *Akfsp.:* characterized by exsolution blebs (OKJ-033) and a weak sub-parallel alignment *Cpx.:* occurs as anhedral - subhedral glomerocrysts (3-4mm) and as single grains < 7mm (OKJ-037); cpx. is schillerised and holds bt., plag., Fe-Ti oxide and apatite inclusions *Ol.:* occurs as interstial fracture altered anhedral grains (2-5mm) and as plag. enclosing glomerocrysts; replaced by Fe-Ti oxides and opx. vermicular intergrowths *Opx.:* occurs as subhedral grains (1.5mm) interstial to plag.; incude apatites and Fe-Ti oxides; extensively altered to mica (OKJ-033,-037) *Bt.:* late stage flakes (1-2mm) include apatite *Apt.:* occurs as euhedral prisms (0.5mm) and as grains (5mm) interstial to cpx. *Fe-Ti oxides:* large grains (1-2mm) are interstial blebs or form vermicular intergrowths. *Ilm.:* occurs as exsolution patches in titano-magnetite.

Gabbro-norite: OKJ-041, OKJ-042

Txt.: show sub-ophitic and strong disequilibrium textures *Plag.:* (0.5 - 2 mm) laths is unclouded and more sericitized than OKJ-004 *Opx.:* forms 3 mm subhedral grains *Cpx.:* forms anhedral grains (4 mm) with abundant bt. and mgt. inclusions *Bt.:* occurs as primary laths, pyroxene and Fe-Ti oxide mantles and as poikilitic flakes (< 5 mm). Dominant grain sizes are 1 - 2 mm. *Apt.:* forms unaltered prisms *Ortho.:* late stage 9 mm grains enclose plag., cpx. and apatite *Fe-Ti oxides:* are primary.

Monzodiorites: OKJ-043, OKJ-044, OKJ-045, OKJ-046

Txt.: very coarse grained (<7 mm), ophitic to subophitic and extensively altered; characterized by presence of quartz and amphibole and high modal orthoclase *Plag.:* grains (2-5mm) are randomly aligned, sericitized but unclouded; show poorly developed lamellar twinning, ragged grain boundaries and evidence of resorption *Cpx.:* (4mm) anhedral fractured phenocrysts are altered along cleavages and fractures *Ol.:* grains (0.5mm) show extensive iron staining and resorption by opx *Opx.:* phenocrysts (4mm)

hold apatite and plag. inclusions and are also replaced by chlorite and white mica *Ortho.:* forms interstial late stage sericitized poikiloblasts which enclose plag., ol., cpx. and apatite *Bt.:* is replaced by opaques and chlorite *Quartz:* small interstitial unaltered grains *Apt.:* occurs as euhedral prisms (0.1 mm) and *Fe-Ti oxides:* euhedral grains (0.5 mm) enclosed by oxides.

Quartz-monzodiorite: OKJ-047

Txt.: coarser grained than monzodiorites *Cpx.:* is mantled by green-brown hornblende *Ol.:* extensively altered by opaques and opx.

Quartz-monzodiorite: OKJ-050

Txt.: mesocumulate, medium grained gabbro with plag. as the cumulate phase and intercumulus ol., cpx. and Fe-Ti oxides *Plag.:* adcumulate growth and zoning occurs *Cpx.:* (<2.5mm) interstial to plag. *Ol.:* (0.5-1.5mm) is surrounded by cpx. or opaque oxides.

Olivine gabbros: OKJ-062, OKJ-031, OKJ-034, OKJ-038,

OKJ-040 *Txt.:* fine (1-2 mm) to coarse (< 7mm) coarse grained and sub-ophitic *Ol.:*glomerocrysts (1-2 or 4 mm) enclose plag., bt. and Fe-Ti oxides; vermicular intergrowths of Fe-Ti oxides and opx rim are common *Cpx.:* schillerized interstial grains (1-3 mm) hold apatite, bt. and Fe-Ti oxide inclusions *Plag.:* laths (1-7mm) are irregularly twinned due to metamorphic clouding (OKJ-038 and -040 are not clouded) *Fe-Ti oxides:* (2-3mm) are associated with bt. and enclose plag. and ol. *Oxides:* occur as both secondary and primary minerals (ilmenite in -38 and -40) *Apt.:* primary minerals (0.1-1.5 mm) prisms or anhedral grains (3 mm) *Akfsp.:* Orth. is a late interstial phase.

Gabbro: OKJ-063

Txt.: coarse grained (5 mm) *Cpx.:* form large (2-6mm) irregular glomerocrysts which hold more inclusions and are less ophitic than in olivine leuco-gabbros; simple twinning is also displayed *Ol.:* subhedral - anhedral interstial grains (1-2mm) are more altered than in ol-leuco-gabbros and are replaced by a vermicular intergrowth of Fe-oxide and opx *Opx.:* occurs as narrow rims around olivine *Plag.:* clouded and sericitized laths (1 - 4mm) hold bt. inclusions and are sub-parallel; lamellar twinning is irregular *Bt.:* 1mm interstial grains are closesly associated with Fe-Ti oxides.

Olivine leuco-gabbro: OKJ-068, OKJ-069

Txt.: ophitic and coarse grained (< 4 mm) *Ol.:* equidimensional, subhedral grains (<3mm) have plag. inclusions (0.5 mm) *Alter.:* appear as opx rims and as chlorite in fractures *Cpx.:* densely schillerized large (4mm) ophitic grains hold plag., bt. and opaque inclusions *Plag.:* zoned subhedral laths (1-3mm) are randomly orientated and show metamorphic clouding *Bt.:* interstial 1 mm flakes *Apt.:* euhedral 0.1 mm prisms *Oxides:* anhedral pyrrhotite and Fe-Ti oxides also occur.

Oligoclase essexite: OKJ-088

Txt.: medium to coarse grained (1-2 mm) *Plag.:* plag. / ortho. ratio = 2:1 (Simpson, 1954) *Amph.:* euhedral to subhedral unaltered inclusion-free crystals *Cpx.:* replaced by amph. *Bt.:* subhedral - anhedral flakes crystallized before and are enclosed by amph. *Mgt.:* exsolution needles present.

Syenites: OKJ-150, OKJ-164

Txt.: intrusion margins show crystal lamination whereas central portions show equigranular textures *Plag.:* interlocking anhedral feldspar crystals (3 mm) with irregular crystal boundaries display symplectic intergrowths; late partial recrystallisation and overgrowth of feldspar phenocrysts in rocks displaying a trachytic texture is indicated by the presence of cpx. inclusions. Exsolution lamellae occur in the ortho. microperthite *Alter.:* features include sericitization of feldspar, corrosion of fayalite to to iddingsite along fractures and rims, ferroedinite amphibole reaction mantles on fayalite and pyroxene and biotite at reaction boundaries *Quartz:* occurs as aggregates interstial to feldspar *Ol.:* Fayalite forms aggregates with ilmenite, clinopyroxene, orthopyroxene, amphibole and apatite *Fe-Ti Oxides:* include ilmenite and magnetite.

Alkaline gabbros: OKJ-084, OKJ-176

Txt.: Coarse grained sub-ophitic *Plag.:* grains are < 7 mm long and show limited alteration *Ol.:* 1-2 mm *Cpx.:* schillerized and inclusion free; occurs as 1-2 mm grains and as 5 mm oikocrysts *Bt.:* forms (primary and/or secondary) Fe-Ti oxide mantles and laths; coarse and fine grained generations characterized by different Rb-Sr values occur *Nepheline:* occurs as highly altered interstial grains.

Table 1.1 Summary of Okenyenya modal abundance (%) and grain size data (mm) relevant to this study. (Modal abundances were obtained by point counting 1000 counts per section. Three perpendicular sections were point counted for selected samples (OKJ-04, -014, -018, -034, -046, -069, -088, -150) to account for preferred orientations.) The "Y" and "X" symbols refer to the average major- and minor-axis grain size dimensions (mm) repectively. The samples analysed for oxygen isotopes in this study are indicated by "*". (Abbreviations used are as for the petrographic descriptions (see Section 3.1 above).)

Sample	*Plagioclase*			*Pyroxene*			*Biotite*			*Olivine*			*Amphibole*			*Quartz*			*Fe-Ti oxide*			*Carbonate*			*Alkali Feldspar*		
	%	X	Y	%	X	Y	%	X	Y	%	X	Y	%	X	Y	%	X	Y	%	X	Y	%	X	Y	%	X	Y
*OKJ-004	57.4	1	6	16.3	0.8	1.3	5.8	0.6	1	8.0	1	1.5	-	-	-	-	-	-	6.7	0.5	1.5	-	-	-	-	-	-
*OKJ-014	8.6	1.5	8	1.6	1.4	2	2.6	0.6	1.2	-	-	-	6.2	1	2	-	-	-	4.3	0.6	1.5	-	-	-	*	1.1	-
*OKJ-018	24.4	2	5	8.4	3	5	5.8	0.02	0.1	1.02	0.1	0.14	29.3	0.8	1.2	-	-	-	16.5	0.2	0.4	tr	0.2	0.3	12.1	2	0.3
*OKJ-031	63.7	0.6	5	18.2	0.9	3.5	5.1	0.5	1.2	2.0	0.8	1.3	-	-	-	-	-	-	3.4	0.6	2	-	-	-	6.2	1	-
*OKJ-033	68.3	3	7	13.0	0.8	4	2.0	0.9	2	2.5	2	5	-	-	-	-	-	-	3.8	0.7	2	-	-	-	2.3	0.5	-
OKJ-034	64.7	1	5	5	0.6	1.4	5.8	0.8	1.2	10.8	0.8	1.2	-	-	-	-	-	-	8	0.6	1	-	-	-	5	0.8	-
OKJ-037	65.2	-	-	13.1	-	-	3.8	-	-	4.3	-	-	-	-	-	-	-	-	4.3	-	-	-	-	-	-	-	-
OKJ-038	69.4	0.7	5	12.0	0.6	3.6	4.5	0.8	2.5	3.7	0.7	0.8	-	-	-	-	-	-	5.7	0.4	2	-	-	-	1.5	0.5	-
OKJ-039	55.5	-	-	11.8	-	-	6.5	-	-	10.1	-	-	-	-	-	-	-	-	10.1	-	-	-	-	-	-	-	-
OKJ-040	54.7	0.7	4	10.5	0.9	2.5	7.0	1.5	4	9.4	0.9	1.1	-	-	-	-	-	-	13.1	0.7	2.1	-	-	-	0.5	1.4	-
OKJ-041	37.2	1.2	5	23.2	2	4	7.1	1.7	5	0.4	0.6	0.8	-	-	-	-	-	-	10.8	0.4	1	-	-	-	9.8	4.4	-
OKJ-043	49.7	1.5	6	5.1	1	4	1.1	1.3	4.5	3.4	0.1	0.5	2.2	1.4	3.6	2.0	0.1	0.2	5.1	0.4	1	-	-	-	28.2	3.4	-
OKJ-044	54.5	0.8	7	4.7	1.5	4.2	1.5	0.8	1.2	1.3	0.7	1	-	-	-	4.1	0.4	0.8	2.1	0.4	0.7	-	-	-	9.1	1.5	-
OKJ-045	46.0	1.8	5	5.2	0.6	3.9	0.5	0.8	1.2	0.5	0.8	0.8	2.5	0.4	1.4	1.7	0.5	0.6	4.2	0.3	0.8	-	-	-	27.6	4	-
OKJ-046	42.8	1.5	6.5	18.4	0.9	4	0.6	0.2	0.5	0.9	0.9	1	-	-	-	4.1	0.2	0.5	3.1	0.4	0.6	-	-	-	20.5	2.1	-
OKJ-047	45.4	1	7	4.4	1	8	-	-	-	3.7	0.8	1.2	2.4	0.4	1.5	8.4	0.4	0.8	3.1	0.5	0.8	tr	0.5	1	27.8	2	1
OKJ-050	70.7	1.9	2.5	16.3	1.6	3	0.7	0.4	1	7.1	1	1.5	-	-	-	-	-	-	3.1	0.6	1.8	tr	0.6	0.7	-	-	0.7
OKJ-061	71.6	-	-	17.0	-	-	4.4	-	-	2.0	-	-	-	-	-	-	-	-	2.0	-	-	-	-	-	-	-	-
OKJ-062	52.7	1	7	19.0	1	3.5	2.7	2	5	19.2	1	4	-	-	-	-	-	-	5.2	0.5	3	-	-	-	-	-	-
OKJ-063	51.6	1	4	37.3	2	6	tr	0.3	1	3.3	0.9	2	-	-	-	-	-	-	2.6	0.8	1.9	-	-	-	-	-	-
OKJ-064	54.0	-	-	36.3	-	-	2.0	-	-	5.6	-	-	-	-	-	-	-	-	5.6	-	-	-	-	-	-	-	-
OKJ-065	70.1	-	-	16.1	-	-	4.1	-	-	4.9	-	-	-	-	-	-	-	-	4.6	-	-	-	-	-	-	-	-
OKJ-066	64.8	-	-	19.2	-	-	1.4	-	-	9.6	-	-	-	-	-	-	-	-	9.6	-	-	-	-	-	-	-	-
OKJ-068	69.2	2	3	16.1	1.5	4	1.6	1.7	1	12.3	2	3	-	-	-	-	-	-	0.1	1	2.5	-	-	-	-	-	-
OKJ-069	50.4	1.8	3.5	37.0	2	4.2	2.7	1	1	4.3	1.2	3	-	-	-	-	-	-	4.2	0.6	1.1	-	-	-	-	-	-
OKJ-088	32.8	0.8	5	3.0	0.3	0.8	3.2	0.5	2	-	-	-	33.5	0.6	2	-	-	-	2.8	0.2	0.3	-	-	-	13.8	0.6	-
OKJ-150	9.7	1	3	tr	0.3	2	4.0	1	2	-	-	-	7.5	1	1	6.4	0.3	0.6	6.1	0.3	1	tr	0.1	0.2	65.1	0.6	0.2
OKJ-164	11.1	1	3	-	-	-	1.7	0.7	1.0	-	-	-	8.5	1	2	4	1	2	2.2	0.1	0.2	-	-	-	69.8	1.5	-
OKJ-176	77.0	1	7	12	1	5	2.0	1	2	2	1	2	-	-	-	-	-	-	4.0	1	2	-	-	-	-	-	-

Table 1.1 (continued)

Sample	*Orthopyroxene*			*Apatite*			*Other minerals*
	%	X	Y	%	X	Y	
OKJ-004	acc	-	-	5.1	0.2	0.7	alteration minerals: 1.3 %
OKJ-014	-	-	-	0.7	0.1	0.2	perthite: 68.2 %, analcite: 2.5 %, nepheline: 3.5 %
OKJ-018	-	-	-	0.7	0.1	0.2	perthite: 2.5 %, trace minerals: sodalite, orthopyroxene
OKJ-031	0.5	0.5	0.8	0.5	0.1	3	
OKJ-033	2.7	0.8	2	5.1	0.1	5	
OKJ-034	2.8	0.3	0.4	2.2	0.1	0.4	
OKJ-037	2.1	-	-	3.3	-	-	
OKJ-038	0.2	0.4	0.4	2.7	0.1	3	
OKJ-039	0.8	-	-	3.4	-	-	
OKJ-040	-	-	-	4.8	0.1	3	
OKJ-041	8.5	0.6	3	2.1	0.4	3	
OKJ-043	0.8	1	4	2	0.1	0.8	
OKJ-044	7.6	1	3.5	0.6	0.2	1	alteration minerals: 5 %
OKJ-045	1.1	1.3	4.1	3.1	0.01	0.1	
OKJ-046	7.0	0.7	3.9	2.4	0.1	0.4	
OKJ-047	0.4	1	1	1.2	0.1	1	alteration minerals: 7.8 %
OKJ-050	-	-	-	0.1	0.2	0.4	
OKJ-061	0.2	-	-	0.8	-	-	
OKJ-062	0.5	0.6	1.8	0.5	0.3	0.4	
OKJ-063	5	0.6	1.2	tr	0.1	0.3	
OKJ-064	3.0	-	-	tr	-	-	
OKJ-065	tr	-	-	tr	-	-	
OKJ-066	tr	-	-	tr	-	-	
OKJ-068	tr	3	5	0.5	0.1	0.2	
OKJ-069	-	-	-	1.1	0.1	0.1	
OKJ-088	-	-	-	1	0.1	0.1	
OKJ-150	-	-	-	0.8	0.1	0.2	
OKJ-164	0.5	0.5	1.2	2.2	0.1	0.6	
OKJ-176	-	-	-	acc	0.1	0.2	nepheline: 3 %

Table 1.2 Bulk rock compositional data (le Roex *et al.*, 1995). The abbreviation "L.O.I." refers to the loss on ignition value.

Sample:	*OKJ-004*	*OKJ-014*	*OKJ-018*	*OKJ-031*	*OKJ-033*	*OKJ-038*	*OKJ-040*	*OKJ-041*	*OKJ-043*	*OKJ-044*	*OKJ-045*	*OKJ-046*	*OKJ-047*	*OKJ-050*
SiO_2	47.2	59.0	47.8	46.9	48.0	44.0	44.3	47.4	50.9	52.6	54.1	54.6	55.0	48.0
TiO_2	0.6	0.5	1.8	1.6	2.1	3.6	3.8	2.7	2.3	2.0	2.1	2.0	2.0	0.5
Al_2O_3	11.8	19.7	17.9	17.1	19.0	16.7	15.7	14.2	16.5	16.5	14.5	14.6	14.9	22.9
Fe_2O_3	1.4	0.5	1.2	1.5	1.3	2.1	2.0	2.0	1.5	1.4	1.5	1.6	1.5	0.8
FeO	9.3	3.1	8.2	10.3	8.4	13.7	13.3	13.2	9.8	9.0	10.1	10.4	9.9	5.0
MnO	0.2	0.01	0.3	0.2	0.2	0.3	0.3	0.3	0.2	0.2	0.3	0.3	0.3	0.1
MgO	17.3	0.9	4.3	6.7	4.2	4.7	5.0	5.2	3.0	2.6	2.6	2.2	2.3	5.3
CaO	8.6	2.1	2.1	11.7	11.3	9.0	9.2	8.5	7.2	6.8	6.1	5.9	6.1	12.8
Na_2O	1.7	6.9	6.9	2.6	2.8	3.1	2.9	3.0	3.1	3.5	3.3	3.3	3.6	2.8
K_2O	0.5	5.6	5.6	0.6	1.1	0.9	1.1	1.7	2.3	2.6	2.5	3.1	2.9	0.3
P_2O_5	0.1	0.2	0.2	0.4	0.9	1.7	1.9	0.3	1.2	1.0	0.9	0.8	0.9	0.0
LOI	0.9	1.7	1.7	1.2	1.2	1.0	1.1	1.4	2.3	2.3	1.7	1.3	1.0	2.1
H2O-	0.1	0.2	0.2	0.2	0.2	0.1	0.1	0.2	0.2	0.2	0.2	0.3	0.2	0.1
Total	99.8	100.1	99.6	100.9	100.7	100.7	100.7	99.9	100.5	100.5	100.0	100.1	100.5	100.6
Zr	64	255	246	37	70	46	70	112	123	186	143	206	167	21
Nb	5.3	120	94	5.4	16.4	18	25	21	29	30	46	39	44	6
Y	20	24	28	15.7	22	31	40	26	41	43	51	45	53	6
Rb	9.7	145	82	12.1	29	19.7	28	40	70	77	85	94	93	6
Ba	149	2686	976	489	619	650	696	890	1128	1319	1154	1356	1525	213
Sr	122	324	669	472	490	539	498	388	390	388	320	300	317	773
Co	82	4.6	33	47	26	22	29	45	19	17	15	10	13	39
Cr	1905	1.7	12.8	85	9.7	2.9	10	19	3	2	3	<2.0	<2.0	65
Ni	643	1.9	24	65	25	4	<4.0	12	<4.0	<4.0	<4.0	<4.0	<4.0	62
V	197	27	186	310	160	116	181	393	140	60	60	49	79	143
Zn	76	55	75	73	70	120	124	124	118	138	138	154	141	27
Cu	76	6.8	41	92	39	12.3	16	20	11	11	11	10	9	29
Nd	7.5	44	19.3	13.2	20.6	36.3	43.8	22.2	39.9	59	59	42.8	46.4	4.3

Table 1.2 Bulk rock compositional data (contd.).

Sample:	*OKJ-062*	*OKJ-063*	*OKJ-068*	*OKJ-069*	*OKJ-084*	*OKJ-088*	*OKJ-150*	*OKJ-164*	*OKJ-176*
SiO_2	47.8	48.2	46.6	47.4	47.8	49.1	61.0	65.2	50.6
TiO_2	1.2	1.1	0.8	1.2	1.4	1.7	0.8	0.8	1.8
Al_2O_3	18.0	15.1	21.1	15.4	14.7	18.5	16.6	14.7	21.5
Fe_2O_3	1.4	1.2	1.0	1.1	1.7	1.4	0.9	0.8	0.9
FeO	9.3	7.9	6.6	7.3	8.3	9.1	4.3	5.2	6.3
MnO	0.2	0.2	0.2	0.1	0.2	0.2	0.2	0.2	0.1
MgO	7.7	8.5	7.5	9.3	6.7	3.4	0.6	0.9	2.2
CaO	10.9	14.3	13.8	15.8	12.7	6.6	2.0	2.3	10.3
Na_2O	2.7	1.9	1.8	1.8	2.8	5.1	5.0	3.8	4.4
K_2O	0.7	0.7	0.3	0.3	2.0	3.4	5.4	5.0	1.3
P_2O_5	0.2	0.1	0.1	0.1	0.3	0.6	0.2	0.2	0.3
LOI	0.9	1.2	0.9	1.0	1.1	2.9	1.8	0.9	0.7
H2O-	0.2	0.2	0.2	0.2	0.4	0.1	0.2	0.0	0.1
Total	100.9	100.7	100.9	101.0	100.0	100.1	99.0	99.94	100.4
Zr	38	55	39	25	131	301	416	347	66
Nb	6	8	6	3	45	103	108	39	24
Y	12	18	13	9	27	31	59	51	18
Rb	15	18	13	7	70	119	143	165	25
Ba	384	331	351	200	792	818	1538	1363	824
Sr	488	354	487	481	613	641	131	130	655
Co	56	45	37	48	42	26	4.9	7	17
Cr	53	239	69	77	152	5	5	13	3
Ni	58	130	98	102	89	14	<1.7	3	4
V	216	218	151	121	230	147	10	27	161
Zn	65	56	46	45	63	64	87	93	43
Cu	103	280	266	107	57	23	2	8	71
Nd	8.7	12.9	6.09	9.15	28.8	34.4	52	42.4	27.8

2.1 Calcite CO_2-extraction technique

The average whole-rock carbon and oxygen isotope compositions of disseminated calcite in selected samples were obtained by following the carbonate CO_2-extraction procedure based on the method of McCrea (1950). The technique involves the decomposition of the carbonates with 100 % phosphoric acid at 25 °C. Samples (30 mg) were pulverized in a grinding mill to less than 200 mesh (< 70 μm). The reaction vessel was then evacuated and both the sample and acid degassed on a vacuum line. Sample bottles were then placed in a water tank at 25°C. After thermal equilibration was reached, the acid was poured from the sample arm into the main body of the tube and placed back into the water tank. CO_2 derived by complete dissolution of calcite after four hours, was collected and cryogenically distilled from H_2O. The reaction time was sufficient for the calcite-phosphoric acid reaction to run to completion. The isotopic composition of the extracted CO_2 was determined using a VG Micromass 602E double-collector ratio mass spectrometer. Raw carbon and oxygen isotope compositions were corrected using a CO_2-acid fractionation factor of 1.01025. The oxygen and carbon isotope compositions are reported with respect to the SMOW and PDB reference scales respectively, and are precise to 0.2 and 0.1 ‰ respectively. The samples were extracted at the same time as a 10 mg split of the pure calcite Namaqualand Marble (NM) standard. The differences between the observed δ values for NM and the accepted values were used to correct the data for drift in the reference gas.

2.2 Notation and fractionation factors

Isotopic ratios are expressed by the δ value given in per mil (‰), which is defined as:

$$\delta X_A = [(R_A - R_{STD}) / R_{STD}] \times 1000$$

where X stands for ^{18}O or ^{13}C, $R_x = (^{18}O/^{16}O)_x$, $(^{13}C/^{12}C)_x$, and R_{STD} is the corresponding ratio in a standard. For oxygen and carbon the δ-values are reported relative to Standard Mean Ocean Water (V-SMOW) and to the Peedee Belemnite (V-PDB).

3.1 Silicate sample preparation and oxygen-extraction technique

Jaw-crushed (Mn-steel jaws) whole rock samples were sieved to obtain -60 to -40 mesh size fractions which were stripped of magnetite by a hand-held magnet. The mafic mineral fractions were separated from the plagioclase using a Frantz Isodynamic Magnetic Separator and the individual grains subsequently handpicked with the use of a binocular microscope. The general absence of quartz from the samples (as indicated by the petrography) indicate the feldspar mineral separates may be considered to be > 98 % pure. The separated minerals were crushed to a fine powder in an agate mortar and pestle and dried at 50 °C for 48 hours before analysis.

The oxygen was extracted from the mineral separates using the silicate stable isotope oxygen-extraction line facility in the Department of Geological Sciences at the University of Cape Town. Samples were loaded into nickel reaction vessels and degassed at 200 °C for 4 hours. The samples (10 mg) were reacted with ClF_3 following the procedure outlined by Borthwick and Harmon (1982). All of the separates were reacted at 550 °C overnight. Nearly all of the analyses were run in duplicate or triplicate. The average difference in the $\delta^{18}O$ value for sample reruns lies below 0.5 ‰ for the plagioclase and below 0.3 ‰ for the pyroxene, biotite and olivine analyses. The yields for most of the minerals lie between 99 % and 101 % . The extracted oxygen was converted to CO_2 with a heated carbon rod and analysed for the $^{18}O/^{16}O$ ratio with a VG 602E mass spectrometer. The average mean deviation of pairs of δ^{46} values obtained for 12 duplicate NBS-28 quartz standard analyses was 0.13.

Table 4.1 Partition coefficients used in the calculation of the bulk rock distribution coefficients, necessitated for the application of assimilation with fractional crystallization (AFC) models (see Chapter 6).

Mineral	*Sr*	*Nd*
Olivine	0.01	0.01
Orthopyroxene	0.01	0.01
Clinopyroxene	0.10	0.30
Plagioclase	2.50[1]	0.08
Amphibole	0.36	0.37
Fe-mica	0.30	0.30
Alkali feldspar	6.00[2]	0.06
Apatite	5.00	21.0
Ti-magnetite	0.01	0.01

Notes:

1. Average for values estimated from the most primitive tholeiitic gabbro plagioclase (An_{63}) composition, with reference to: 1) the Korringa (1971) plot of the distribution of Sr between plagioclase and melt, as a function of the anorthite content of the feldspar, and 2) other values typically stated for a basaltic liquid composition (Cox, Bell & Pankhurst, 1979).

2. Estimated from the average tholeiitic gabbro alkali feldspar (An_3) composition with reference to the Korringa (1971) Sr versus the feldspar An composition plot. This value represents the average of values of the observed data (3) and an extrapolation of the calculated curve (9), at a feldspar composition of An_3.

Other sources of data: McKenzie & O'Nions (1991); le Roex (1985); Schnetzler & Philpotts (1968); Schnetzler & Philpotts (1970); Hart & Dunn (1993).